# DYNAMIC PVDF SENSOR BASED MONITORING OF SINGLE POINT CUTTING PROCESSES

A Thesis
Presented to
The Academic Faculty

by

Vinh Nguyen

In Partial Fulfillment
of the Requirements for the Degree
Master of Science in the
School of School of Mechanical Engineering

Georgia Institute of Technology
December 2016

# DYNAMIC PVDF SENSOR BASED MONITORING OF SINGLE POINT CUTTING PROCESSES

Approved by:

Dr. Shreyes Melkote, Advisor
School of Mechanical Engineering
*Georgia Institute of Technology*

Dr. Thomas Kurfess
School of Mechanical Engineering
*Georgia Institute of Technology*

Dr. Steven Liang
School of Mechanical Engineering
*Georgia Institute of Technology*

Date Approved: October 20th, 2016

# ACKNOWLEDGEMENTS

I would like to greatly thank the students and faculty of the PMRC for help with their support. I would like to thank greatly Steven Sheffield, Louis Boulanger, Brandon Royal, and Nathan Mauldin for their aid in conducting machining experiments and fabricating parts. In addition, I would like to thank Kyle French, Anh Nguyen, and Vladimir Bortkevich of the ME Electronics shop for their electrical expertise. I would like Siemens Energy for providing feedback and funding for this project. I would like to thank Dr. Melkote for his guidance as an advisor. I would also like to thank Dr. Liang and Dr. Kurfess for their time to be on my committee. I would like to thank my family and many friends for making sure I never forget the value of being a good person.

# TABLE OF CONTENTS

Page

ACKNOWLEDGEMENTS ..... iii

LIST OF TABLES ..... vi

LIST OF FIGURES ..... vii

NOMENCLATURE ..... x

SUMMARY ..... xiii

CHAPTER 1 INTRODUCTION ..... 1

Motivation and Problem Statement ..... 1

Research Objectives ..... 3

Proposed Approach ..... 4

Thesis Outline ..... 5

CHAPTER 2 LITERATURE REVIEW ..... 6

Machining Process Monitoring ..... 6

Monitoring of Cutting Forces in Single Point Cutting ..... 8

PVDF Based Sensing Applications ..... 10

On-line Recognition of Chatter in Single Point Cutting: Sensors and Algorithms ..... 11

Summary ..... 16

CHAPTER 3 PVDF SENSOR BASED DYNAMIC CUTTING FORCE MEASUREMENT IN TURNING ..... 17

Introduction ..... 17

Turning Force Measurement System Modeling ..... 17

Signal Flow Modeling ..... 22

Experimental Verification ..... 23

Summary ..... 30
CHAPTER 4 PVDF SENSOR BASED BORING TORQUE MEASUREMENT ..... 32
Introduction ..... 32
Boring Torque Measurement System Modeling ..... 32
Signal Flow Modeling ..... 32
Experimental Verification ..... 35
Summary ..... 41
CHAPTER 5 ON-LINE CHATTER DETECTION ..... 42
Introduction ..... 42
Sensing and Processor System Requirements ..... 42
Algorithm Description and Implementation ..... 44
Methodology ..... 44
Turning Experiments ..... 56
Turning Results ..... 62
Boring Experiments ..... 68
Boring Results ..... 72
Summary ..... 77
CHAPTER 6 CONCLUSIONS AND RECOMMENDATIONS ..... 78
Original Contributions ..... 78
Main Conclusions ..... 78
Future Work and Recommendations ..... 80
APPENDIX ..... 82
REFERENCES ..... 87

# LIST OF TABLES

Page

Table 1. Cutting conditions for turning tests for sensor calibration. ..... 25

Table 2. Cutting conditions for boring tests..... 37

Table 3. Cutting conditions for turning tests for chatter detection. ..... 62

Table 4. Cutting conditions for boring tests..... 71

# LIST OF FIGURES

Page

Figure 1. Overall approach. ..... 5

Figure 2. Example of an automated process monitoring chain. ..... 7

Figure 3. Example picture of PVDF thin film sensor [52]. ..... 10

Figure 4. Frequency response of several MEMS microphones [103]. ..... 12

Figure 5. PVDF rosette configuration for outer diameter turning. ..... 18

Figure 6. Signal flow for single-point cutting force measurement system. ..... 18

Figure 7. Schematic of a PVDF sensor element. ..... 20

Figure 8. Example measurement system frequency response. ..... 23

Figure 9. Force measurement setup for turning. ..... 24

Figure 10. PVDF signal comparison with dynamometer for dynamic $Fy$ (Test 12). ..... 26

Figure 11. PVDF signal comparison with dynamometer for $Fz$ (Test 17). ..... 27

Figure 12. PVDF signal frequency decomposition comparison with dynamometer (Test 17). ..... 27

Figure 13. PVDF signal comparison with dynamometer for $Fx$ (Test 8). ..... 28

Figure 14. PVDF signal comparison with dynamometer for dynamic radial force component (Facing). ..... 29

Figure 15. PVDF signal comparison with dynamometer for dynamic radial force component (Threading Tool). ..... 29

Figure 16. Force measurement setup for boring. ..... 33

Figure 17. PVDF rosette configuration for a boring tool. ..... 34

Figure 18. Data logging equipment for boring sensor validation. ..... 36

Figure 19. PVDF signal comparison with dynamometer dynamic torque component (Test 1). ..... 38

Figure 20. PVDF signal comparison with dynamometer dynamic torque component (Test 5). ..... 38
Figure 21. PVDF signal comparison with dynamometer dynamic torque component (Test 8). ..... 39
Figure 22. PVDF signal frequency decomposition comparison with dynamometer (Test 8). ..... 39
Figure 23. Intersecting hole condition. ..... 40
Figure 24. PVDF signal comparison with dynamometer dynamic torque component (Test 12). ..... 40
Figure 25. Chip regeneration in orthogonal cutting [104]. ..... 45
Figure 26. Example CMM data and workpiece surface. ..... 48
Figure 27. Example autocorrelation functions. ..... 50
Figure 28. DWT example schematic. ..... 53
Figure 29. SGWT example ..... 54
Figure 30. Case 1 tool path. ..... 56
Figure 31. Example feed force data (Case 1). ..... 57
Figure 32. Case 2 tool path ..... 58
Figure 33. Example feed force data (Case 2). ..... 59
Figure 34. Case 3 tool path. ..... 60
Figure 35. Example feed force data (Case 3). ..... 61
Figure 36. 1st Autocorrelation Coefficient (Test 1). ..... 63
Figure 37. 1st Autocorrelation Coefficient (Test 6). ..... 64
Figure 38. 1st Autocorrelation Coefficient (Test 7). ..... 64
Figure 39. SGWT algorithm results (Test 3). ..... 65
Figure 40. SGWT algorithm results (Test 6). ..... 65
Figure 41. SGWT algorithm results (Test 8). ..... 66
Figure 42. FFT algorithm results (Test 2). ..... 67

Figure 43. FFT algorithm results (Test 5). 68
Figure 44. FFT algorithm results (Test 9). 68
Figure 45. Boring case tool path. 69
Figure 46. Example turning vs. boring comparison. 70
Figure 47. Frequency decomposition of unstable and stable cutting. 70
Figure 48. 1st Autocorrelation Coefficient (Test 1). 72
Figure 49. 1st Autocorrelation Coefficient (Test 12). 73
Figure 50. SGWT algorithm results (Test 2). 74
Figure 51. SGWT algorithm results (Test 6). 75
Figure 52. FFT algorithm results (Test 11). 76
Figure 53. FFT algorithm results (Test 9). 76

# NOMENCLATURE

$a$ = Radial depth of cut in orthogonal cutting (m)

$a_i$ = Approximation coefficient of discrete wavelet transform at decomposition level $i$

$a_k$ = Autocorrelation coefficient at time difference $k$

$B$ = Shannon entropy of a signal

$c_k$ = Autocovariance function at time difference $k$

$c_y$ = System damping (N/m/s)

$C_F$ = Capacitance in the charge amplifier feedback loop (F)

$d_i$ = Detail coefficient of discrete wavelet transform at decomposition level $i$

$d_{ij}$ = Piezoelectric modulus that relates the electric displacement along axis $i$ to the mechanical stress along axis $j$ (C/N)

$D$ = Diameter of cutting tool (m)

$\varepsilon(t)$ = Bending strain (m/m)

$E_i$ = Young's modulus of the PVDF sensor along axis $i$ (N/m$^2$)

$E_t$ = Young's modulus of the tool (N/m$^2$)

$F(t)$ = Time series dynamic cutting force (N)

$F_x$ = Radial dynamic force component (N)

$F_y$ = Tangential dynamic force component (N)

$F_z$ = Feed dynamic force component (N)

$g[n]$ = Low pass filter

$G$ = Shear modulus of the tool (N/m$^2$)

$G_{Cut}(s)$ = Continuous time transfer function matrix between cutting forces and strain at the location of the PVDF sensor

$G_{PVDF}(s)$ = Transfer function matrix between the strain measured by the PVDF sensor and the charges generated in the electrodes of the PVDF sensor

$h_0$ = Undeformed chip thickness (m)

$h(t)$ = Chip thickness (m)

$h[n]$ = High pass filter

$H$ = Distance from the center of PVDF sensor to the neutral axis with respect to bending moment created by $F$ (m)

$I_p$ = Polar moment of inertia ($m^4$)

$I_{zz}$ = Area moment of inertia ($m^4$)

$k_y$ = System stiffness (N/m)

$K_{Cut}$ = Orthogonal cutting force coefficient ($N/m^2$)

$K_{Feed}$ = Feed force calibration constant (V/N)

$K_{Rad}$ = Radial force calibration constant (V/N)

$K_T$ = Boring torque calibration constant (V/Nm)

$K_{Tan}$ = Tangential force calibration constant (V/N)

$L$ = Distance from the idealized concentrated force to the center of the PVDF sensor (m)

$m_y$ = System mass (kg)

$N$ = Number of samples

$p_i$ = Probability mass function of a sample

$P_R$ = Power ratio of the top two largest Fast Fourier Transform peaks

$q(t)$ = Electric charge generated in the electrodes of a PVDF sensor (C)

$q_A$ = Total electric charge generated in the electrodes of PVDF sensors in the axial rosette configuration (C)

$\Phi(s)$ = Frequency response transfer function

$S$ = Sampling period (s)

$T(t)$ = Time series of cutting torque (Nm)

$v_{ij}$= Poisson ratio of the PVDF sensor material; it represents the contribution of the normal strain along axis $i$ to the normal strain along axis $j$

$V(t)$ = Time series of voltage output of charge amplifier (V)

$V[n]$ = Discrete voltage samples collected by the data logging unit (V)

$V_A(t)$ = Time series of voltage output of anti-aliasing filter (V)

$\omega_c$ = Chatter vibration frequency (Hz)

$\psi(t)$ = Mother wavelet of a continuous wavelet transform

$X$ = Discretized sample dataset of a signal

$X_F$ = Discrete Fourier Transform of a signal

$X_\omega$ = Continuous wavelet transform of a signal

$\gamma(t)$ = Torsional shear strain (%)

$y(t)$ = Instantaneous displacement between the tool and workpiece (m)

# SUMMARY

A low-cost, high fidelity measurement system consisting of a thin film Polyvinylidene Fluoride (PVDF) piezoelectric strain rosette and data logging electronics has been designed, fabricated, and evaluated for monitoring the dynamic cutting forces and torque in single-point cutting processes, specifically turning and boring. Physics-based models are used to relate the measured voltage to the process forces and torques. By means of key assumptions about particular strain components, simplified PVDF strain sensor rosettes are developed to isolate the particular strains of interest. Wired and wireless communication methods to transmit the dynamic strains measured by the sensors to a data logging base station are demonstrated. The proposed methods are experimentally validated through comparison with quartz-based piezoelectric cutting force and torque dynamometers. In addition, the performance of several chatter detection algorithms applied to turning force and boring torque data is evaluated with a focus on embedded electronic automation. The dynamic cutting force data is acquired from turning experiments by varying the initial workpiece geometry, while the dynamic torque data is acquired from boring experiments performed on industrial rotor compressor discs. For chatter detection in turning, spectral analysis is demonstrated to be the most robust algorithm and is shown to be capable of detecting dynamic instability before physical damage to the part occurs. For chatter detection in boring, autocorrelation modeling is demonstrated to be the most computationally efficient of the techniques evaluated.

# CHAPTER 1

# INTRODUCTION

## Motivation and Problem Statement

Single point machining processes such as turning and boring are used extensively in manufacturing applications, including gas turbine rotor and stator production. Though analytical methods exist to predict the cutting forces and dynamic instability in such processes [1, 2], they do not account for process uncertainties. Sources of process uncertainty that are difficult to model include inhomogeneity in workpiece material properties, and tool breakage/wear, etc., which in turn can negatively impact part quality and productivity of the operation. Therefore, the machining process requires on-line system monitoring in addition to physics-based modelling to maximize production and minimize costs.

Cutting forces and torques in machining in general, and single-point cutting in particular, are of particular practical significance for process monitoring since they can be used as a robust proxy for the detection of tool breakage, wear, and self-excited chatter vibrations [3, 4]. Current state-of-the-art for accurate measurement of forces in single-point cutting consists of platform type quartz-based piezoelectric force dynamometers. Piezoelectric sensors consist of a material that produces charge when undergoing deformation or temperature change. However, these force sensing systems suffer from several limitations including: 1) high cost, 2) difficulty in incorporating them into the machine tool system without compromising the system dynamic stiffness, and 3) limited bandwidth (typically < 4 kHz). Therefore, a low-cost, highly sensitive, nonintrusive measurement method is required to realize real-time process monitoring in a production environment.

Though there exist analytical models to identify cutting conditions that avoid chatter [5-8], they do not account for a wide range of process related uncertainties mentioned earlier. Also, structural dynamic characteristics of the workpiece/tool/fixture/machine tool system change as a function of the machining parameters including tool position and fixturing and are therefore difficult to characterize. Therefore, real-time detection of dynamic instability, i.e. chatter, is still necessary for active chatter suppression during the cutting process. Though multiple chatter detection methods for turning and boring have been proposed by the research community, the corresponding algorithms have yet to be implemented on the factory floor.

Various reasons exist for the failure to apply on-line chatter detection methods in a production environment. Generally, the sensors and detection algorithms are developed and validated in a laboratory setting and do not consider the demands of production environments including reconfigurability, cost, and sources of noise. As a result, chatter monitoring systems proposed by researchers are limited by at least one of the following drawbacks: 1) the sensors used to robustly acquire data for processing are costly (such as piezoelectric microphones and quartz-based dynamometers), 2) the chatter detection algorithms fail to consider various events or machine tool setups that can change the signal's behavior, such as tool breakage, changing cutting parameters, pre-existing geometric discontinuities in the workpiece (e.g., holes, steps, etc.), 3) the chatter monitoring methodologies cannot accommodate automated machine tool correction or practical data logging, and 4) the computing hardware used for signal acquisition and processing tend to be intrusive and expensive, as is the case with contract vendors who have to reconfigure the CNC software architecture to facilitate chatter detection/suppression.

Polyvinylidene Fluoride (PVDF) piezoelectric strain sensors are seen as a potential candidate for nonintrusive machine tool monitoring due to their flexibility in mounting, wide frequency bandwidth (with resonant frequency above 10 MHz), high strain sensitivity

(~10 mV/με), and low cost (~$5 per sensor) [9]. The PVDF strain sensor is constructed by sputtering PVDF onto a thin polymer film, which can then be easily attached to a host structure. Thus, the PVDF thin film sensor produces a corresponding charge when the host structure is strained elastically. The development and use of PVDF thin film sensors for monitoring the dynamic forces in end milling [10] and in non-machining applications [11-15] have been reported.

While PVDF-based sensing has been evaluated for end milling, PVDF-based force sensing has not been developed nor validated for single-point cutting processes such as turning and boring. In single-point cutting processes, the tool is in continuous contact with the workpiece. Thus, ideally the cutting force should be a steady state signal (termed static force). In this thesis, dynamic forces are defined as variations about the static forces. Dynamic forces measured by the PVDF sensor can be used to characterize process states including tool breakage, wear, and self-excited vibrations [2, 3]. In summary, the need for low cost, flexible, and robust systems for on-line monitoring of single-point cutting processes such as turning and boring serve as the primary motivation for this research. As a result, a new machining process monitoring system consisting of PVDF piezoelectric thin film sensing is researched.

## Research Objectives

In light of the problems discussed above, this research aims to develop innovative, low-cost, and non-intrusive sensing systems for monitoring the dynamic cutting forces and torque in single-point cutting processes, specifically turning and boring, and to evaluate the performance of several computationally efficient chatter detection algorithms suitable for embedded application. The specific objectives of this research are:

1. Develop quantitative physics-based measurement system models for PVDF sensing of dynamic forces in turning and dynamic torque in boring processes.

2. Demonstrate robust, on-line measurement of the dynamic cutting forces and torques in turning and boring, respectively, using the PVDF sensors and measurement system models developed in this thesis.
3. Establish efficient turning and boring chatter detection methods suitable for implementation in high speed embedded electronic platforms.

The research objectives of this thesis are accomplished through a comprehensive literature review of prior work followed by design, analysis, and rigorous experimental validation of the proposed approaches.

## Proposed Approach

The overall approach for process monitoring of turning and boring processes is shown in Figure 1. The cutting forces and torque in turning and boring, respectively, elastically deform the cutting tool. The PVDF piezoelectric thin film sensor rosette measures the dynamic strains produced in the tool at the location of the sensor and converts the strains to cutting forces/torque using physics-based measurement system models developed in this thesis. The sensed signals are then processed by the embedded microcontroller-based electronics using algorithms developed in this thesis to detect the onset of chatter before chatter marks occur on the workpiece. If chatter alarm is issued by the monitoring system, corrective action can be taken by the machine tool controller but, for certain environments, simply recording the alert can be sufficient.

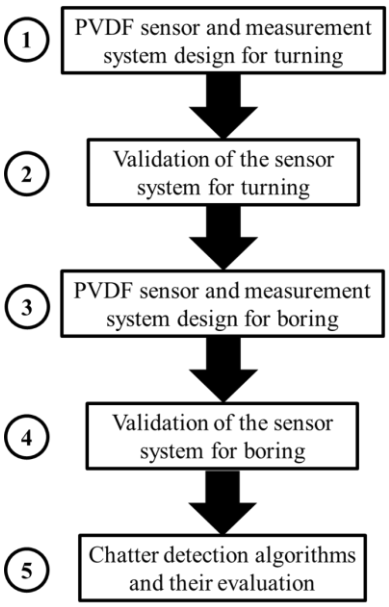


Figure 1. Overall approach.

## Thesis Outline

The remainder of this thesis is organized as follows. Chapter 2 presents a comprehensive review of prior work and existing external sensor-based technologies. Chapter 3 introduces a novel PVDF piezoelectric strain sensor based method for monitoring dynamic feed, radial, and tangential forces in turning and its experimental validation. Chapter 4 introduces a simplified PVDF piezoelectric strain sensor configuration for monitoring the dynamic torque in boring and its experimental evaluation. Chapter 5 discusses various mathematical algorithms for on-line chatter detection and experimental evaluation of the proposed methods. Finally, the conclusions and future recommendations of this work are given in Chapter 6.

# CHAPTER 2

# LITERATURE REVIEW

A literature review of prior research is presented in this chapter. The review is divided into four sections: 1) developments in monitoring of machining processes with an emphasis on single-point cutting, 2) a more specific overview of monitoring of cutting forces in single-point cutting, 3) PVDF sensor based applications, 4) on-line algorithms for chatter detection in single-point cutting processes.

## Machining Process Monitoring

Monitoring of the machining process is vital to the success of automated manufacturing. The topic has been extensively investigated by researchers [3, 16, 17]. A variety of sensors including microelectromechanical systems (MEMS) accelerometers [18], acoustic emission sensors [19], thin film strain gauges [20, 21], and thermocouples [22, 23] have been used for monitoring machining processes including milling, drilling, turning, grinding, lapping, and chemical mechanical processing. However, several challenges related to practical implementation of such sensing technology still remain [3]. Because machining is performed with a wide variety of cutting tools, part geometries and materials, and cutting conditions, the sensor packaging and their corresponding algorithms must be robust and adaptable to changes in all possible variables. In addition, use of sensors incurs additional cost and maintenance. The machine characterization from the sensor information must be checked, relayed to a network or computer, and then the appropriate action must be taken. Figure 2 shows the major steps involved in an automated process. Each arrow in the process represents a physical connection in the loop (e.g. wire). As a result, from an implementation standpoint, sensors are often viewed as expensive, inefficient, and inaccurate when compared to the alternative of a trained operator.

Therefore, low-cost, nonintrusive, wireless sensors have emerged as a promising candidate for machining process monitoring.

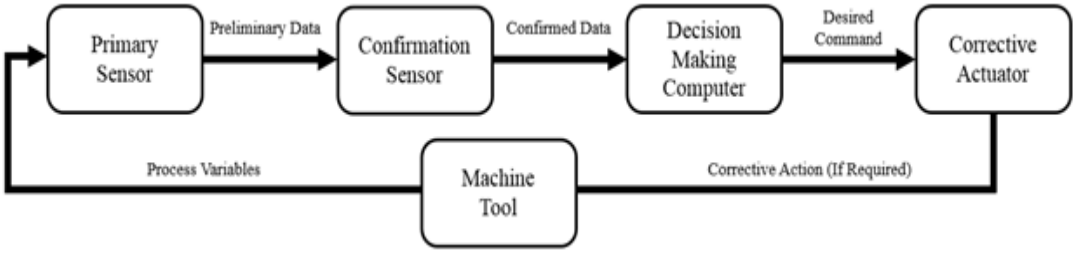


Figure 2. Example of an automated process monitoring chain.

Recently, the application of embedded and wireless sensing in machining has attracted the interest of the research community as a way to implement nonintrusive yet robust sensing systems. Several researchers [24-26] have identified and evaluated wireless monitoring system requirements and potential faults for implementation of wireless standards in turning applications in production environments. Even though researchers continue to investigate the integration of wireless capability into the factory system architecture [27-30], sensors that exploit the flexibility of the wireless standard must also be implemented in order to fully realize machining process monitoring.

Wireless and embedded sensing have been previously demonstrated for the collection of temperature, vibration, sound, and force data. Ho, et al. [31] developed a wireless cutting temperature data acquisition system for the turning process using a standard thermocouple coupled with Bluetooth transmission. Several researchers [32-34] demonstrated the applicability of thermal sensors embedded in the spindle or under the rake face of the tool. However, temperature data cannot be easily correlated to other machining process events such as chatter or tool breakage. Aruväli, et al. [35] used a solid state MEMS accelerometer attached to the carriage of a lathe to correlate vibration data with machine tool faults. Work done by [36] and [18] used a wireless piezoelectric

vibration sensing system and a MEMS accelerometer to detect tool wear. However, accelerometers are susceptible to transients unrelated to the cutting process such as table rapid decelerations and tool carriage rotations. Acoustic emission sensors embedded in the tool [37, 38] and utilizing a Doppler radar [39] have been demonstrated for monitoring tool wear. Unfortunately, acoustic emission sensors have not been studied in surroundings resembling a production environment and are susceptible to background noise emitted from sources including nearby machines. Though filtering techniques exist to filter normally distributed acoustic background noise, strong harmonics (e.g. another machine chattering nearby) are more difficult to isolate and physically identify when the source is unknown. Among the large number of machining process variables, cutting forces are of practical significance since they can be used as a robust proxy for the detection of tool breakage, wear, and self-excited vibrations [3, 4]. Cutting forces are directly related to physics-based modeling of machining process, and are therefore the most robust and accurate parameter for machining process monitoring.

### Monitoring of Cutting Forces in Single Point Cutting

Current state-of-the-art for accurate measurement of forces in single-point cutting consists of platform-type quartz-based piezoelectric force dynamometers [40]. These types of sensors exhibit the high sensitivity and sensor frequency bandwidth required for the collection of single-point cutting force data. However, they suffer from several limitations including 1) the sensors used to robustly acquire data for processing are costly (such as piezoelectric microphones and quartz-based dynamometers), 2) the chatter detection algorithms fail to consider various events or machine tool setups that can change the signal's behavior, such as tool breakage, changing cutting parameters, pre-existing workpiece geometric discontinuities (e.g., holes, steps, etc.), 3) the chatter monitoring methodologies cannot accommodate automated machine tool correction or practical data logging, and 4) the computing hardware used for signal acquisition and processing tend to

be intrusive and expensive. Many CNC machine tools are equipped with spindle power monitors that can be accessed via universal protocols such as MTConnect [41-43]. However, such access methods (e.g. measurement of spindle load and axis position) are primarily limited in machining process monitoring due to insufficient sampling rate required to detect chatter, which typically occurs at higher frequencies.

Researchers have developed and demonstrated innovative cutting force measurement systems in order to overcome the drawbacks of current state-of-the-art methods. Cutting force measurements by integrating force/torque sensors into the housing are an example of recent innovation [44-46]. These methods require special installation techniques that vary significantly from machine-to-machine and can be corrupted by inertial forces. Implementation of metal foil strain gauges for monitoring of forces in turning [20, 47, 48] and boring [49] have been demonstrated. Though strain gauges have proven to be sufficient for static cutting force measurements, these sensors suffer from the drawback of low resonant frequencies and DC excitation noise for dynamic cutting force measurements. Costly circuit and rosette design techniques are required to overcome such limitations. Researchers have attempted to supplement strain gauges with accelerometers to indirectly calculate the dynamic forces [20, 50], though such accelerometers still suffer from the limitations including susceptibility to inertia forces. Totis, et al. [51] developed an adaptable piezoelectric force ring for a mill-turn machine, but such sensors are cost-prohibitive. These drawbacks severely inhibit the practical implementation of on-line cutting force monitoring and emphasize the need for a flexible and low-cost dynamic force measurement system for single-point cutting processes such as turning and boring that can be implemented in an industrial environment.

## PVDF Based Sensing Applications

PVDF based piezoelectric strain sensors have been shown to be potential candidates for sensing applications where only the dynamic or quasistatic strain signals are of interest. An image of a typical PVDF sensor in comparison to a coin is reproduced in Figure 3.

Figure 3. Example picture of PVDF thin film sensor [52].

The PVDF polymer can be laminated onto a sheet of polyester, resulting in a very thin sensor film (~40 μm) [53]. PVDF's piezoelectric properties result in the sensor producing a charge when it is dynamically strained. The charge can then be converted to voltage using a charge amplifier. The voltage is measured by a DAQ (Data Acquisition), which can be correlated to the strain. PVDF's low thickness and high conformability (due to its flexibility) minimize its impact on the host structure's dynamics. This property is particularly important for mounting to host structures that have complex shapes or possess low stiffness. In addition, the PVDF polymer facilitates the decoupling of strain components in a general strain field due to its different strain sensitivities along its two in-plane axes. Instead of an external power supply, piezoelectric PVDF sensors require a charge amplifier circuit. Thus, the PVDF dynamic output voltage is independent of the supply voltage, making it ideal for adaptable remote sensing solutions. In addition, PVDF sensors are inexpensive (~$5 per sensor) when compared to state-of-the-art quartz-based piezoelectric dynamometers (~$30,000 without associated charge amplifier and cabling).

PVDF-based sensing has been demonstrated in multiple applications, thus showing flexibility not only in mounting, but also in implementation. PVDF-based dynamic force sensors have been demonstrated for fault detection in both metallic [15] and ceramic [11]

materials along with a large variety of biomedical applications [12-14]. For example, PVDF sensors were used for dynamic force sensing in microscale applications where MEMS-based sensors cannot be used because of their fragility and complex packaging [54-56]. In [57], PVDF was used in the form of a wire to isolate and measure the radial wall motions of a fluid-filled pipe. An exotic use of PVDF thin film sensing application is shown in [58], where a strip of PVDF was mounted on the outside of a shoe to measure dynamic dance movements. However, research involving the validation of PVDF-based sensors generally involve qualitative analysis [59, 60], and quantitative physics-based models relating dynamic strain to force while considering thermal effects are rare [61]. PVDF sensor-based monitoring applications have been recently demonstrated for force sensing in end milling [10, 62] and tool wear monitoring in face milling [63], where the cutting force signal is inherently dynamic.

### On-line Detection of Chatter in Single Point Cutting: Sensors and Algorithms

Various sensing methods have been proposed for the detection and quantification of chatter in single-point cutting. Along with appropriate sensitivity, an acceptable sensor must possess a wide flat band frequency response to detect the possible frequency range of chatter vibrations. Chatter frequencies can range from 100 Hz to as high as 4000 Hz [64]. Possible process signals for chatter detection include vibrations [65-83], force [67, 76, 80, 84-90], acoustic emission [70, 71, 76, 91-93], process induced optical response [87, 94], motor current [69], temperature [95], surface roughness [86, 95], and ultrasound waves [96]. Force, acceleration, acoustic emission, and spindle current/power are the most commonly used process signals for chatter detection in machining [64].

Accelerometers are commonly used for chatter detection due to their ease of mounting and wide frequency response. However, piezoelectric accelerometers commonly used in machining vibrations research are costly, although cheaper MEMS accelerometers have been used for chatter detection in milling processes [18, 97, 98]. However, in the

context of chatter detection, accelerometers cannot easily isolate the location of the vibrations of the entire structure whether or not such vibrations are the result of dynamic instability. Thus, the chatter signal to noise ratio can be low for inexpensive accelerometers, especially when attempting to detect chatter in its incipient stage. Acoustic emission sensors are relatively non-intrusive to the machining process and have been used for real-time chatter detection in single-point cutting. However, acoustic sensors often require extensive signal processing to isolate the chatter signal from acoustic signals dependent on other process parameters [99]. In addition, most low-cost acoustic emission sensors do not yield a flat frequency response under 100 Hz. A typical frequency response of a MEMS microphone is shown in Figure 4. Monitoring of spindle motor current/power for chatter detection has been demonstrated not only for chatter detection in turning, but also in milling [100, 101]. Though the spindle electrical current offers a relatively simple and nonintrusive signal for chatter detection, the measurement parameter suffers from the drawback of narrow bandwidth. For example, Heidenhain has clearly specified frequency bandwidth limitations (no higher than 100 Hz) on their motor current based chatter suppression technology [102].

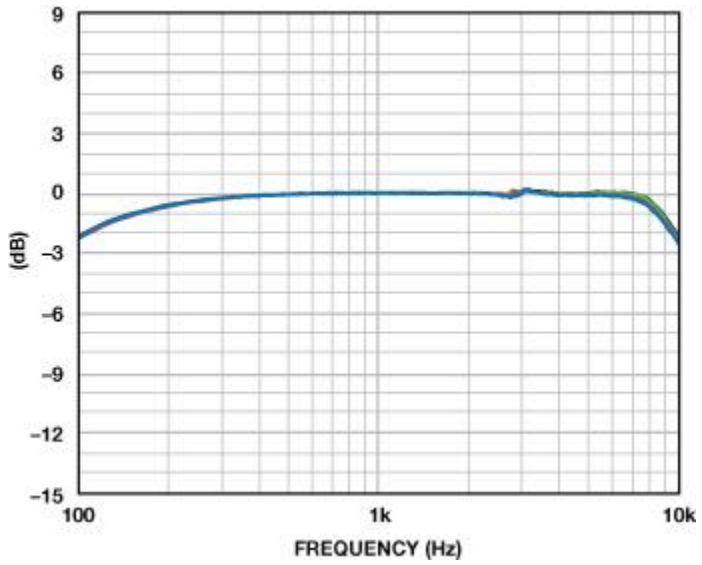


Figure 4. Frequency response of several MEMS microphones [103].

Vibrations associated with the machining process affect instantaneous chip thickness, which in turn affects cutting forces. Therefore, cutting force has been identified as a robust signal output by the machining process for detection of chatter due to its direct relationship with dynamic instability [2, 104, 105]. In addition, force and strain measurements can be used to isolate and amplify the chatter signal in the location/direction of interest [61]. However, measurement of cutting force with the desired bandwidth and sensitivity for detection of the onset of chatter requires can be expensive and intrusive (e.g., piezoelectric force dynamometers). Thus, the use of a low-cost thin-Film PVDF strain sensor for chatter detection through the measurement of the dynamic cutting force signal is proposed in this thesis. When the PVDF sensor is attached to the tool shank, a high signal to noise ratio (SNR) can be achieved due to the reduced direct signal transmission path between the sensor and the cutting zone. In addition, as shown by Ma, et al. [61] PVDF sensors can be configured into rosettes to isolate the strain/force component of interest. However, a chatter detection algorithm is still required.

Ideally, a chatter detection algorithm should be designed to enable automated real-time machine tool correction, but in certain environments, simply detecting the onset of dynamic instability can be sufficient to prevent irreparable damage to the workpiece and/or the machine tool system. Chatter detection algorithms have been developed for both milling and single-point cutting, although the force signals in the two processes are inherently different. While milling cutting force signals are largely dominated by tooth passing frequency dependent harmonics [106-109], single-point cutting force signals resemble dynamic noise about a static mean [2, 21] in the simplest case. In addition, single-point cutting force signals can also contain spindle speed dependent harmonics along with nonstationary features due to complex toolpaths, continuously varying cutting process parameters (such as continuously varying spindle speed to ensure constant surface speed in a face turning operation), and preexisting discontinuities in the workpiece geometry (e.g.

holes, slots, etc.). Thus, certain assumptions used in milling chatter detection algorithms, such as constant harmonics [110-113], cannot be made in single-point cutting. Note that while Suprock, et al. [114] compensated for changing spindle harmonics through the use of multiple bandpass filters over time as the center frequency varies, the technique works best when using real-time spindle speed measurements, thus inducing a significant lag between the real and theoretical values.

Algorithms developed for chatter detection in milling processes are not examined in this review for the reasons mentioned previously. However, chatter detection algorithms that have demonstrated applicability to both milling and single-point cutting are examined. Prior work on chatter detection algorithms for single-point cutting generally apply three types of signal processing methods, including (i) statistical analysis on time domain data [65, 66, 69, 71-73, 84, 85, 90, 115], (ii) spectral decomposition based analysis including Fourier transform and wavelet transform [67, 68, 76, 77, 80, 82, 87, 94, 116], and (iii) machine learning techniques such as Artificial Neural Networks (ANN) and support vector machines [78, 81, 89, 95, 96, 117].

An interesting method for detecting chatter in turning processes involves processing multiple sensor signals. Calculation of the coherence function between two sensor signals, as reported in [71, 72], has shown promise due to its normalization capability, thus reducing susceptibility to variations in the cutting conditions. Elias, et al. [69] demonstrated the use of Cross-Recurrence Quantification Analysis (CRQA) as a method for combining statistical time series data from multiple sensors and examining the change in CRQA parameters as an indication of chatter. However, increasing the number of sensors also increases the cost, thus limiting its wide-scale use.

Artificial Neural Networks have been shown as a promising technique for early detection of chatter. ANNs are a type of machine learning algorithm that assigns weights to inputs (neurons) based on their correlation to an output state of the system. Thus, as more inputs are fed to the network, the weights adapt and the algorithm is trained. ANNs

have been successfully demonstrated for epileptic seizure detection [118-121] and bearing fault detection [122-124]. However, chatter detection methods based on machine learning algorithms suffer from the drawback that extensive training and classification is required.

A reason for the failure to implement on-line chatter detection methods is a lack of robustness of the existing methods to process variations encountered in a production environment. Generally, algorithms are developed and validated in a laboratory setting, where the effect of some of the process variables is assumed to be negligible. In addition, the algorithms are validated for very simple machining cases, which are not representative of production applications. For example, some algorithms are successfully validated with toolpaths that slowly increase the depth of cut [5, 85]. These algorithms do not consider robustness against pre-existing workpiece geometric discontinuities such as steps, predrilled holes, etc., which can trigger false alarms. From a signal shape perspective, these geometric discontinuities act as nonlinearities and produce non-stationary signals. To compensate for these geometric variations, some of the previously mentioned algorithms require system identification prior to on-line implementation. This limits algorithm flexibility since each individual setup needs to be experimentally characterized.

One of the most significant barriers to on-line chatter detection is the computational cost. Though low-cost, non-intrusive machine tool sensing systems have been demonstrated, the hardware for processing the sensor output relies on off-the-shelf personal computers. Such computing platforms tend to be bulky and costly compared to the sensors used. In an experimental/research setting, such validation is appropriate, but some algorithms tested with a computer system cannot be practically implemented on a microcontroller-based embedded system, which has limited memory and processing speed. An ideal chatter detection system is one that executes the algorithm computation on an embedded processor due to its flexibility and low-cost. A proposed low-cost, nonintrusive embedded chatter detection system will be presented in this thesis along with computational criteria for embedding the algorithm into a microcontroller.

## Summary

It can be deduced from the literature survey presented in this chapter that existing methods for monitoring the cutting force and/or torque in single-point cutting processes are intrusive, prohibitively expensive, possess limited bandwidth, or are dependent on the workpiece material. Therefore, low-cost PVDF sensors are a promising candidate for dynamic cutting force. In addition, the reported methods for on-line chatter detection suffer from at least one of the following drawbacks: 1) possible sensitivity to transient events in machining other than chatter vibrations, 2) high memory requirement, and 3) high computational cost. To promote widespread adoption of chatter recognition monitoring, it is proposed that chatter algorithms be designed to overcome the foregoing drawbacks and have the memory and computational efficiency required for implementation in embedded systems instead of on off-the-shelf personal computers.

# CHAPTER 3

# PVDF SENSOR BASED DYNAMIC CUTTING FORCE MEASUREMENT IN TURNING

## Introduction

In this chapter, novel PVDF-based strain sensor-based methods for measuring the dynamic force components in the feed, radial, and tangential directions in the turning process are presented. In the following sections of this chapter, the overall dynamic force sensing methodology and approach are described, followed by experimental validation, discussion of results and conclusions.

## Turning Force Measurement System Modeling

This section describes the force measurement system for turning. Consider the schematic shown in Figure 5. The PVDF sensor(s) glued to the tool shank is (are) wired to the piezoelectric and anti-aliasing signal conditioning electronics, which are in turn wired to a data logging unit. The dynamic cutting forces acting on the insert elastically deform the tool shank. The dynamic elastic strains generated in the host structure at the PVDF sensor location then produce electric charges at the electrodes due to the piezoelectric effect.

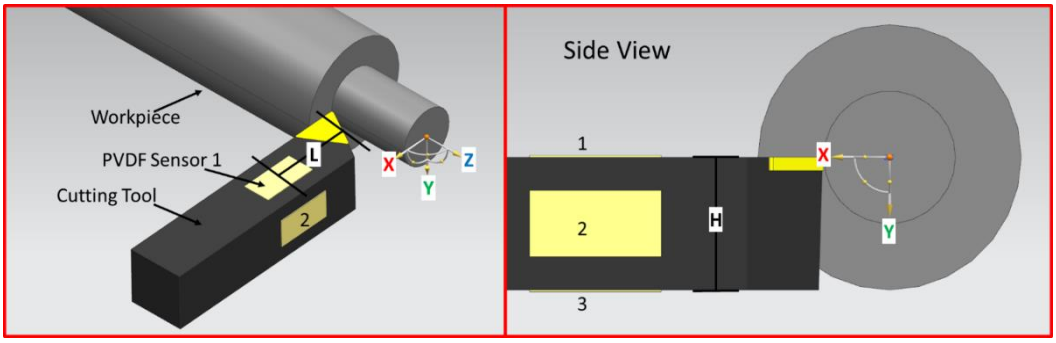


Figure 5. PVDF rosette configuration for outer diameter turning.

The charges are then converted into voltage signals using a charge amplifier. The voltage signal is processed by an anti-aliasing filter before being read by a data acquisition unit. The general signal flow for both turning and boring is shown in Figure 6.

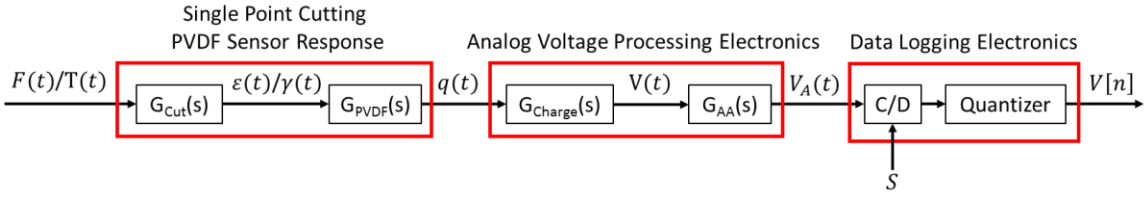


Figure 6. Signal flow for single-point cutting force measurement system.

In Figure 6, $F(t)$, $T(t)$, $\varepsilon(t)$, $\gamma(t)$, $q(t)$, $V(t)$, $V_A(t)$, $V[n]$, and S denote the dynamic cutting force component, the dynamic cutting torque, PVDF bending strain response, PVDF torsional shear strain response, charge generated at the sensor electrodes, voltage signal output by the charge amplifier, voltage signal output by the anti-aliasing filter, digital voltage samples collected by the data logging unit, and the sampling period, respectively. Between turning and boring, $G_{Cut}(s)$ and $G_{PVDF}(s)$ will differ while the rest of the signal flow remains the same. Note that $T(t)$ and $\gamma(t)$ relate to the boring process described in the following chapter. $F(t)$ and $\varepsilon(t)$ correspond to turning processes, and the derivation for these parameters will be described in this section.

Dynamic strains experienced by the turning tool are measured by the PVDF sensor rosette and used to calculate the dynamic force component of interest. Figure 5 illustrates the strain gauge rosette used to measure the dynamic force components in the radial (X), feed (Z), and tangential (Y) directions using PVDF sensors at location $i$ ($i = 1,2,3$).

In the following derivation, it is assumed that the cutting forces can be approximated as three point loads acting at a location equal to half the radial depth of cut measured from the free end of the tool, though in reality the forces are distributed across the tool-workpiece contact. To obtain the tangential dynamic force component ($F_y$), only one PVDF sensor ($i = 1$) is needed if the axial and torsional strains are assumed to be negligible compared to the bending strain. It is also assumed that the small strain theory of elasticity is applicable. These assumptions can also be applied to obtain the dynamic feed force ($F_z$) with PVDF sensor $i = 2$. Note that the following derivation of the relationship between the measured dynamic strain and the dynamic force component is for the dynamic tangential force component. The derivation approach is identical for the dynamic feed force component. The derivation for the dynamic radial force ($F_x$) is presented later.

Treating the tool as a cantilever beam with square cross-section clamped in the tool holder, the bending strain generated in the tool at the location of the PVDF sensor $i = 1$ can be found using the standard bending formula

$$\varepsilon_1 = \frac{F_y L H}{2 E_t I_{zz}} = \frac{6 F_y L}{E_t H^3} \tag{1}$$

where $L$ is the distance between the center of the PVDF sensor and $F_y$, $H$ is the cross sectional height of the tool, $E_t$ is the Young's Modulus of the tool, and $I_{zz}$ is the area moment of inertia. It was shown by Ma, et al. [61] that the axial strain is usually 1-2 orders of magnitude lower than the bending strain given by Eq. (1). Using the derivation of PVDF charge output for a single PVDF sensor formulated by Ma, et al. [61], and assuming the

pyroelectric effect is negligible, the general charge output of the PVDF sensor configuration shown in Figure 7 can be written as

$$q = \frac{\int [\varepsilon_1 (d_{31} E_1 + \upsilon_{12} d_{32} E_2) + \varepsilon_2 (d_{32} E_2 + \upsilon_{21} d_{31} E_1)] dA_3}{1 - \upsilon_{21} \upsilon_{12}} \quad (2)$$

where $d_{ij}$ is the piezoelectric modulus relating the electric displacement along axis $i$ to the mechanical stress along axis $j$ (all axes are shown in Figure 7), $\upsilon_{ij}$ is the Poisson's ratio of the PVDF sensor material and represents the contribution of the normal strain along axis $i$ to the normal strain along axis $j$, $E_i$ is the Young's modulus of the PVDF sensor along axis $i$. Note that while Figure 7 shows the PVDF sensor to be flat, the model studies the change in deformation from the sensor's initial state, which can be flat when attached to a square shank turning tool or curved on a cylindrical boring bar.

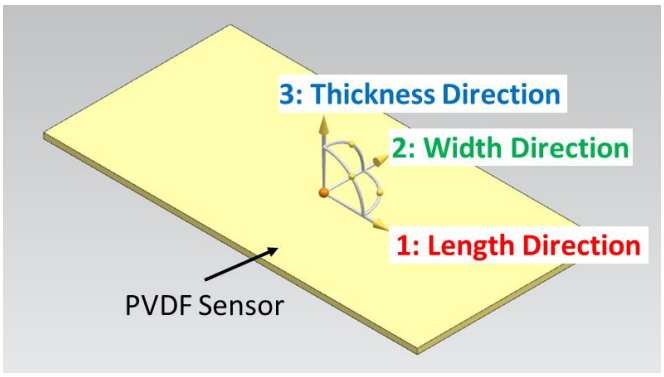


Figure 7. Schematic of a PVDF sensor element.

However, relating $\varepsilon_2$ to $\varepsilon_1$using the Poisson's ratio, assuming $d_{32} << d_{31}$ [125], and substituting Eq. (1) into Eq. (2) results in the following relation between the charge developed at the sensor location and the corresponding force component

$$q_1 = \frac{6LA_3[d_{31}E_1(1-\upsilon_t\upsilon_{21})]}{E_t{H_y}^3(1-\upsilon_{21}\upsilon_{12})}F_y \tag{3}$$

where $\upsilon_t$ is the host structure's Poisson's ratio. Because the PVDF sensor is mounted parallel to the tool's longitudinal axis and is therefore not sensitive to in-plane shear strains, Eq. (3) can be used to solve for $q_2$, which in turn can be used to determine the dynamic feed force, $F_z$.

To determine the dynamic radial force, $F_x$, the corresponding axial strain must be isolated. The axial strain is expressed as

$$\varepsilon_a = \frac{F_x}{E_t H^2} \tag{4}$$

Instead of using the configuration developed by Ma, et al. [61], a simplified sensor configuration is proposed in Figure 5 to meet the sensor mounting (size) constraints of the turning tool holder. Using the PVDF sensors $i$ = 1, 3 to cancel the bending strains while assuming that the torsional strains are negligible, the total charge can be written as

$$q_A = q_1 + q_3 \tag{5}$$

Note that the addition notation is used because axes 3 of the sensors $i = 1, 3$ lie in opposite directions. Assuming that the same PVDF sensors are used (therefore, $d_{ij}$, $v_{ij}$, and $E_i$ are the same) and both sensors experience the same axial strain, substituting Eq. (2) and (4) into Eq. (5) yields the following equation relating charge output to the dynamic radial cutting force

$$q_A = \frac{2\varepsilon_a A_3[d_{31}E_1(1-\upsilon_t\upsilon_{21})]}{1-\upsilon_{21}\upsilon_{12}} = \frac{2A_3[d_{31}E_1(1-\upsilon_t\upsilon_{21})]}{E_t H^2(1-\upsilon_{21}\upsilon_{12})}F_x \quad (6)$$

After relating the piezoelectric charge to the cutting forces in turning, a charge amplifier converts the charge to voltage, thus facilitating data acquisition by an A/D converter. The following section describes how this process relates to the PVDF model.

**Signal Flow Modeling**

The derivation of the remainder of the signal flow in Figure 6 can be used to relate the voltage to the dynamic force and dynamic torque for all the PVDF sensor configurations discussed in this thesis. In order to record the data electronically, the output charge is converted to voltage using a charge amplifier circuit. Therefore, the resulting voltage as a function of charge is expressed as

$$\mathrm{V(t)} = \frac{\mathrm{q}}{\mathrm{C_F}} \quad (7)$$

where $C_F$ is the capacitance in the charge amplifier feedback loop. The voltage signal is then processed by a low pass filter with a cutoff frequency of no more than half the sampling rate in order to mitigate the aliasing effect. The filtered signal is then read by a data acquisition unit, thus transforming the analog signal into the discrete domain with sample time $T$. Figure 8 illustrates the idealized frequency response of the measurement system. Note that the charge amplifier response is 0 at 0 Hz, and therefore, any frequencies lower than $f_1$ will be attenuated. Though the charge amplification circuitry depends on the electrical requirements, the general components that determine $f_1$ are the values pertaining to the feedback capacitors and resistors.

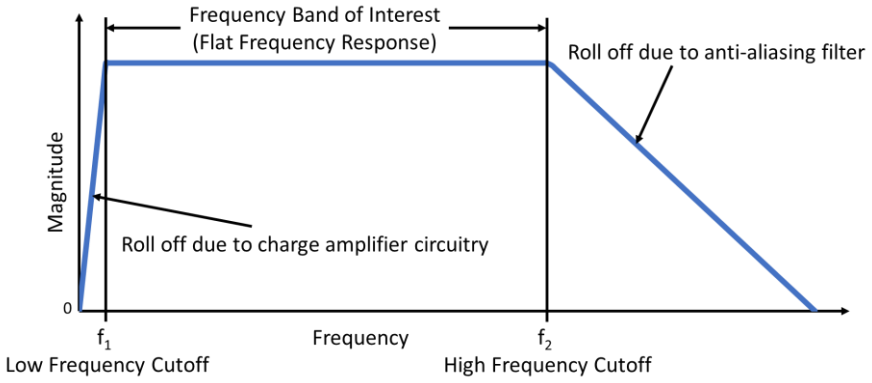


Figure 8. Example measurement system frequency response.

By substituting Eq. (7) into Eq. (3) and Eq. (6), $K_{Tan}$ and $K_{Rad}$ for turning can be written as

$$V = K_{Tan}F_y, \qquad K_{Tan} = \frac{6LA_3[d_{31}E_1(1-\upsilon_t\upsilon_{21})]}{C_F E_t {H_y}^3(1-\upsilon_{21}\upsilon_{12})} \tag{8}$$

$$V = K_{Rad}F_x, \qquad K_{Rad} = \frac{2A_3[d_{31}E_1(1-\upsilon_t\upsilon_{21})]}{E_t H^2(1-\upsilon_{21}\upsilon_{12})} \tag{9}$$

Note that Eq. (11) and Eq. (12) imply a linear relationship between the voltage output and force.

## Experimental Verification

A set of turning experiments were performed on Aluminum 6061 and AISI 1018 steel (Rockwell B70) to validate the PVDF measurement system. A Kistler 9257B 3-axis Force Component Dynamometer was used as the reference signal for comparison. Both signals were digitally recorded with a National Instruments cDAQ-9178 at a sampling rate of 12 KHz. The cut-off frequency of the PVDF signal charge amplifier was set to 7.24 Hz while the anti-aliasing filter was an 8-order low pass Bessel filter with a cut off frequency

of 5.5 KHz. A Bessel filter was chosen over a Butterworth filter to produce a linear phase response at the filter output.

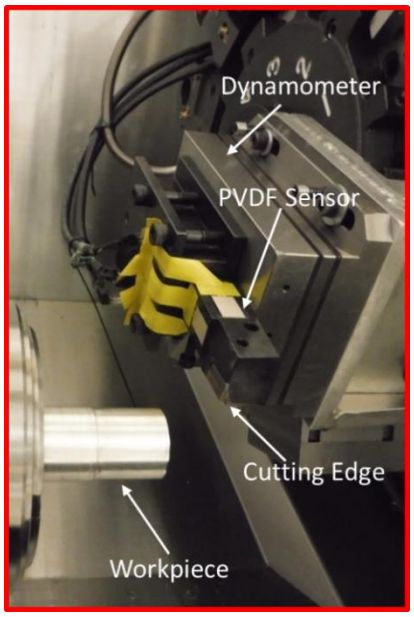


Figure 9. Force measurement setup for turning.

Because certain material and geometric constants are not known exactly, $K_{Tan}$ (which also corresponds to $K_{Feed}$ for the dynamic feed force component) and $K_{Rad}$ have to be calibrated. Note that since different host structures have different geometric and mechanical properties (e.g. cross-sectional area and Young's Modulus), the sensor configuration has to be recalibrated for different tools. The results of sensor calibration are shown in Table 1 for the outer diameter longitudinal turning tests. The length of cut in each test was 25.4 mm and was performed with a right hand turning tool (Valenite MTGNR-16-4D). All cuts were performed without coolant. Note that while other toolpaths and cutting tools were tested and will be discussed later, they were not used for sensor calibration.

Table 1. Cutting conditions for turning tests for sensor calibration.

| Test No. | Spindle Speed (RPM) | Cutting Speed (m/min) | Depth of Cut (mm) | Feed (mm) | Material | $K_{Tan}$ (mV/N) | $K_{Feed}$ (mV/N) | $K_{Rad}$ (mV/N) |
|---|---|---|---|---|---|---|---|---|
| 1 | 500 | 40 | 1.27 | 0.254 | AL 6061 | 2.89 | 2.49 | 4.33 |
| 2 | 1000 | 80 | 1.27 | 0.254 | AL 6061 | 3.15 | 2.65 | 4.18 |
| 3 | 2000 | 160 | 1.27 | 0.254 | AL 6061 | 3.06 | 2.75 | 5.08 |
| 4 | 2500 | 200 | 1.27 | 0.254 | AL 6061 | 2.78 | 2.69 | 4.65 |
| 5 | 1500 | 120 | 0.635 | 0.254 | AL 6061 | 3.02 | 2.12 | 2.96 |
| 6 | 1500 | 120 | 0.9525 | 0.254 | AL 6061 | 3.15 | 2.35 | 2.94 |
| 7 | 1500 | 120 | 1.5875 | 0.254 | AL 6061 | 2.41 | 3.01 | 5.24 |
| 8 | 1500 | 120 | 1.905 | 0.254 | AL 6061 | 3.19 | 2.69 | 5.10 |
| 9 | 1500 | 120 | 1.27 | 0.076 | AL 6061 | 3.03 | 3.68 | 3.00 |
| 10 | 1500 | 120 | 1.27 | 0.152 | AL 6061 | 3.09 | 3.05 | 5.03 |
| 11 | 1500 | 120 | 1.27 | 0.330 | AL 6061 | 2.76 | 2.81 | 5.21 |
| 12 | 1500 | 120 | 1.27 | 0.406 | AL 6061 | 2.89 | 2.45 | 3.70 |
| 13 | 1000 | 80 | 0.635 | 0.127 | ST 1018 | 2.92 | 2.79 | 3.24 |
| 14 | 1500 | 120 | 0.635 | 0.127 | ST 1018 | 2.98 | 3.57 | 3.18 |
| 15 | 2000 | 160 | 0.635 | 0.127 | ST 1018 | 2.59 | 2.34 | 2.99 |
| 16 | 1500 | 120 | 0.3175 | 0.127 | ST 1018 | 3.52 | 4.22 | 5.21 |
| 17 | 1500 | 120 | 0.9525 | 0.127 | ST 1018 | 3.08 | 2.75 | 3.86 |
| 18 | 1500 | 120 | 0.635 | 0.063 | ST 1018 | 2.72 | 3.10 | 4.18 |
| 19 | 1500 | 120 | 0.635 | 0.190 | ST 1018 | 3.28 | 2.05 | 3.22 |

The average values for $K_{Tan}$, $K_{Feed}$, and $K_{Rad}$ were determined to be 2.92 mV/N, 2.82 mV/N, and 4.07 mV/N, respectively. Figures 10 to 12 show representative results of the turning tests. Recall that the PVDF sensor can only measure the dynamic component of force and not the static component. Therefore, to permit comparison of the PVDF signal with the forces measured by the piezoelectric force dynamometer, all signals shown in the figures have been transformed to zero mean but the actual cutting forces measured by the piezoelectric force dynamometer vary about a non-zero static mean. Figures 10 and 11 show that for $F_y$ and $F_z$, respectively, the PVDF signals appear to match the dynamometer dynamic force signals quite well. Figure 12 shows the frequency decomposition of the measured dynamic force profiles presented in Figure 11. For comparison, the spectra are

normalized by the magnitude of the maximum frequency. At lower frequencies, the PVDF sensor and dynamometer reference signals are similar. This is because stable cutting frequencies detected by the sensors are a function of the spindle frequency, which is relatively low (25 Hz) compared to the sampling rate. However, the PVDF sensor frequency decomposition exhibits a particular harmonic (4688 Hz) that the dynamometer does not show. This could be due to the inherent differences in the frequency/electromagnetic circuitry characteristics of the dynamometer and cutting tool/PVDF sensor systems, specifically the electromagnetic interference resulting from lower quality shielding for the PVDF sensor system. The sensor-tool configuration frequency response from an impact hammer impulse width of 0.55ms is shown in the Appendix. Note that the frequency magnitude is approximately unity magnitude until the impact hammer frequency. Frequency response characteristics are presented in datasheets for the PVDF thin film sensor [9] and the cutting force dynamometer [40].

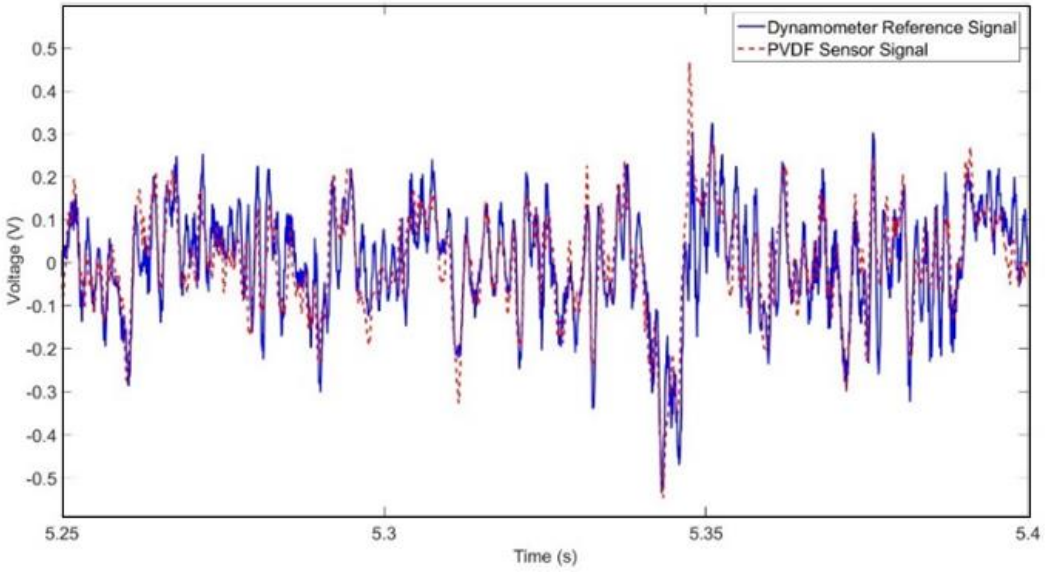


Figure 10. PVDF signal comparison with dynamometer for dynamic $F_y$ (Test 12).

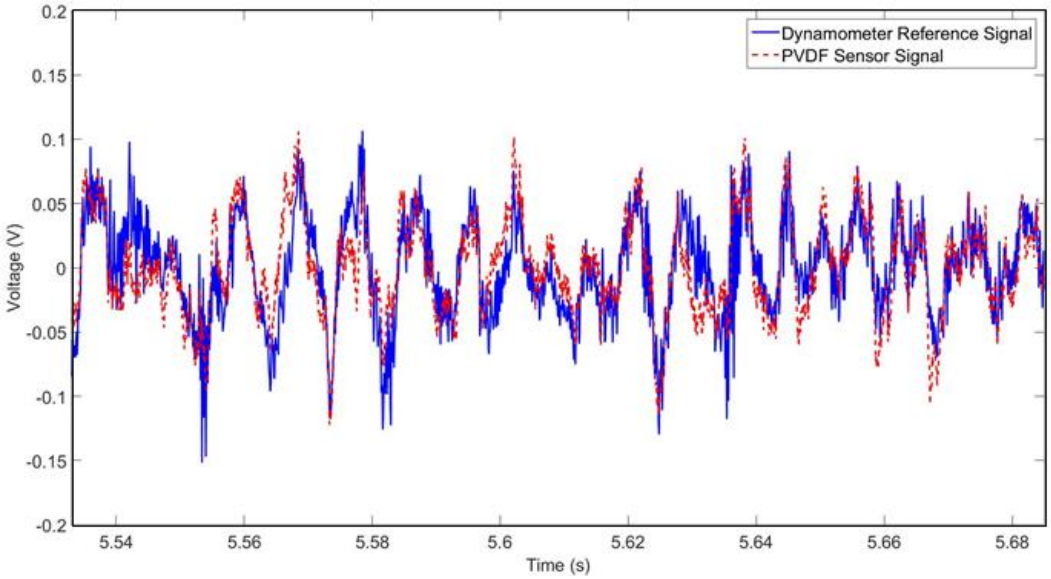


Figure 11. PVDF signal comparison with dynamometer for $F_z$ (Test 17).

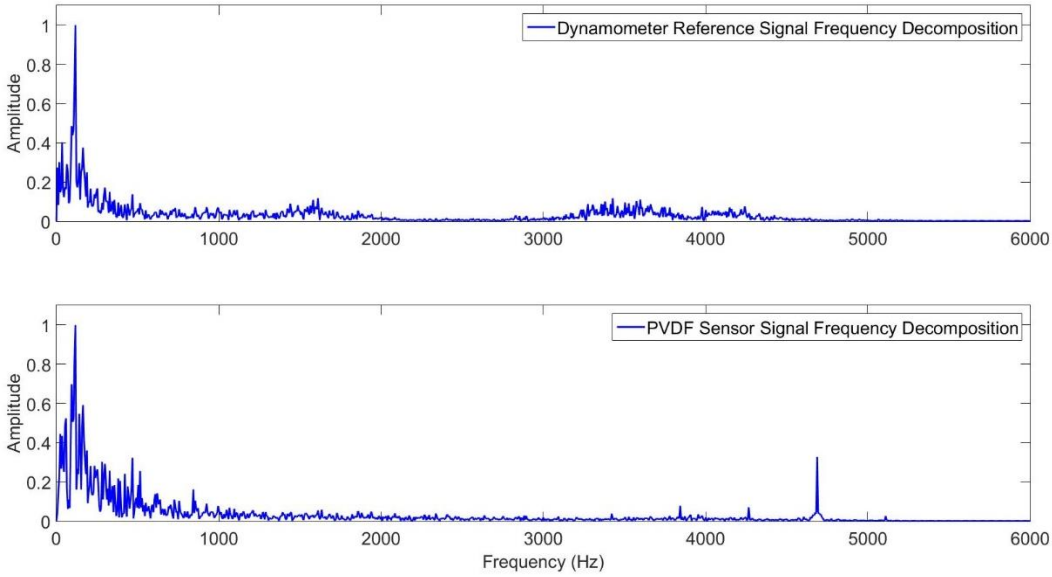


Figure 12. PVDF signal frequency decomposition comparison with dynamometer (Test 17).

The radial PVDF and dynamometer reference signals show some differences, as seen in Figure 13. In addition, the individual values for $K_{Rad}$ appear to vary much more in comparison to the other constants. This is because the point of contact between the right

hand turning tool and workpiece induces a torsional strain that is not cancelled by the configuration using two PVDF sensor, thus distorting the signal. Using the force data procured from experimentation, the torsional strain was determined to be ~45% of the axial strain. Special test cases were run to determine when the PVDF sensor data for the radial dynamic force is in better agreement with the Kistler dynamometer data.

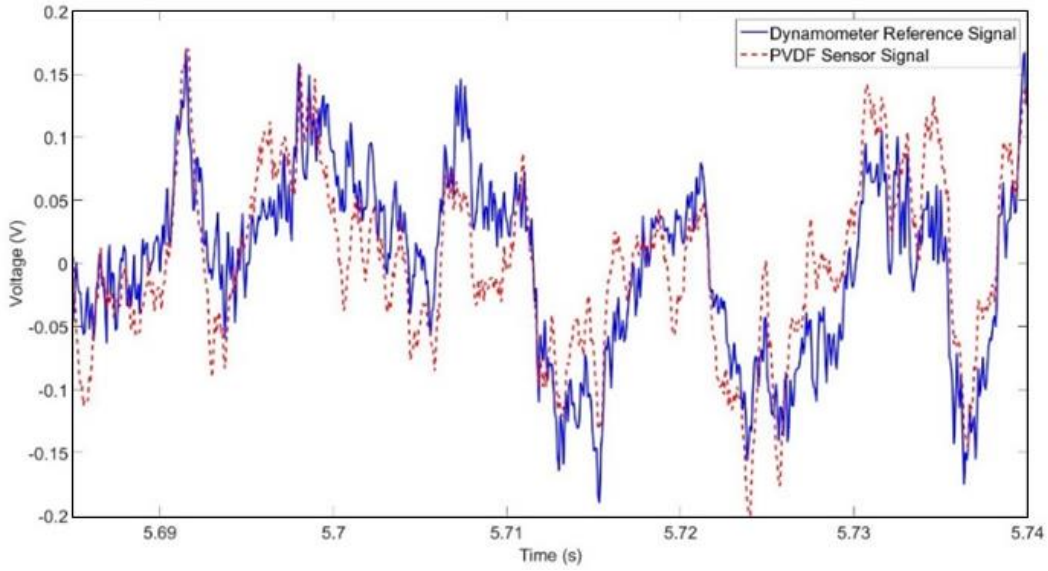


Figure 13. PVDF signal comparison with dynamometer for $F_x$ (Test 8).

Figure 14 shows the results for a facing operation. In this operation, the $F_x$ force matches more closely than in the previous tests. This is because, during the facing operation, the feed force is aligned with $F_x$, thus increasing the axial strain generated in the tool. Figure 15 shows the PVDF $F_x$ response for a straight longitudinal turning test performed using a threading tool (Kennametal DVVNN-163D) instead of the right-handed turning tool listed in Table 1. In this test, the responses are in better agreement because the force is concentrated closer to the axis of the tool, thus reducing the torsional strain. The harmonic response shown in Figure 15 was present in all the test cases with the threading

tool even though no chatter was observed. This response could be the result of the system being asymptotically stable (harmonics are present but do not grow).

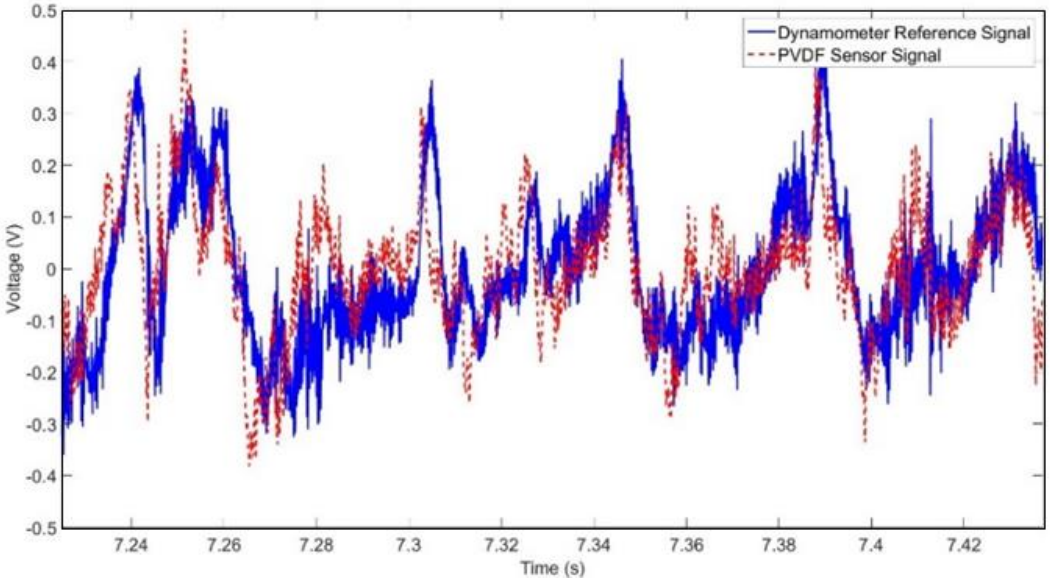


Figure 14. PVDF signal comparison with dynamometer for dynamic radial force component (Facing).

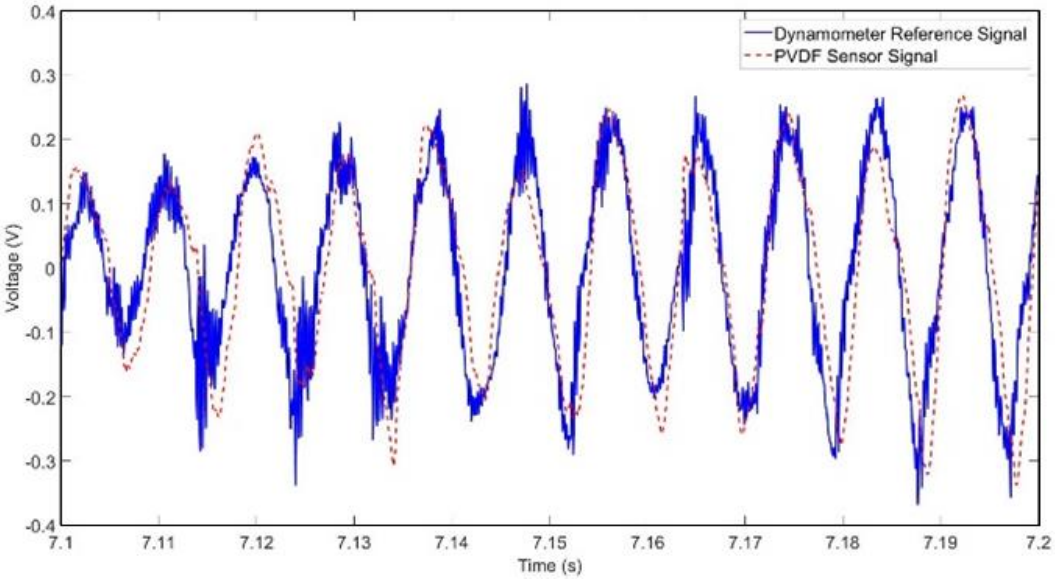


Figure 15. PVDF signal comparison with dynamometer for dynamic radial force component (Threading Tool).

## Summary

A novel, low cost and non-intrusive method for monitoring the dynamic components of the cutting forces in turning was proposed, designed and validated. The force monitoring methodology takes advantage of a low cost PVDF sensor, which yields a combination of high flexibility, low electromagnetic interference, wide bandwidth, high dynamic range, and high strain sensitivity along the different geometric axes of the sensing element. Physics based models have been developed to relate the charge produced by the PVDF sensor to dynamic cutting forces. PVDF signals were acquired using an in-house developed charge amplifier and a commercial DAQ. Though wireless functionality is not incorporated in the turning case, a wireless transmitter, implemented for the rotating boring bar in Chapter 4, can easily be adapted to the turning case. In addition, schematics for wireless PVDF-based monitoring of turning processes developed after the experiments described in this chapter is provided in the Appendix. The measured PVDF sensor signals were found to be in reasonably good agreement with those measured by the reference piezoelectric force dynamometer. For measuring the radial cutting force using a simplified dual sensor configuration, turning processes involving facing toolpaths and threading tools were identified to yield better agreement with the dynamometer-based reference signal. When the material constants of the cutting tool and the PVDF sensor are known, they can be used directly in Eqs. (8) and (9) to transform the PVDF sensor signals into cutting force signals independent of the machining parameters or workpiece material. In this case, no calibration is needed for the measurement system to function. However, in this work, because certain geometric constants are not known, the PVDF sensor signal was calibrated against the dynamometer force signal. The PVDF sensor cannot measure the static strain component in turning due to the inevitable charge decay at the sensor electrodes, but, if desired, the sensor can be supplemented with a standard metal foil strain gauge to obtain

the entire reference signal. Such a combination would alleviate the sensitivity requirements of the associated electronics, thus reducing cost. The PVDF sensor signal represents a slightly distorted version of the cutting force signal and is useful in applications where only the AC content of the cutting forces is of interest. If the exact shape of the dynamic force is not required, then the simplified rosettes can still be correlated with the machining responses of interest including tool wear, tool breakage, and chatter. The sensor and its associated electronics require more robust packaging in order to withstand external disturbances typically encountered in a production environment, including coolants and automatic tool changing.

# CHAPTER 4

# PVDF SENSOR BASED BORING TORQUE MEASUREMENT

## Introduction

In this chapter, a novel, PVDF-based sensor for measuring the dynamic torque acting on a boring tool are presented. In contrast to the work of Ma et al. [62], a simplified, two sensor configuration attached to the rotating boring bar is used to measure the dynamic cutting torque component. Other improvements over the work of [62] include demonstration of a real-time wireless transmitting device and an improved digital filter design that does not require the use of a recovery inverse-filter.

## Boring Torque Measurement System Modeling

Figure 16 shows the experimental setup for boring. For non-rotating boring tools mounted in a lathe, Eq. (3) and (6) can be used to obtain the corresponding forces. However, for rotating boring bars, particularly those used in a machining center, the dynamic torque is of interest. As with the turning case, the PVDF sensors glued to the tool shank are wired to the piezoelectric and anti-aliasing signal conditioning electronics designed and built in-house, which are in turn wired to a data logging unit. Note that this section describes how $T(t)$ and $\gamma(t)$ depicted in Figure 6 are related to the boring process, and provides their derivation.

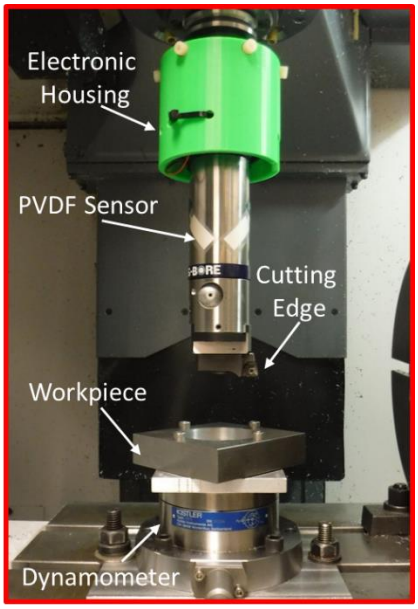


Figure 16. Force measurement setup for boring.

Using the torsion formula, the shear strain $\gamma$ produced in the boring bar can be related to the dynamic boring torque as

$$\gamma = \frac{D}{2GI_p}T = \frac{16}{\pi GD^3}T \tag{10}$$

where $D$ is the diameter of the boring bar, $G$ is the shear modulus of the boring bar, $I_p$ is the polar moment of inertia, and $T$ is the dynamic cutting torque. In contrast to the four PVDF sensor model used by Ma et al. [62], a model using two PVDF sensors in the configuration shown in Figure 17 is proposed. Though most boring bars are large enough to support the four PVDF sensor configurations, using two sensors reduces the circuit complexity and the computational error stack-up.

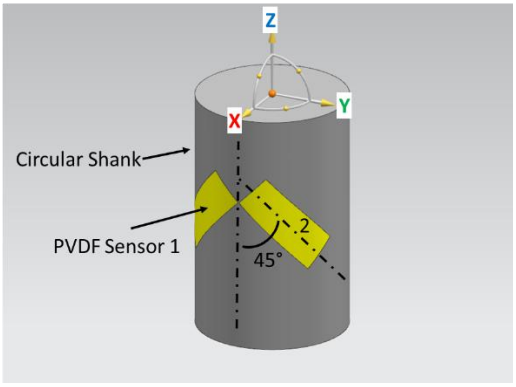


Figure 17. PVDF rosette configuration for a boring tool.

In this configuration, subtracting $\varepsilon_{1/2,1}$ and $\varepsilon_{1/2,2}$ cancels the axial and thermal strains experienced by the host structure. The shear strain $\gamma$ can be found from $\varepsilon_{1/2,i}$ using the following expression derived from Mohr's Circle

$$\varepsilon_{1,1} = \varepsilon_{2,2} = \frac{\gamma}{2} + \alpha_1 \Delta T$$
$$\varepsilon_{1,2} = \varepsilon_{2,1} = -\frac{\gamma}{2} + \alpha_1 \Delta T \tag{11}$$

Therefore, subtracting $q_2$ from $q_1$ using Eq. (2) and making similar assumptions about $d_{32}$ as in the case of the turning tool, the charge output of the torque PVDF sensor configuration can be written as

$$q_T = \frac{16A_3[E_1 d_{31}(1 - v_{21})]}{\pi G D^3 (1 - v_{21} v_{12})} T \tag{12}$$

However, a key assumption in the derivation of Eq. (12) is that bending strains produced in the boring bar are negligible. While this assumption is applicable for multi-insert boring tools, a single insert boring bar was used in this thesis to test its validity.

Therefore, it is expected that the PVDF torque signal from the single insert boring bar will experience some distortion due to the bending strains.

## Signal Flow Modeling

The derivation of the rest of the PVDF-based boring dynamic torque measurement model follows the same steps as for the turning model presented earlier provided a charge amplifier and anti-alias filter are used as shown in Figure 6. Under these conditions the PVDF-based boring dynamic torque measurement system also exhibits the same frequency characteristics as shown in Figure 8. As in turning, the material and geometric constants can be combined into a singular constant $K_T$ relating voltage to the torque by substituting Eq. (12) into Eq. (7). This results in the following formula

$$V = K_T T, \qquad K_T = \frac{16A_3[E_1 d_{31}(1-\upsilon_{21})]}{C_F \pi G D^3 (1-\upsilon_{21}\upsilon_{12})} \tag{13}$$

## Experimental Verification

To validate the PVDF measurement system for boring, a set of boring tests were performed. A Kistler 9272 drilling force dynamometer was used to provide a reference signal for the cutting torque. Similar to the turning experiments, the dynamometer signal was recorded by a National Instruments cDAQ-9178 at a sampling rate of 12 KHz. The PVDF signal was sampled by a MK20DX256VLH7 microcontroller with 16-bit resolution. For real-time wireless communication, a RN41 Bluetooth transmitter (IEEE Standard 802.15.1) was used to communicate with a corresponding RN41 Bluetooth receiver connected to a laptop. The PVDF wireless transmission electronics were attached to a 3D printed housing that was concentrically mounted to the boring bar. Though the MK20DX256VLH7 can sample faster than 400 KHz, the RN41 could only send data at 13 KHz without significant packet loss. Therefore, the sampling rate for the PVDF signal was 13 KHz, while the charge amplifier cutoff was configured to be 7.24 Hz and the anti-

aliasing low pass cutoff was 5.5 KHz. Figure 18 shows the electronic data logging equipment used for experimental validation.

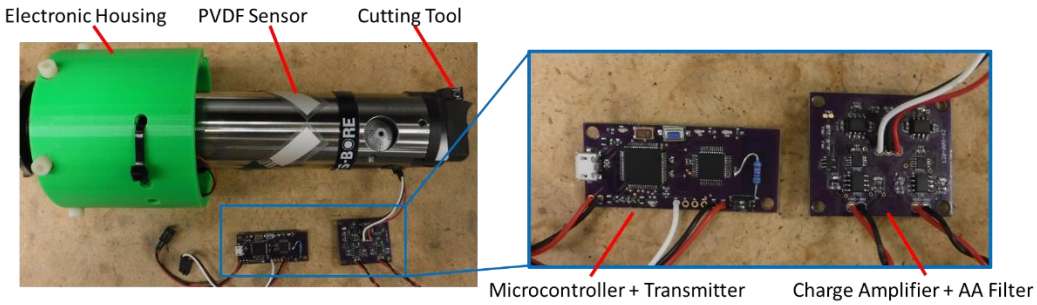


Figure 18. Data logging equipment for boring sensor validation.

For all boring experiments, the PVDF sensors were adhesively bonded to a 50 mm body diameter by 280 mm projection length single insert boring head (ISCAR BHFI MB16-MB50). The length of cut was 5.08 mm. Table 2 shows the test conditions for experimental validation along with the empirically determined $K_T$ for each test. Tests 12-14 correspond to a unique workpiece geometry that will be described later. The average sensitivity was calculated to be 30.15 mV/Nm, which is ~10 times more sensitive than the PVDF rosette formulation tested by Ma et al. [62] for an equivalent shaft diameter and feedback capacitance.

Table 2. Cutting conditions for boring tests.

| Test No. | Spindle Speed (RPM) | Cutting Speed (m/min) | Radial Depth of Cut (mm) | Feed (mm) | Material | Intersecting Hole Geometry | $K_T$ (mV/Nm) |
|---|---|---|---|---|---|---|---|
| 1 | 120 | 15.5 | 1.78 | 5.08 | 1018 ST | No | 29.09 |
| 2 | 120 | 15.5 | 1.78 | 7.62 | 1018 ST | No | 30.58 |
| 3 | 120 | 15.5 | 1.78 | 2.54 | 1018 ST | No | 35.48 |
| 4 | 150 | 19.5 | 1.78 | 5.08 | 1018 ST | No | 30.10 |
| 5 | 135 | 17.4 | 1.78 | 5.08 | 1018 ST | No | 30.13 |
| 6 | 120 | 15.5 | 1.27 | 5.08 | 1018 ST | No | 29.35 |
| 7 | 120 | 15.5 | 2.29 | 5.08 | 1018 ST | No | 31.98 |
| 8 | 120 | 15.5 | 1.78 | 5.08 | AL 6061 | No | 28.70 |
| 9 | 120 | 15.5 | 1.78 | 7.62 | AL 6061 | No | 30.49 |
| 10 | 150 | 19.5 | 1.78 | 5.08 | AL 6061 | No | 29.11 |
| 11 | 120 | 15.5 | 2.29 | 5.08 | AL 6061 | No | 28.86 |
| 12 | 120 | 15.5 | 1.78 | 5.08 | 1018 ST | Yes | 27.70 |
| 13 | 150 | 19.5 | 1.78 | 5.08 | 1018 ST | Yes | 31.37 |
| 14 | 120 | 15.5 | 2.29 | 5.08 | 1018 ST | Yes | 29.13 |

Figures 17 to 19 show representative results of the dynamic torque comparison between the PVDF-based sensor system and the torque measured by the Kistler drilling dynamometer. Though the dynamic torques measured by the two methods are in reasonable agreement, they are not as good as the results shown in Figure 10 and Figure 11. The main reason for the observed discrepancy is the assumption of negligible bending strain. Using the thrust force from the dynamometer force data, the bending strain was calculated to be 35% of the torsional strain. An interesting point to note is that, when testing AL 6061, the workpiece/dynamometer assembly generated chatter vibrations, and the agreement between the PVDF and dynamometer signals was better, as shown in Figure 21. A comparison of the frequency decompositions for the data in Figure 21 is shown in Figure 22. As in turning, the harmonics tend to agree in the lower frequency range (<2000 Hz), and some disagreement is evident at the higher frequencies. During stable cutting, the dynamic force signals resemble Brownian noise in the frequency domain. Therefore, the

PVDF and dynamometer signals tended to agree more when the frequency distribution exhibited clear harmonics.

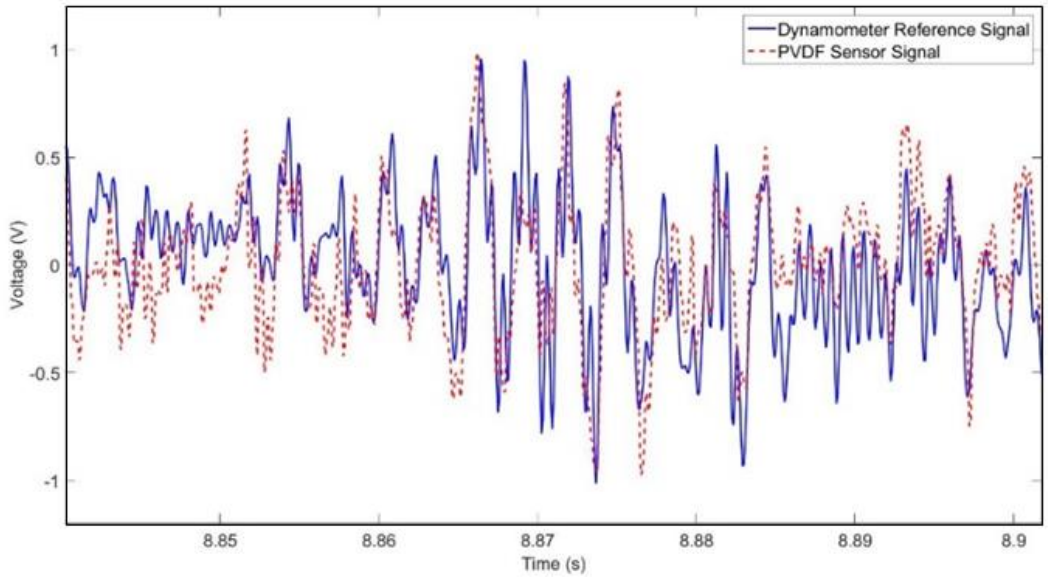


Figure 19. PVDF signal comparison with dynamometer dynamic torque component (Test 1).

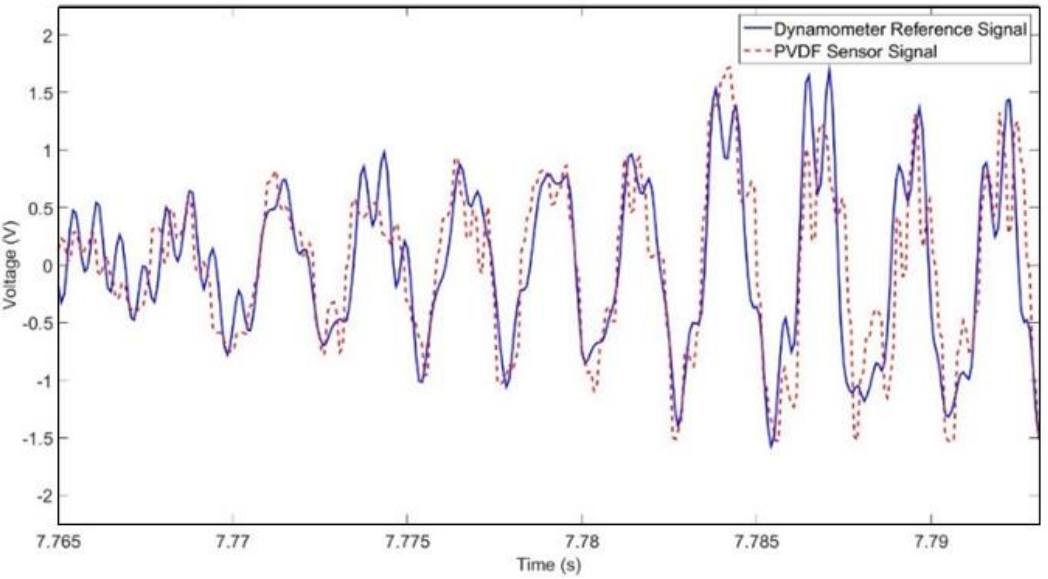


Figure 20. PVDF signal comparison with dynamometer dynamic torque component (Test 5).

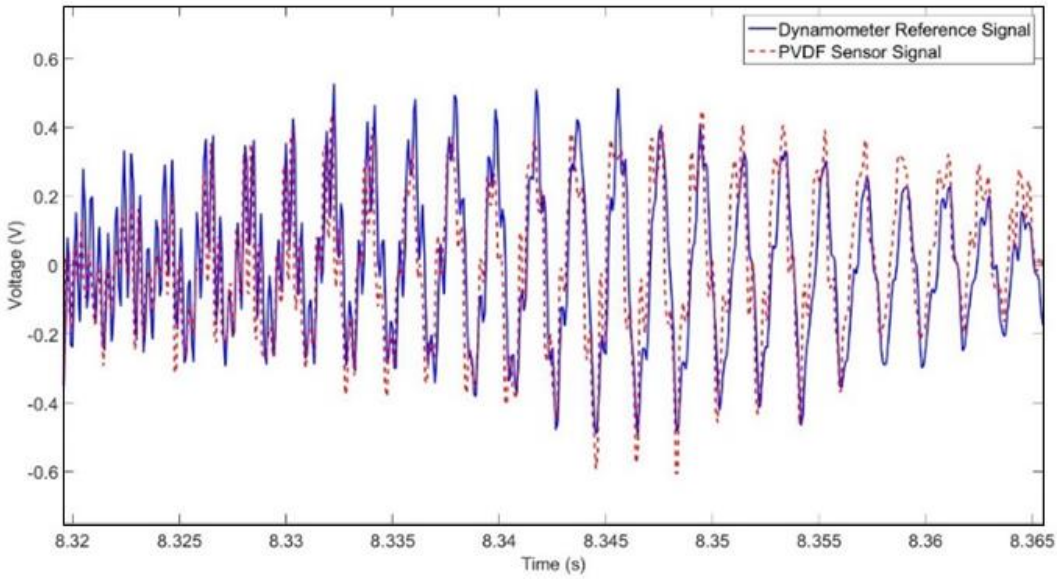


Figure 21. PVDF signal comparison with dynamometer dynamic torque component (Test 8).

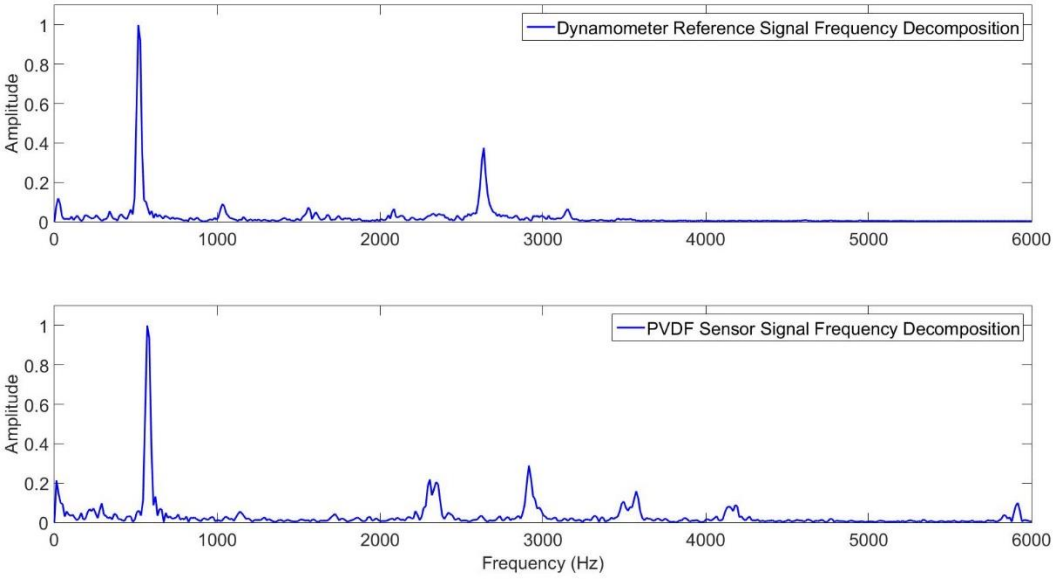


Figure 22. PVDF signal frequency decomposition comparison with dynamometer (Test 8).

In addition to the conventional hole enlargement experiments, another workpiece geometry shown in Figure 23 was tested. In this configuration, one of two intersecting holes is enlarged, thus introducing a harmonic at the spindle frequency so low (2 Hz) that

the PVDF sensor should not be able to detect it. During experimentation, it was indeed established that the PVDF sensor system does not capture such a low harmonic. However, Figure 24 shows that the PVDF dynamic measurement response still compares favorably with the dynamometer's response.

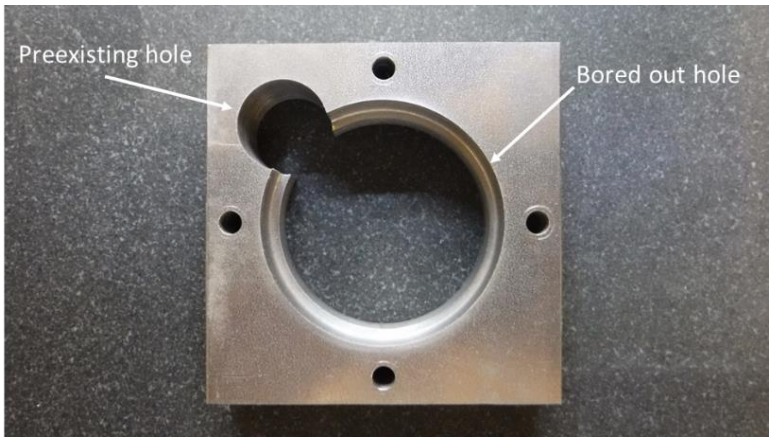


Figure 23. Intersecting hole condition.

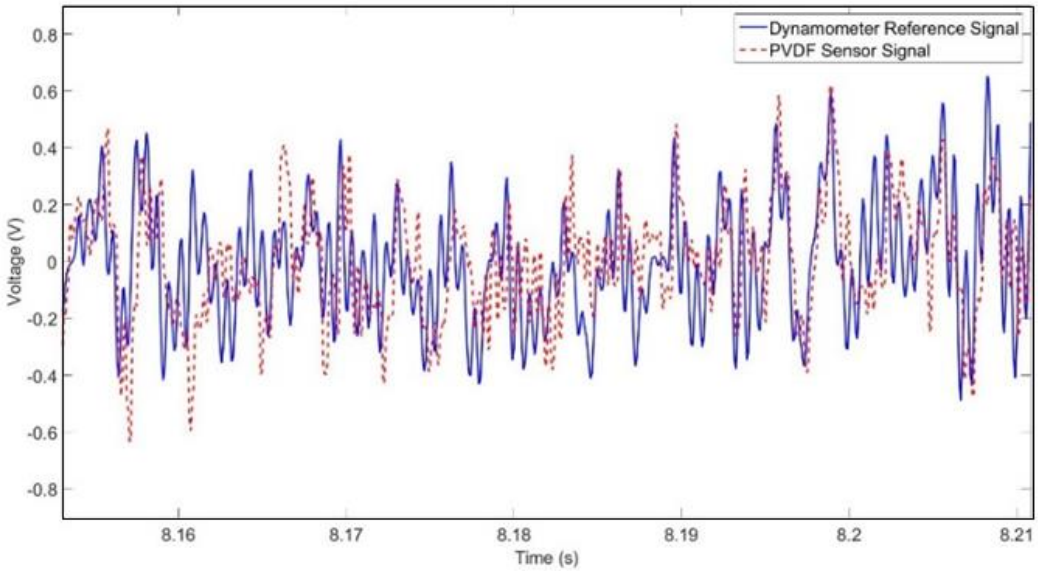


Figure 24. PVDF signal comparison with dynamometer dynamic torque component (Test 12).

## Summary

A novel, low cost and non-intrusive method for monitoring the cutting torque in the boring process has been proposed, designed and validated. Physics based models have been developed to relate charges produced by the simplified two PVDF sensor rosette to the dynamic cutting torque. A wireless data acquisition system, developed in-house, was used to measure the PVDF sensor signals. Experimental results showed some discrepancy in the PVDF signal compared to the piezoelectric dynamometer-based reference signal due to the assumptions made in the physics based model relating the piezoelectric charge to the dynamic torque. Ideal tool/workpiece setups and cutting phenomena were identified to yield better agreement with the dynamometer-based reference signal. The PVDF sensor was shown to be better suited for measuring high frequency signals as opposed to low frequency harmonics. If the exact shape of the dynamic torque is not required, then the simplified rosette can still be correlated with the machining responses of interest including tool wear, tool breakage, and chatter.

# CHAPTER 5

# ON-LINE CHATTER DETECTION

## Introduction

This chapter evaluates the performance of three chatter detection algorithms for the turning and boring processes with the eventual goal of developing embedded sensor-based process monitoring automation. The objective of chatter detection in this thesis is to detect chatter in its early stages and prior to the appearance of chatter marks on the workpiece surface. Three chatter detection algorithms, based on the following three methods, were evaluated: 1) 1$^{st}$ Autocorrelation Coefficient, 2) Wavelet Transform, and 3) Fast Fourier Transform. To evaluate the algorithms, cutting force data were gathered from a number of turning scenarios consisting of varying workpiece geometries using a piezoelectric force dynamometer. Boring data were gathered for a single toolpath with varying machining parameters using the PVDF sensor configuration outlined in Chapter 4.

In the following sections, the general sensor and processor requirements for chatter detection are described. A description of the signal shape during stable cutting versus unstable cutting is then presented. This is followed by derivations of the three chatter algorithms evaluated in this thesis. Then, the various turning conditions for chatter algorithm validation are presented. Description of the boring chatter detection problem is also presented. The results of applying each chatter algorithm to detect chatter in turning and boring are presented followed by discussion of the results.

## Sensor and Processor System Requirements

In order for an algorithm to detect chatter instability before the occurrence of chatter marks on the workpiece surface, the sensing system must be low-cost, robust, and

nonintrusive. Specifically, a sensing and monitoring system with the following features is required:

- Utilize a sensor flexible enough that it can robustly transform the measured time series signal into a voltage time series to be recorded by a microprocessing unit. Chatter detection sensors including strain gauges [21, 50], piezoelectric thin-film sensors, and microphones [93] have been investigated in the literature but are not the primary focus of this chapter. For chatter algorithm development and evaluation purposes, a 3-axis cutting force dynamometer is used due to its high frequency bandwidth and nonstationary signal shape while the PVDF thin film measuring system presented in Chapter 4 is used subsequently to evaluate its effectiveness for chatter detection in the boring process.
- Use a microprocessor that performs the majority of on-line chatter detection calculations. Low cost and low profile embedded microcontroller series including Arduino [126], mbed [127], and BeagleBoard [128] are suitable for this application. However, their onboard memory and processing power are severely limited compared to a current state-of-the art personal computer. For example, an Arduino Due can store 512 kB of flash memory (~64,000 double variables) while MATLAB running on a Dell XPS 8700 can store at least 900 MB (~112,500,000 double variables) [129]. Such memory limitations adversely impact mathematical calculations including complex numbers, matrix operations, and digital filtering. For this research, the benchmark processor unit was a MK20DX256VLH7 (72 MHz clock, 256 kB memory) microcontroller using the Arduino environment [130]. This microprocessor was selected for its low cost and its flexibility in being configured as an embedded system (Teensy 3.1) or as an Integrated Circuit that can be soldered onto a prototype printed circuit board with minimal supplementary components.
- Use a receiver for collecting the chatter algorithm output. After the measured signal is processed by the algorithm, the output needs to be sent to a receiver. Examples of a

receiver include a standalone DAQ system, the machine tool controller, or a webserver. Having the microcontroller unit process the data to produce a compressed output (e.g. is there chatter or not?) reduces the computational burden on the receiver unit and allows for flexible implementation. Transmission methods to transfer the algorithm's results to the receiver include an RS-232 cable, Bluetooth, and Secure Digital (SD) storage. Examples of devices to receive the algorithm's results include machine tools for autonomous adaptation of cutting speed or feed for chatter avoidance and cloud based storage for productivity monitoring.

## Algorithm Description and Implementation

Three chatter detection algorithms, based on the following three methods, were evaluated:

- 1st Autocorrelation Coefficient
- Wavelet Transform
- Fast Fourier Transform

These methods were chosen due to their relatively low computational and memory requirements, which are suited for embedded processing units. The ultimate goal of each algorithm is to collect and process the sensor data in real time, and compute parameters that are sensitive to the onset of dynamic chatter instability before chatter marks appear on the workpiece surface. The algorithms were implemented in MATLAB, although the computational feasibility of the algorithm was also tested on the proposed MK20DX256VLH7 microcontroller.

## Methodology

To recognize chatter from a measured signal, the corresponding signal shape and pattern must be first identified. In this work, chatter is defined a dynamic instability in machining that is characterized by self-induced vibrations, which produce poor workpiece

surface finishes [104]. Figure 25 provides a basic illustration of the underlying mechanism of regenerative chatter [104], which is commonly encountered in machining operations.

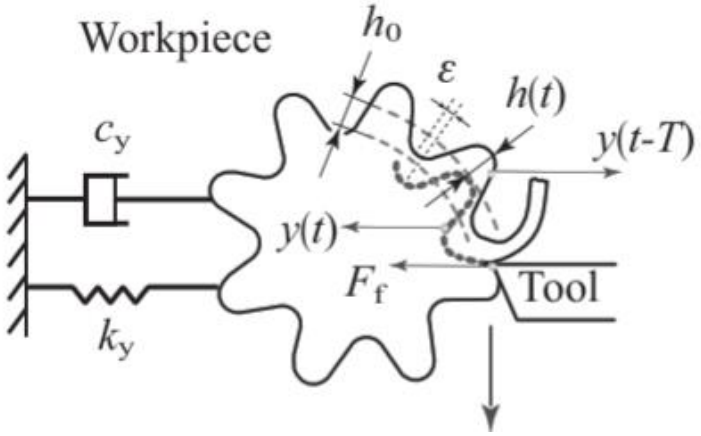


Figure 25. Chip regeneration in orthogonal cutting [104].

The following derivation will provide a simplified example of the distinct regenerative chatter behavior to be identified for autonomous detection. As established in [104], the single degree of freedom equation of motion for orthogonal cutting is as follows

$$m_y\ddot{y(t)} + c_y\dot{y(t)} + k_y y(t) = F_{Cut}(t) = K_{Cut}ah(t) \tag{14}$$

where $y(t)$ is the displacement of the workpiece, $a$ is the radial depth of cut, $h(t)$ is the undeformed chip thickness, and $K_{Cut}$ is the orthogonal cutting force coefficient. Note that in the case of single point cutting, the orthogonal model can be mapped to oblique coordinates, which can then be resolved into the machine tool coordinates via a transformation matrix as a function of constant cutting tool geometry. Initially, the surface of the part is smooth before the first spindle revolution. However, every revolution leaves behind a wavy surface because of the bending vibrations of the shaft in the feed direction $y$. When the second revolution starts, the part experiences modulations both due to the

current workpiece/tool vibrations and the surface undulations produced in the previous spindle revolution. Thus, a change in the instantaneous undeformed chip thickness is produced, which can be described mathematically as follows

$$h(t) = h_0 - [y(t) - y(t - S)] \tag{15}$$

where $h_0$ is the nominal undeformed chip thickness, $S$ is the spindle speed, and therefore $[y(t) - y(t - S)]$ is the dynamic instantaneous undeformed chip thickness. Substituting Eq. (15) into Eq. (14), and transforming the equation into the Laplace domain, the transfer function between the nominal undeformed chip thickness and dynamic undeformed chip thickness is given by

$$\frac{h(s)}{h_0(s)} = \frac{1}{1 + (1 - e^{-sT})K_{cut}a\Phi(s)} \tag{16}$$

where $\Phi(s)$ is the frequency response transfer function. Assume that the root of the characteristic equation is $s = \sigma + j\omega_c$, where $\omega_c$ is the frequency at which the part deforms in the $y$ direction (or the chatter frequency). If the root has a positive real part ($\sigma > 0$), the time domain solution will have a positive exponent. Thus, the amplitude of the system's displacement will exponentially increase while modulating at frequency $\omega_c$. Over time, the system will become unstable, thus resulting in chatter. If the root's real part is negative ($\sigma < 0$), the time domain solution shows that the vibration will subside with time. Thus, the vibration amplitude at frequency $\omega_c$ goes to 0. Stability lobe diagrams identifying stable/unstable cutting conditions can be derived by analyzing the critical stability at $\sigma = 0$.

In single-point cutting, the dynamic chip thickness oscillates about a constant chip thickness value. In this thesis, the signal waveform corresponding to a constant chip

thickness is identified as static, and the signal waveform resulting from the varying chip thickness about the average chip thickness is identified as dynamic. From the previous derivation, an increasing periodic signal waveform would be identified as chatter. Note that the stable single-point cutting process may have harmonics, though they will not grow in magnitude. However, a random disturbance needs to be added to account for the various random processes also present in the actual process, e.g. material inhomogeneities, noise in the measurement system, etc. In light of the central limit theorem, the aggregation of all these random processes can be modeled as a Gaussian white noise about the static signal. Gaussian noise is assumed to have no correlation with the dynamic state of the cutting process. Thus, for single-point cutting, when the cutting process is stable, the dynamic cutting force is dominated by Gaussian white noise. During the transition from stable cutting to unstable cutting, the vibration at the chatter frequency starts to grow and eventually dominates the cutting force signal after chatter is fully developed. Figure 26 shows a representative CMM measurement of a turned workpiece and a picture of the corresponding machined surface exhibiting chatter marks.

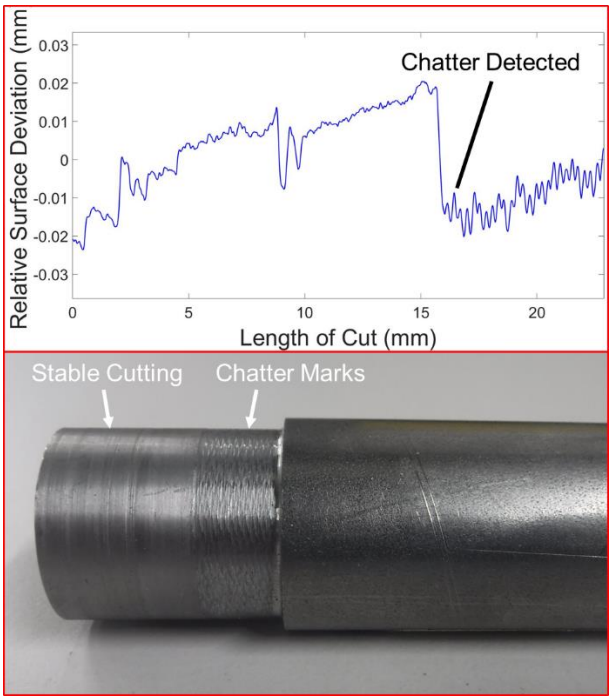


Figure 26. Example CMM data and workpiece surface.

### 1st Autocorrelation Coefficient

The autocorrelation function is the basis of the first chatter detection algorithm to be described. Autocorrelation is the cross-correlation of a signal with itself at different points in time [131]. The autocorrelation function is useful in determining a data set's level of correlation. Information entropy, also a way to measure system correlation, has been demonstrated to have properties that are similar to the autocorrelation function [132] and calculation of system entropy has been used for chatter detection in single-point cutting [85, 93]. The calculation of Shannon Entropy of a dataset $X$ with samples $\{x_1, \cdots x_n\}$ is given as follows:

$$B = -\sum_{i}^{n} p_i \log p_i \tag{17}$$

where $p_i$ is the probability mass function of a sample. However, the $log$ operation used in the entropy analysis is computationally expensive for embedded processor systems. On the MK20DX256VLH7, a single $log$ operation takes ~50 μs while a single multiplication (e.g., when computing the autocorrelation) on the MK20DX256VLH7takes ~0.063 μs. Therefore, the autocorrelation function was determined to be a more practical tool for implementation in embedded processor systems. The autocovariance function is defined as

$$c_k = \frac{1}{N}\sum_{t}^{N-k}(X_t - \bar{X})(X_{t+k} - \bar{X}) \tag{18}$$

The autocorrelation function consists of the coefficients $\{a_1, \cdots a_n\}$. Thus, the value of autocorrelation coefficient at time difference $k$ is defined as follows:

$$a_k = \frac{c_k}{c_0} \tag{19}$$

where $c_0$ is the variance function, which is defined as:

$$c_0 = \frac{1}{N}\sum_{t}^{N}(X_t - \bar{X})^2 \tag{20}$$

The autocorrelation function exhibits the following properties:

- The autocorrelation function is both symmetric and Hermitian.
- The continuous autocorrelation function reaches its peak at zero lag ($k = 0$).
- The autocorrelation of white noise will have a strong peak at $k = 0$ and will be 0 at all other $k$.

- The Wiener–Khinchin theorem [133] relates the autocorrelation function to the power spectral density via the Fourier transform.

Using the previously mentioned properties and the previously stated methodology, it is possible to identify a signal white noise, and therefore as stable. Examples of autocorrelation functions of a representative sinusoidal signal ($f(x) = \sin x$) and of random noise (mean = 0 and standard deviation = 1) are shown in Figure 27.

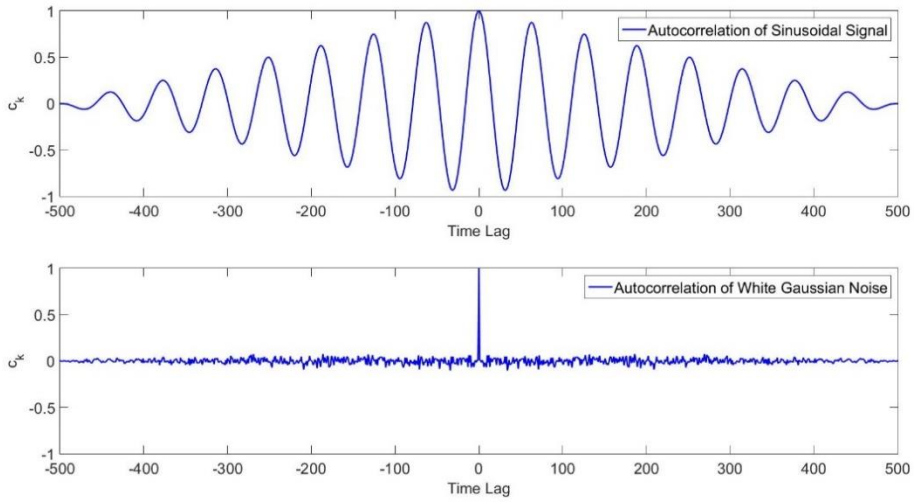


Figure 27. Example autocorrelation functions.

Note that $c_k = 1$ at $k = 0$ for both waveforms. However, for random noise, $c_k \approx 0$ at all other values of $k$. Thus, the autocorrelation function can be examined at a single time lag point to check for randomness. In particular, to test for randomness, the autocorrelation coefficient for $k = 1$ can be tested against the confidence interval for rejection of the null hypothesis that the data is random [4]. The autocorrelation value at a particular time lag is defined as the 1st autocorrelation coefficient. For completeness, the chatter variable to be monitored is defined as follows

$$a_1 = \frac{\sum_t^{N-1}(X_t - \bar{X})(X_{t+1} - \bar{X})}{\sum_t^{N}(X_t - \bar{X})^2} \tag{21}$$

In this work, the absolute value of the 1st autocorrelation coefficient is known to be close to 0 when the data is random, and close to 1 when the data is perfectly correlated. When chatter develops, a specific periodicity emerges, and the data becomes more correlated, thus bringing the 1st autocorrelation coefficient closer to 1. The benefits of this algorithm include computational efficiency ($O(\sim 10N)$) addition and multiplication operations) and minimal onboard storage requirements. In addition, a normalized threshold can easily be set to detect the onset of chatter, and the chatter frequency can be identified by calculating the entire autocorrelation function [134].

In the current work, the 1st autocorrelation coefficient was calculated every 500 points. This window helps minimize the moving average effect, though a linear fit can be subtracted from the windowed data to produce a zero mean dataset. However, the force data obtained when the tool is not cutting can be strongly correlated due to natural sensor characteristics (in this case, the MAINS hum). Therefore, computer generated, normally distributed random numbers are added to the raw force data to distinguish between the non-cutting and chatter cases.

**Second Generation Wavelet Transform**

A mathematical method of interest for chatter detection is the wavelet transform. Multiple chatter algorithms have been developed using wavelet transforms [116, 135, 136], and wavelet transforms have been demonstrated on embedded systems [137]. The continuous wavelet transform (CWT) of a signal $x(t)$ is defined as [138]

$$X_\omega = \frac{1}{|a|^{1/2}} \int_{-\infty}^{\infty} x(t)\psi\left(\frac{t-b}{a}\right) dt \tag{22}$$

where $a$ and $b$ are scaling and translational wavelet parameters, respectively, of the mother wavelet $\psi(t)$. The wavelet parameters are a function of the type of wavelet (e.g. Hermitian, Poisson, Shannon, etc.). The CWT can also be described as a convolution of the input data signal with a set of functions generated by the mother wavelet. By convolving the signal with the wavelet, certain frequencies of the time domain signal are amplified while others are minimized depending on the scaling parameter. Thus, simultaneous time-frequency resolution can be controlled. Analogous to how the Fast Fourier Transform (FFT) is to the Fourier Transform, the discrete wavelet transform (DWT) is to the CWT. The DWT involves decomposing a signal into approximation and detail coefficients through a series of filter banks as follows.

$$a_i = (x * g)[n] = \sum_{k=-\infty}^{\infty} x[k]g[n-k]$$
$$d_i = (x * h)[n] = \sum_{k=-\infty}^{\infty} x[k]h[n-k] \quad (23)$$

where $a_i$ and $d_i$ are the approximate and discrete coefficients, respectively, at decomposition level $i$, $g$ is the low pass filter, and $h$ is the high pass filter. These filter banks act as wavelets in the CWT derivation. The approximation coefficients produce better low frequency resolution, while the detail coefficients produce better high frequency resolution. By continually decomposing the approximation coefficients into next level approximation and detail coefficients, multiple bands can be examined, thus achieving sufficient time-frequency resolution if the appropriate number of decompositions is performed. Figure 28 shows an example schematic of a 3 level decomposition DWT with a sampling rate of 12 KHz.

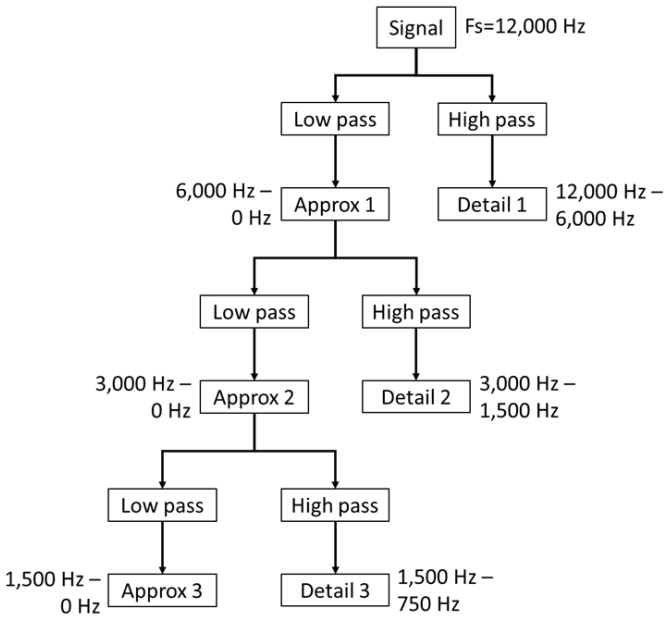


Figure 28. DWT example schematic.

Note that the Discrete Wavelet Transform takes only $O(N)$ for a particular decomposition. This paper evaluates the computationally efficient Second Generation Wavelet Transform (SGWT) as a method suitable for embedded microcontroller applications. The SGWT involves application of the lifting scheme, which is the act of factorizing filter bank convolution and subsampling onto even and odd samples, thus reducing the number of operations by an order of two [139]. Through the lifting scheme, the wavelets are not designed in the frequency domain while retaining the favorable wavelet properties of multiresolution capability and computational efficiency. Figure 29 shows a schematic of the SGWT. The basic steps for the SGWT are as follows:

1. Split the input signal into odd and even samples.
2. A Predictor operator is applied to the even values and the output is subtracted from the odd samples. The result is the detail coefficient.
3. The Update operator is applied to the detail coefficient, and the output is added to the even samples. The result is the approximation coefficient.

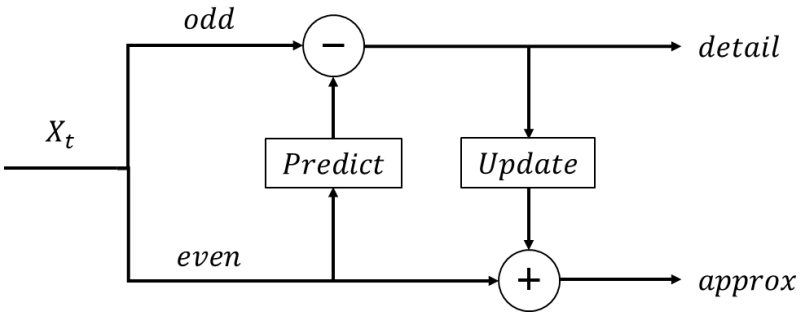


Figure 29. SGWT example

In this work, the lifting scheme corresponds to the Haar-Wavelet [137]. Thus, the Predictor Operator is the identity multiplication while the Update Operator is division by 2. Note that the chosen sorting, predicting, and updating operations are computationally efficient for the MK20DX256VLH7 microcontroller (~3N add and multiplication operations per decomposition while the odd/even sort requires minimal computation). The SGWT however does require significant memory if all decompositions are to be stored. Therefore, this thesis recommends identifying and monitoring the decomposition level that is most sensitive to chatter. Decomposing straight from the raw signal to the band of interest, as opposed to performing stage-like decompositions, also saves computation cost.

**Fast Fourier Transform**

The Fast Fourier Transform (FFT) is a computationally efficient method of performing the Discrete Fourier Transform (DFT). The DFT signal transformation can be described as [140]:

$$X_F = \sum_{n=0}^{N-1} x_n e^{-i2\pi m \frac{n}{N}} \qquad m = 0, \dots, N-1 \tag{24}$$

When analyzing the cutting force data in the spectral domain, it was determined that a stable harmonic in the single-point cutting process is accompanied by other harmonics of similar power. However, during the onset of chatter, a dominant frequency emerges, with associated frequencies emerging shortly thereafter. Therefore, comparing the magnitudes of the two largest peaks in the FFT can demonstrate if a particular frequency is emerging as dominant. The application of the FFT to chatter detection involves performing the transformation on a mean-shifted set of points, identifying the two highest peaks, and then calculating their ratio. If a cut becomes unstable, the ratio of the peaks will increase as the power at a particular frequency becomes large. Thus, a threshold can be established. The resulting parameter can be expressed as:

$$P_R = \frac{P_1}{P_2} \tag{25}$$

where $P_1$ and $P_2$ are the amplitudes corresponding to the two highest peaks. $P_R$ can be chosen through experimentally procuring cutting data and tuning the parameter to the desired threshold.

The computation complexity of the FFT is $O(N \log N)$. To calculate the frequency of the two largest peaks after creating the FFT, a binary search algorithm can be used. Note that if the sampling frequency is low enough such that the FFT bins are not susceptible to noise, the autocorrelation matrix and a corresponding eigenvalue method can be used to identify the highest two frequencies without computing the entire frequency spectrum [110]. However, because no assumptions are made about the frequency behavior of the cutting system dynamics, the largest sampling frequency was chosen. Thus, in this work, while it is possible to use the eigenvalue method to identify the largest frequency component [141], calculating the second largest frequency with appropriate resolution would require an autocorrelation matrix so large that it would need more computations than

computing an entire FFT. However, if the required frequency resolution is known, then the sampling rate could be lowered to facilitate the eigenvalue method.

## Turning Experiments

For the acquisition of cutting force data during stable and unstable cutting, three turning process scenarios were analyzed. The differences between the three cases involved changing the pre-existing workpiece geometry and toolpath. Variation of other parameters, such as the workpiece material, tool feed rate, and cutting speed were found to change the chatter frequency and signal magnitude, but did not change the signal shape itself.

### Case 1

Figure 30 illustrates the basic toolpath for Case 1, which involves a linear, outer diameter longitudinal turning pass. The radial depth of cut increases gradually as the tool traces an inclined linear path. Chatter occurs once a threshold depth of cut is reached [104]. This case will be used as a baseline test case for the chatter detection algorithms evaluated in this study.

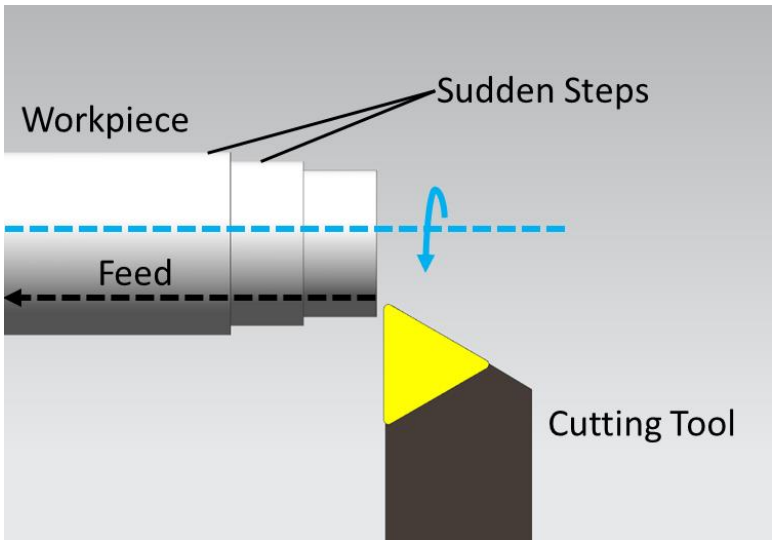


Figure 30. Case 1 tool path.

Figure 31 shows an example of the feed force data acquired in this case. If there is no runout, the signal should ideally represent a Gaussian distribution with a linearly increasing mean. The cutting force signal for this particular case is non-stationary. Depending on the algorithm, the force data can be adjusted to yield favorable statistical properties through various data transformations (e.g. periodically subtracting the mean or adding white noise). Note that stable and unstable cutting are defined by the existence of chatter marks. In this research, dynamic instability is defined as the occurrence of chatter marks on the workpiece surface. By using the tool feed rate in conjunction with the CMM data, the chatter marks on the workpiece can be synchronized with the force data.

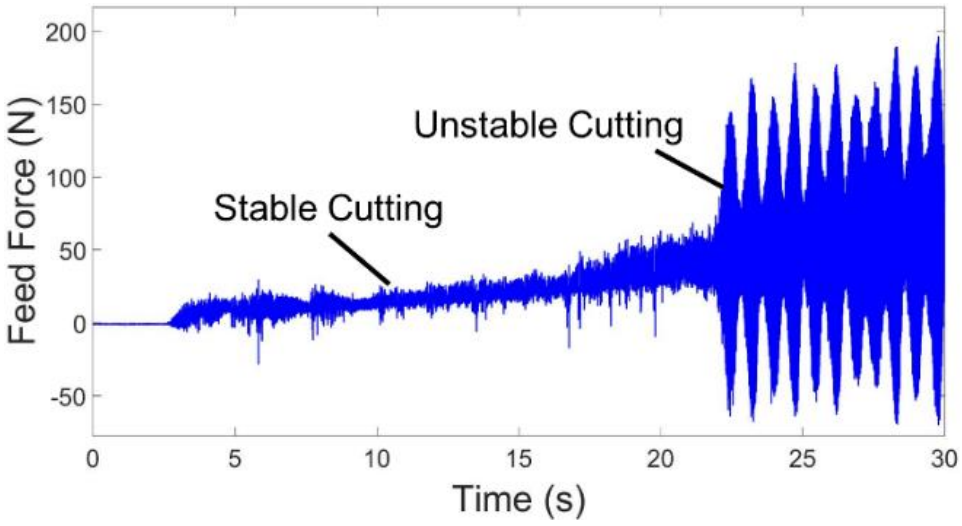


Figure 31. Example feed force data (Case 1).

**Case 2**

This case involved cutting along a toolpath parallel to the workpiece longitudinal axis. However, the radial depth of cut increases along the feed direction due to steps on the workpiece surface (see Figure 32). The magnitude of the depth of cut increase differs between the individual tests. In some cases, the sudden increase will induce chatter, while in other cases, chatter will not occur when the radial depth of cut changes.

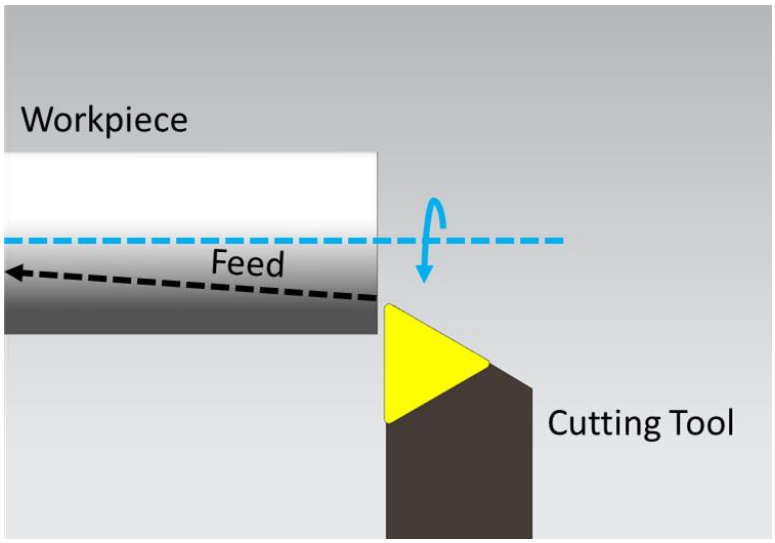


Figure 32. Case 2 tool path

Figure 33 shows representative feed force data for Case 2. In this test, the first depth of cut increase did not induce chatter. Chatter however did occur when the cutting tool encountered the second step increase in the depth of cut. An ideal chatter algorithm will only trigger an alarm when the step causes dynamic instability. In addition, if the depth of cut increase triggers chatter, the event is similar to when chatter occurs immediately upon sudden entry of the tool into the part instead of gradual tool engagement with the part.

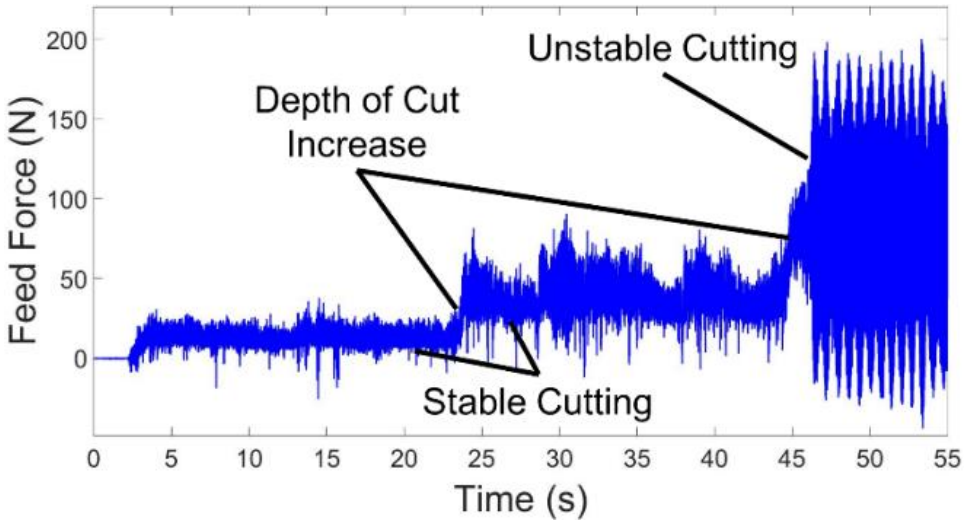


Figure 33. Example feed force data (Case 2).

**Case 3**

Like Case 2, Case 3 involved cutting along a toolpath that is parallel to the workpiece longitudinal axis. A pre-existing hole was drilled into the part perpendicular to the workpiece axis thereby disrupting the constant depth of cut. Figure 34 shows the basic toolpath. In some of the Case 3 tests, dynamic instability occurred when the tool encountered the hole. However, the more significant phenomenon under investigation is the case of a completely stable cut, as shown in Figure 34.

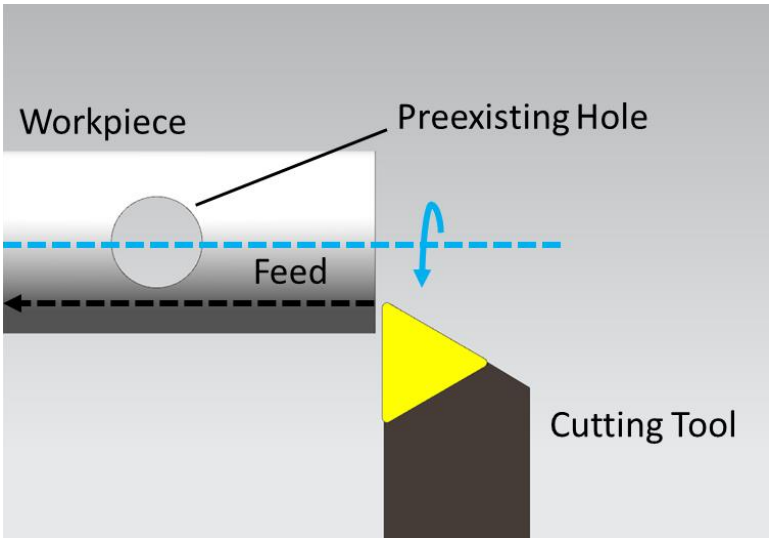


Figure 34. Case 3 tool path.

In Figure 35, the cut is completely stable because there were no visible chatter marks on the workpiece surface. The cyclical variation in the feed force evident in Figure 35 is due to intermittent cutting as the tool repeatedly passes over the hole. When the tool encounters the hole, it suddenly loses contact with the workpiece. During this transition, the tool bends in the direction opposite to the cutting force vector, much like when a compressed spring is released. This springback is detected by the dynamometer, as seen by the negative force values in Figure 35. Chatter detection algorithms were tested to determine if the characteristics exhibited by a stable cut, such as in this case, give rise to a false alarm.

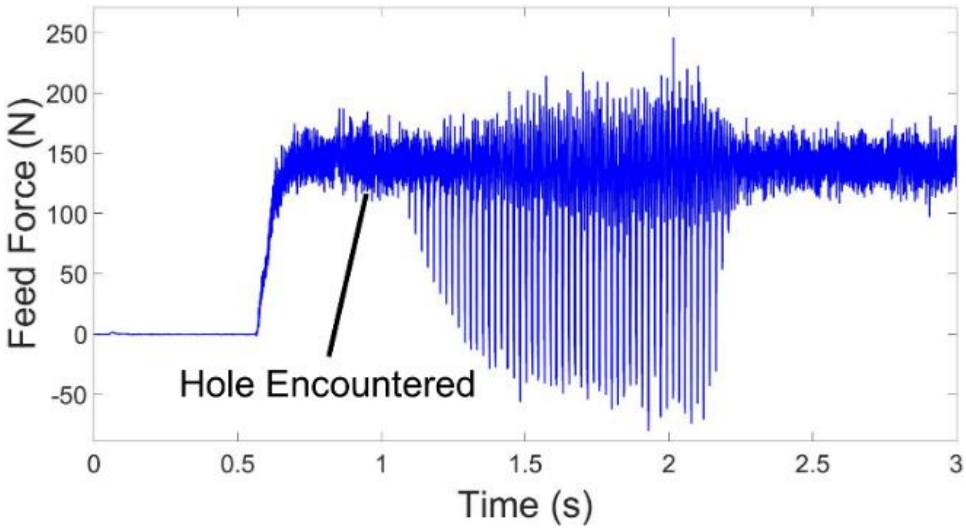


Figure 35. Example feed force data (Case 3).

The single point turning tests corresponding to Cases 1-3 were performed on an Okuma Spaceturn LB2000EX. A Kistler 9257B dynamometer was used to measure the cutting forces. Cutting force was used as the sensed variable since it is readily measured with high fidelity and is sensitive to dynamic chatter instability. A National Instruments cDAQ-9178 data acquisition system was used at a sampling rate of 12 KHz to acquire the force data; per the Nyquist criterion, this sampling rate allows chatter frequencies up to 6 KHz to be detected. All turning tests were performed with a right hand toolholder (Valenite MTGNR-16-4D) with no coolant. The onset of chatter is marked by the appearance of a characteristic pattern on the workpiece surface. A Hexagon Metrology Coordinate Measuring Machine (CMM) was used to confirm the occurrence of chatter marks on the machined surface, thus synchronizing the physical occurrence of chatter with the cutting force data. The cutting parameters are summarized in Table 3.

Table 3. Cutting conditions for turning tests for chatter detection.

| Test No. | Case No. | Spindle Speed (RPM) | Feed (mm) | Workpiece Material | Occurance of Chatter Along Length (mm) |
|---|---|---|---|---|---|
| 1 | 1 | 1000 | 0.025 | 1018 ST | 8.38 |
| 2 | 1 | 1000 | 0.025 | 1018 ST | 1.04 |
| 3 | 1 | 1000 | 0.025 | 1018 ST | 7.01 |
| 4 | 2 | 1000 | 0.025 | 1018 ST | 12.60 |
| 5 | 2 | 1000 | 0.025 | 1018 ST | 14.88 |
| 6 | 2 | 1000 | 0.025 | 1018 ST | 16.66 |
| 7 | 3 | 1500 | 0.025 | AL 6061 | N/A |
| 8 | 3 | 1500 | 0.025 | AL 6061 | N/A |

## Turning Results

### 1st Autocorrelation Coefficient

To calculate an allowable threshold to detect chatter, the inverse of the 95% confidence bands for testing randomness of a data set specified by [131] was used. A threshold of 0.877 was calculated, meaning that if the absolute value of $a_1$ is greater than 0.877, chatter is detected. Figure 36 illustrates the algorithm result when applied to the force data corresponding to Case 1.

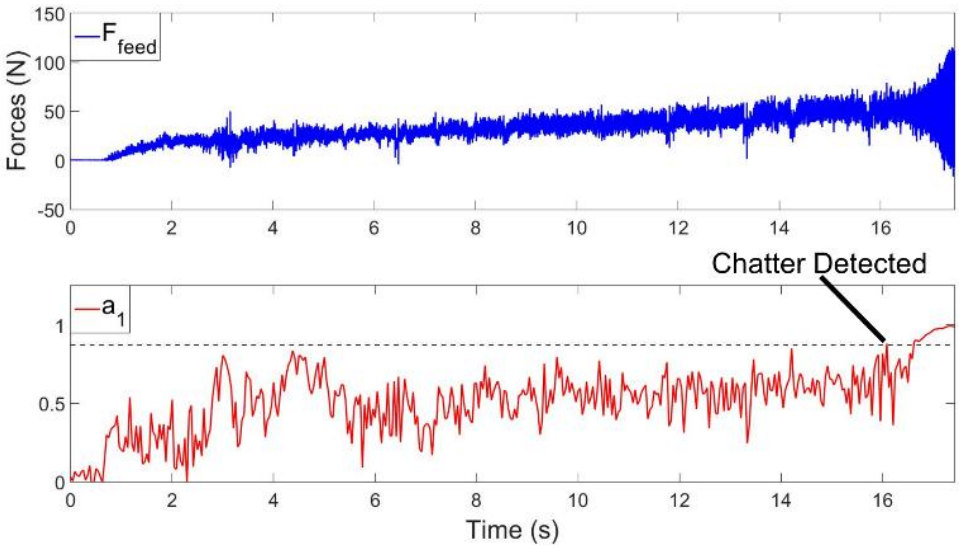


Figure 36. 1st Autocorrelation Coefficient (Test 1).

In this test, chatter was detected 1,430 ms before chatter marks appeared on the workpiece. Note that $a_1$ continues to approach 1 as the force data grows in magnitude. Therefore, this test demonstrates that the algorithm output does not produce a false alarm, and the threshold can be adjusted depending on algorithm robustness and automated corrective action requirements (e.g. adjustment of tool feed or cutting speed). However, stable cutting harmonics can also produce correlated data, thus triggering a false alarm for this algorithm. Figure 37 illustrates the results of a test corresponding to Case 2. This is an instance of stable correlated data, and therefore the algorithm triggers an alarm. However, after the alarm is issued, $a_1$ decreases, thus showing that the signal is not increasing in magnitude, which would be required for dynamic instability. Further support for this conclusion is derived from the CMM data shown in Figure 26, which show that chatter marks occur approximately near the third step cut by the tool while a false alarm is triggered at the second step. The 1st autocorrelation algorithm also triggers a false alarm for Case 3, where cutting over the hole exhibits a strongly correlated, but stable signal, as shown in Figure 38.

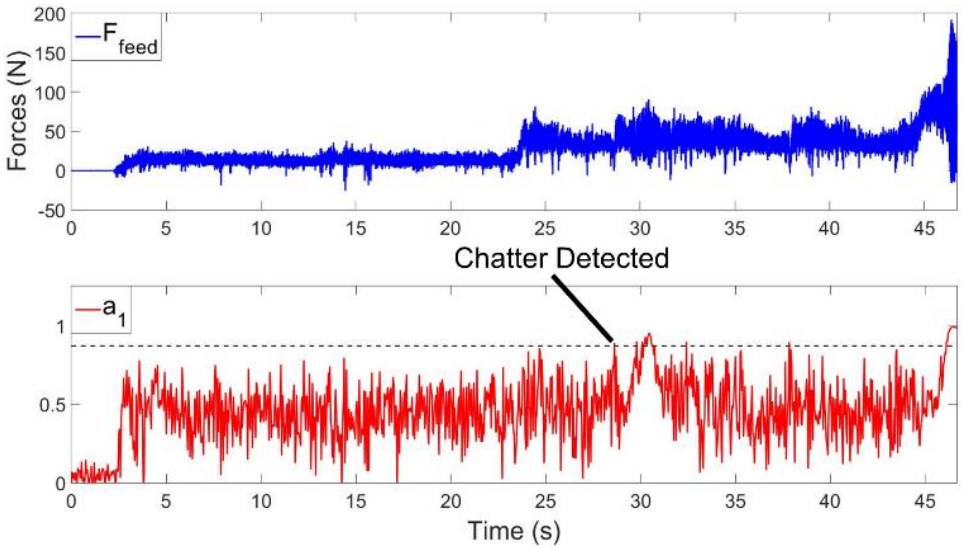


Figure 37. 1st Autocorrelation Coefficient (Test 6).

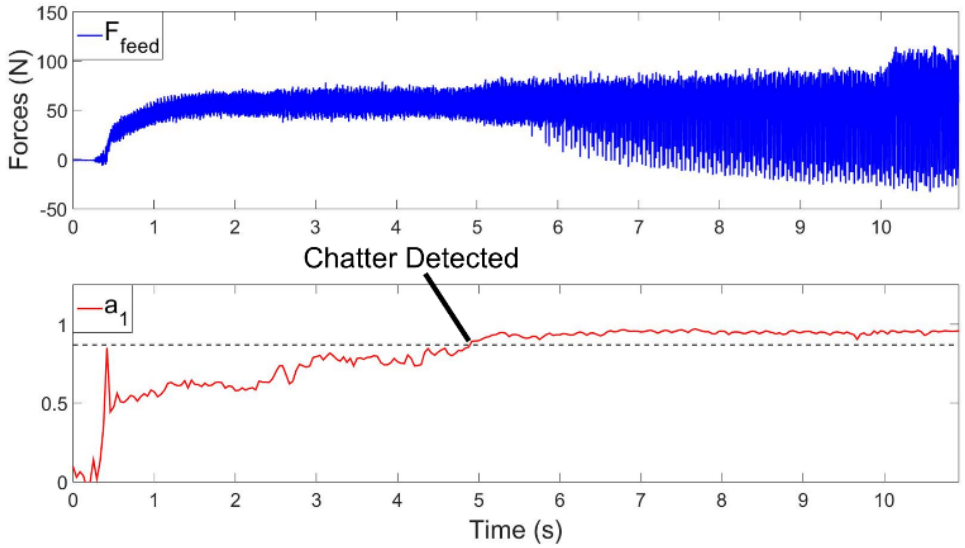


Figure 38. 1st Autocorrelation Coefficient (Test 7).

**Second Generation Wavelet Transform**

For turning, seven wavelet decompositions were performed. Level 2 to 6 wavelet detail components are shown in Figure 39 and Figure 40 for Case 1 and Case 2,

respectively. It appears that the level 6 detail decomposition signal produces the highest magnitude at the onset of chatter and therefore demonstrates the most sensitivity to the chatter frequency. The result is logical as the level 6 decomposition corresponds to a 93.75 Hz to 187.5 Hz filter bank, and the chatter frequency in this case is 108.4 Hz. The differences in cutting condition from Case 1 to Case 2 do not seem to affect the algorithm's sensitivity to chatter.

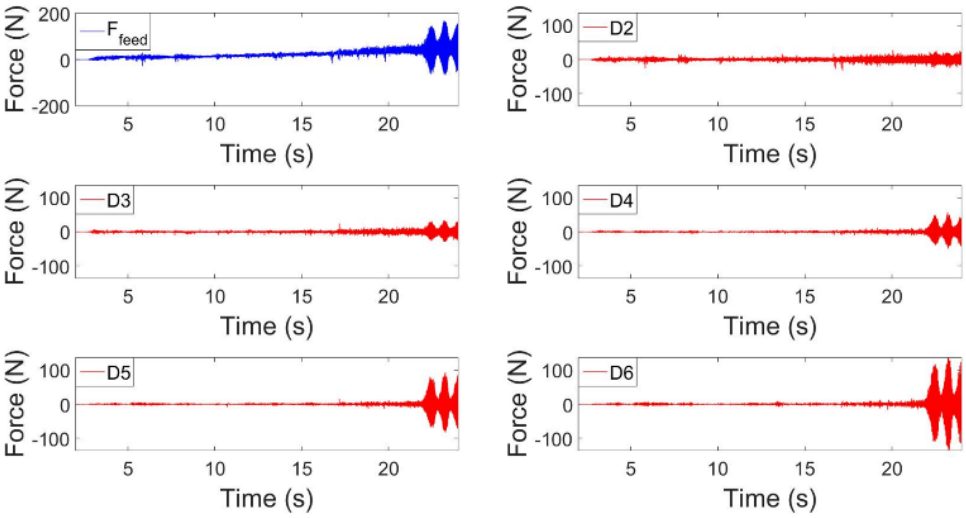


Figure 39. SGWT algorithm results (Test 3).

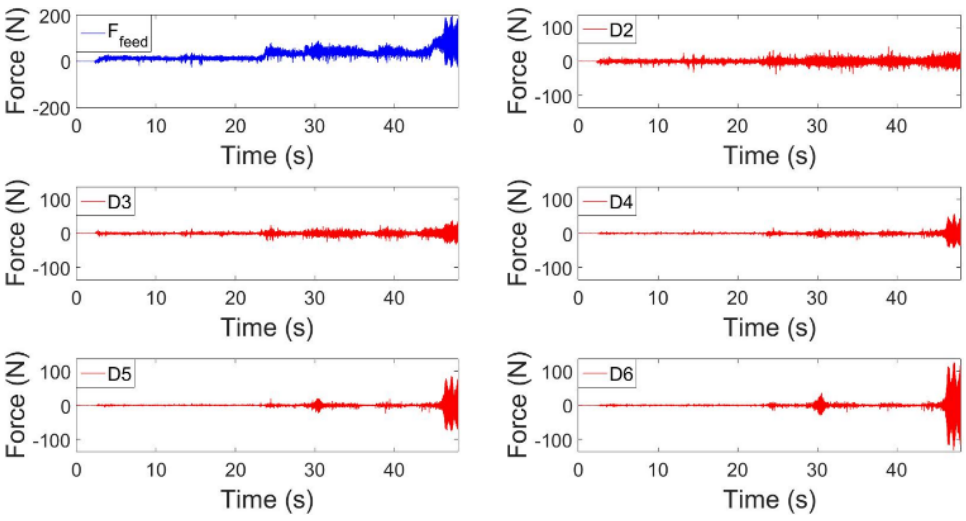


Figure 40. SGWT algorithm results (Test 6).

However, the level 6 decomposition of the SGWT does not demonstrate significant sensitivity to a strongly induced harmonic, as shown in Figure 41. This is because Case 3 has multiple stable frequencies that exhibit strong resolutions in all the decompositions, as opposed to the onset of chatter, which tends to yield a single emerging frequency. Another disadvantage of the Wavelet Transform is the number of decompositions requires prior knowledge of the chatter frequency, which is not always known or is constantly changing (especially in the case of constant surface speed cutting). A method of autonomously identifying dynamic instability instead of visualizing the decomposition sensitivity is also required in order for the SGWT to be effective in chatter detection.

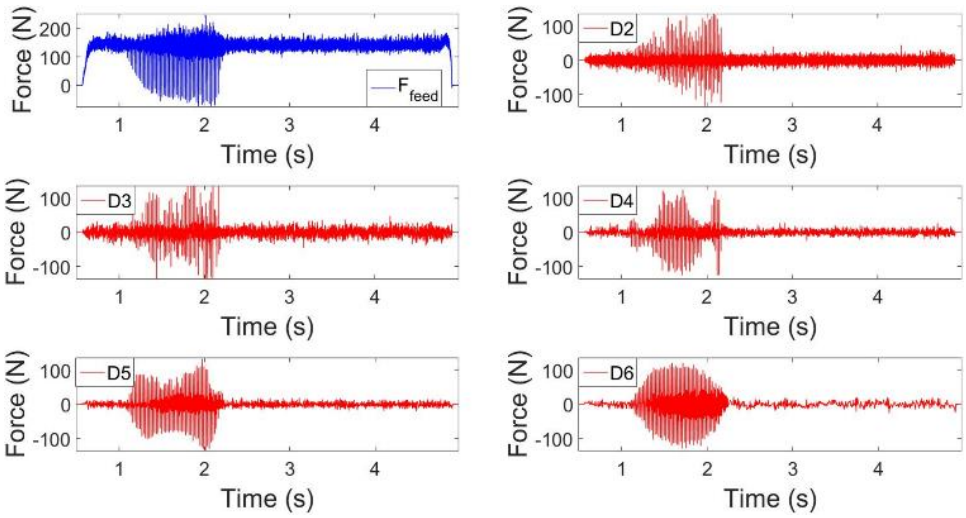


Figure 41. SGWT algorithm results (Test 8).

**Fast Fourier Transform**

In this work, the threshold for the FFT power ratio $P_R$ is taken as 5 by using a safety factor of 1.75 for the highest $P_R$ observed during stable cutting for Case 3. As with the autocorrelation algorithm, computer generated normally distributed random numbers are added to the raw force data in order to distinguish between the cutting and non-cutting

cases. With the MK20DX256VLH7, a 1024 point FFT requires 42.8 ms of computation time, while brute force searching for the two largest magnitudes takes 2 ms. However, a 1024 point FFT appears to be the largest number of possible bins without running into memory constraints. Therefore, a 1024 point FFT was used in the algorithm evaluations. Figure 42 shows the algorithm's application to force data for Case 1. In this case, chatter was detected 465 ms before chatter marks appeared on the workpiece.

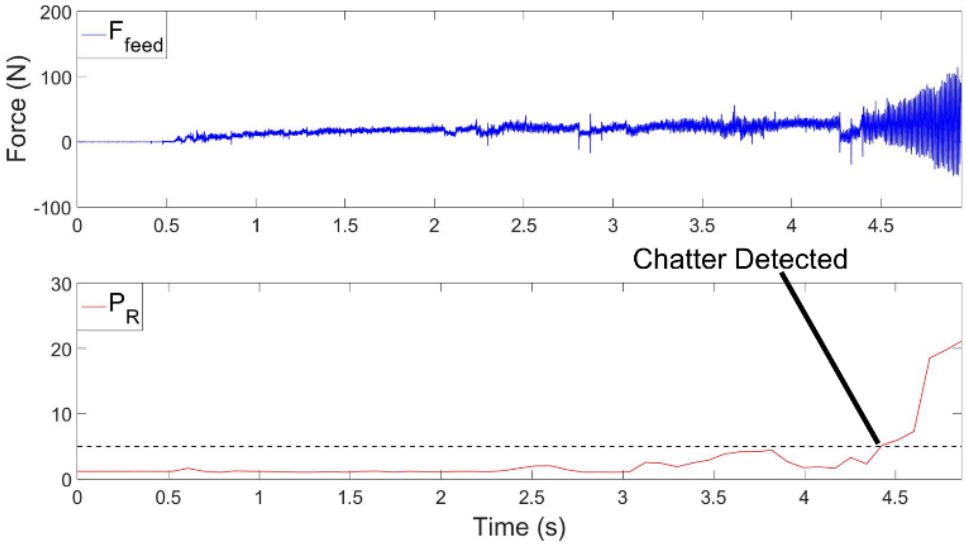


Figure 42. FFT algorithm results (Test 2).

Figure 43 and Figure 44 show the algorithm performance for Cases 2 and 3, respectively. In Case 2, chatter was detected 1,147 ms before chatter marks appeared on the workpiece surface. Sudden steps in the radial depth of cut did not appear to trick the algorithm into triggering a false alarm. This is because the sudden transients mostly affect the 1$^{st}$ bin of the FFT; and because this bin is not considered, transient effects are mitigated. For Case 3, the FFT algorithm did not trigger any alarms, because even though the total spectrum power increased, no singularly emerging harmonic was produced.

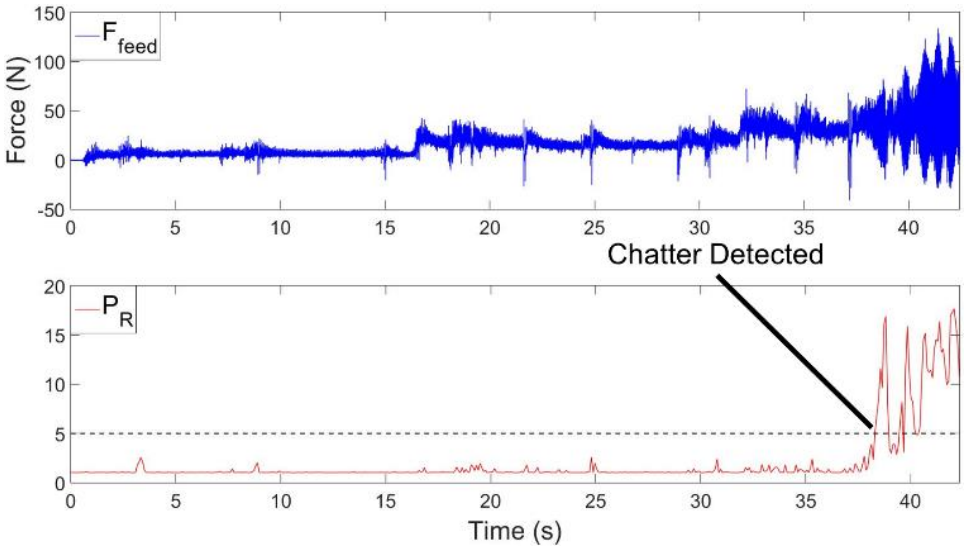


Figure 43. FFT algorithm results (Test 5).

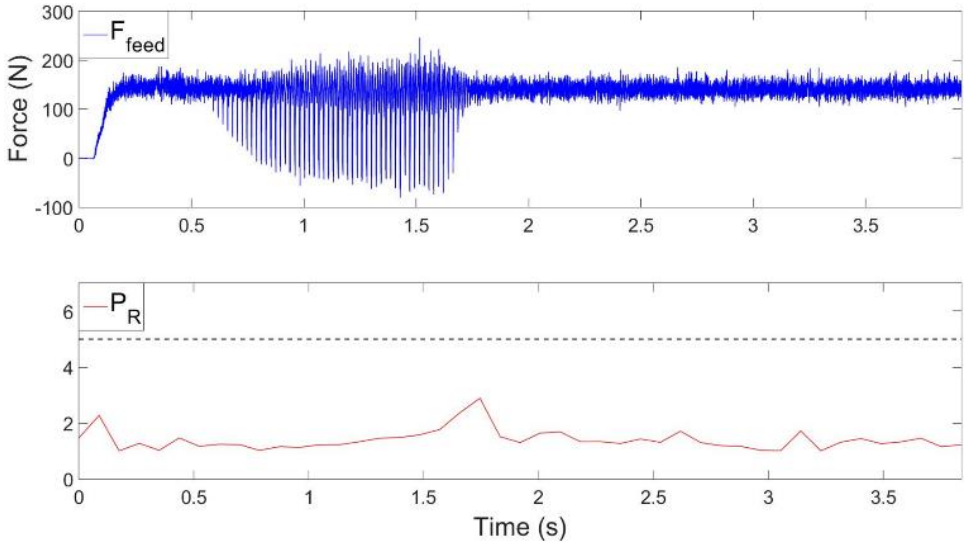


Figure 44. FFT algorithm results (Test 9).

## Boring Experiments

Unlike the turning case, for the acquisition of boring torque data during stable and unstable cutting, only one scenario was analyzed. This is due to the simpler toolpaths used

for boring holes. Figure 45 shows the toolpath schematic for the boring case, which involves a linear, inner diameter boring pass.

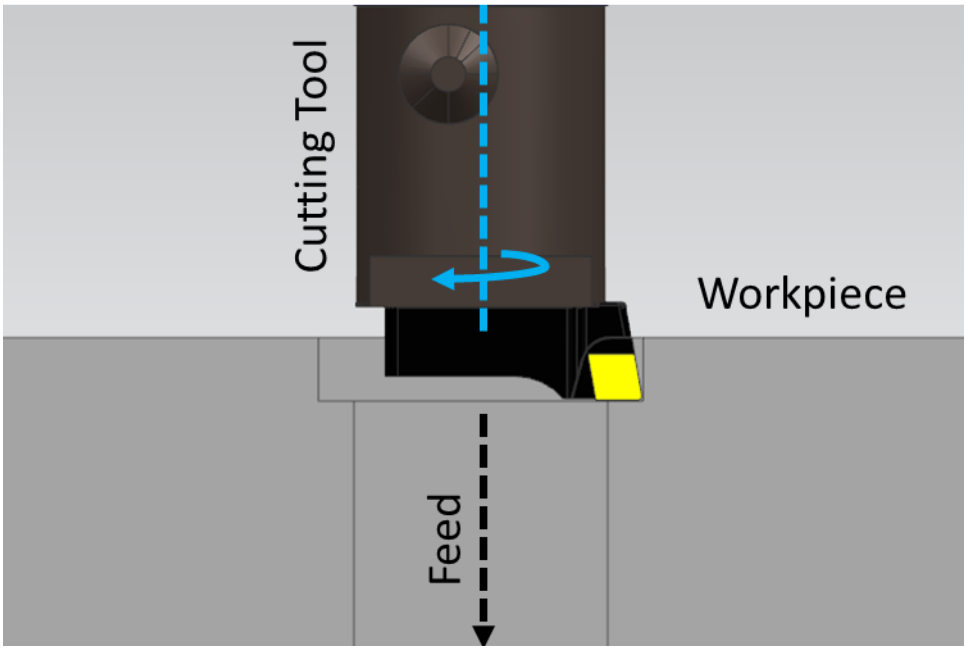


Figure 45. Boring case tool path.

Note that the radial depth of cut remains constant throughout the entire toolpath. Thus, chatter does not develop gradually and therefore time of chatter recognition before marks occur on the workpiece could not be acquired. However, the PVDF configuration isolates torque, and therefore the boring signal shape resembles that of turning. Figure 46 shows a comparison of cutting forces in an outer diameter turning test and cutting torques in a boring test. The signal shapes are similar in that they exhibit noise about a static mean. In fact, the primary difference between turning and boring is that the boring tool has symmetric principle axes of stiffness while a turning tool tends to have a stiffness in one direction that is greater than in all other directions [142]. Though the root cause for chatter is different, the force signal shape characteristics for chatter recognition are unchanged. Analytical models for chatter in boring are limiting because they do not account for the

mode coupling effect. Thus, the emphasis of this thesis is on recognizing boring chatter instead of modelling the nature of chatter in boring processes.

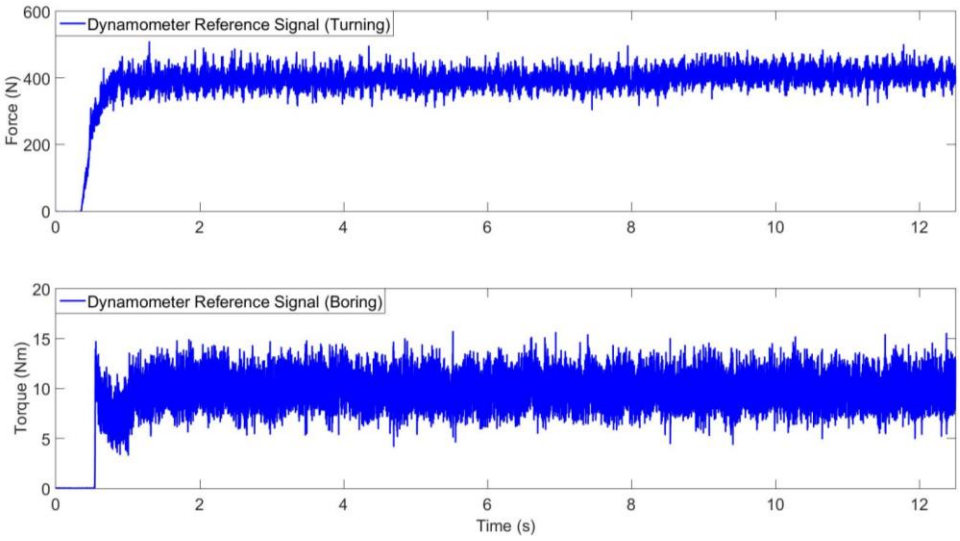


Figure 46. Example turning vs. boring comparison.

Figure 47 shows the power spectra of both the unstable and stable cutting torque signals. Note that the unstable cutting torque yields a single dominant frequency at 252 Hz in comparison to other peaks in the decomposition.

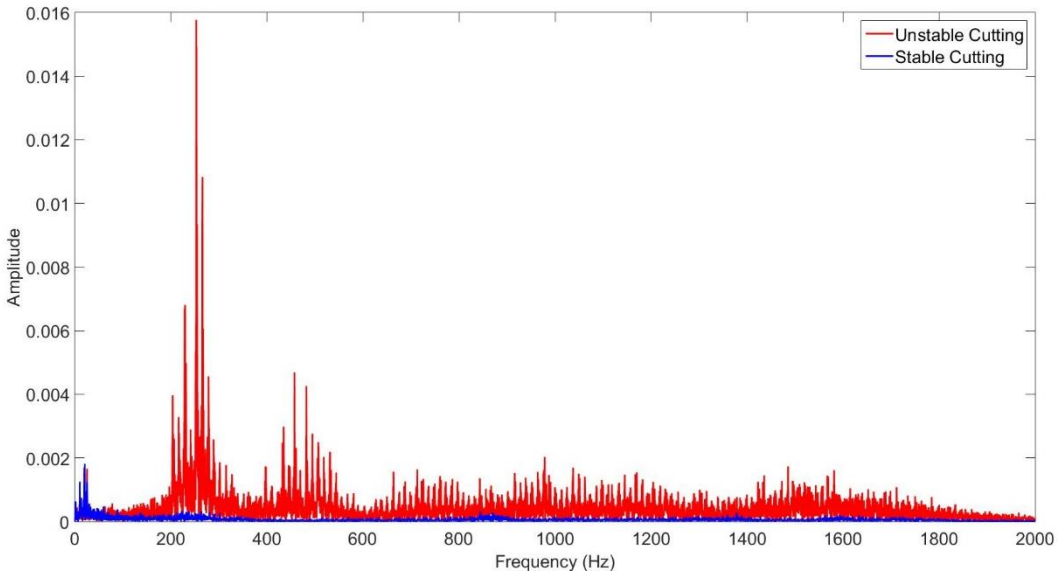


Figure 47. Frequency decomposition of unstable and stable cutting.

The PVDF sensor configuration developed in Chapter 4 was used to measure the cutting torque. The sampling rate for the PVDF signal was 13 KHz while the charge amplifier cutoff was configured to be 7.24 Hz and the anti-aliasing low pass cutoff was 5.5 KHz. Though the PVDF sensing system's frequency bandwidth capability to distinguish chatter was demonstrated in [62], the PVDF measuring system was not used in conjunction with an on-line algorithm to detect chatter.

All boring tests were performed with a single-insert boring bar (ISCAR BHFI MB16-MB50 with CAT-40 holder) with a CAT-40 to CAT-50 adapter. The tests were performed on a boring machine (Liné Machine Tools, Vegamill TF218) located in the Siemens Energy facility in Charlotte, North Carolina. Other parameters such as the workpiece material, tool feed rate, and cutting speed were changed to test algorithm robustness. The test conditions are summarized in Table 4.

Table 4. Cutting conditions for boring tests.

| Test No. | RPM | Feedrate (mm/min) | Depth of Cut (mm) | Length of Cut (mm) | Chatter? |
|---|---|---|---|---|---|
| 1 | 540 | 90 | 0.635 | 70 | Yes |
| 2 | 540 | 90 | 0.635 | 70 | Yes |
| 3 | 540 | 90 | 0.1905 | 70 | Yes |
| 4 | 540 | 90 | 0.1905 | 70 | Yes |
| 5 | 520 | 210 | 0.1905 | 70 | No |
| 6 | 520 | 210 | 0.1905 | 70 | No |
| 7 | 520 | 210 | 0.1905 | 70 | No |
| 8 | 520 | 210 | 0.1905 | 70 | No |
| 9 | 520 | 210 | 0.1905 | 70 | No |
| 10 | 650 | 210 | 0.635 | 70 | Yes |
| 11 | 650 | 210 | 0.635 | 70 | Yes |
| 12 | 594 | 70 | 0.1524 | 90 | No |
| 13 | 594 | 70 | 0.1524 | 90 | No |

## Boring Results

### 1st Autocorrelation Coefficient

For boring, the 1st autocorrelation coefficient was calculated every 1000 points. This window helps to minimize the moving average effect, though alternatively a linear fit can be subtracted from the windowed data to produce a zero mean data set. In the case of boring, the electronics were powered by a 3.7 volt lithium ion battery, and therefore the torque signal did not experience distortion from 50/60 Hz electrical noise typically associated with an AC power source. However, for consistency with the turning case, computer generated, normally distributed random numbers were added to the raw torque data. As with the turning case, the same threshold of 0.877 was calculated using the inverse of the 95% confidence bands for testing randomness of the data set. Figure 48 shows a representative result obtained when the algorithm is applied to the PVDF torque data corresponding to Test 1 (Table 4).

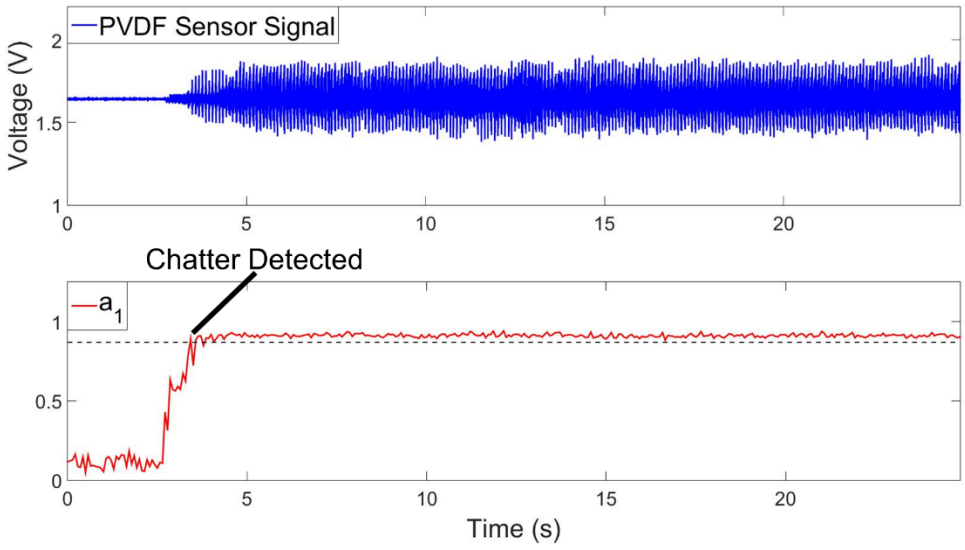


Figure 48. 1st Autocorrelation Coefficient (Test 1).

In this test, chatter was detected when the tool contacted the workpiece. Note that $a_1$ continues to approach 1 as the force data grows in magnitude. Therefore, as in the turning case, this test demonstrates that the algorithm output does not produce a false alarm, and the threshold can be adjusted depending on algorithm robustness and automated corrective action requirements (e.g. adjustment of tool feed or cutting speed). Figure 49 shows the results of Test 12, where the entire cut was stable. Unlike in the turning case, $a_1$ does not increase in magnitude above the threshold. This is the case for boring operations because the effect of runout is not present because the boring operation follows a previous drilling/boring pass. Thus, the 1st Autocorrelation Coefficient method is more robust than in the turning case while still enjoying the computational efficiency advantages over the other algorithms.

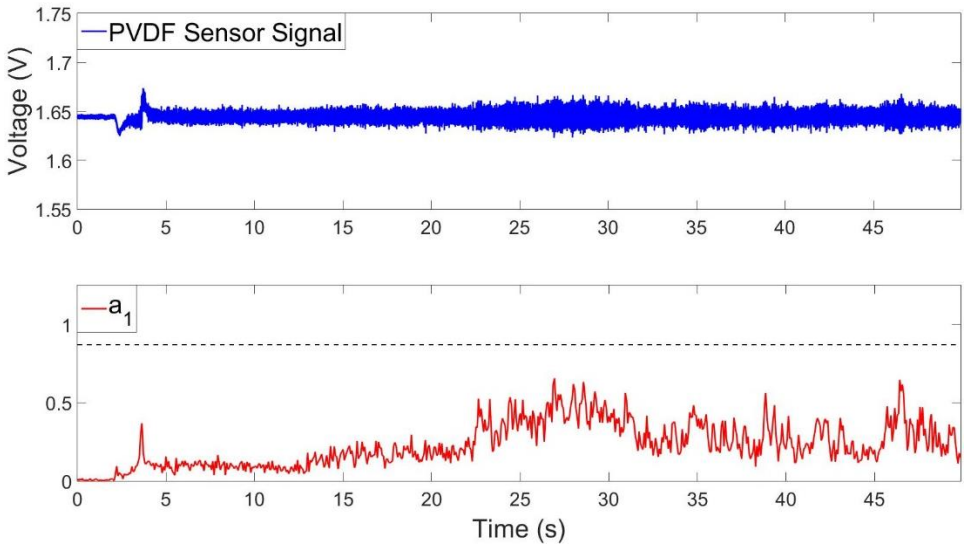


Figure 49. 1st Autocorrelation Coefficient (Test 12).

**Second Generation Wavelet Transform**

Similar to turning, 7 wavelet decompositions were computed for the boring case. Level 2 to 6 wavelet detail components are shown in Figure 50 and Figure 51 for Test 2

and Test 6, respectively. In contrast to turning, the SGWT does not consistently produce a decomposition with the highest sensitivity. Figure 50 shows that decomposition levels 3 to 5 produce the highest signal magnitude during unstable cutting. However, note that the magnitude decreases when decomposing the signal to level 6. This is because the level 6 decomposition corresponds to a 101.56 Hz to 203.12 Hz filter bank, and the chatter frequency in this case is ~275 Hz. Thus, the frequency of interest lies outside of 6$^{th}$ level decomposition band. This error reinforces the notion that the chatter frequency must be known prior to implementing the algorithm to prevent unnecessary computations. Note that Figure 51 shows a completely stable cut, and the sensitivity differences in the decomposition bands are difficult to identify visually.

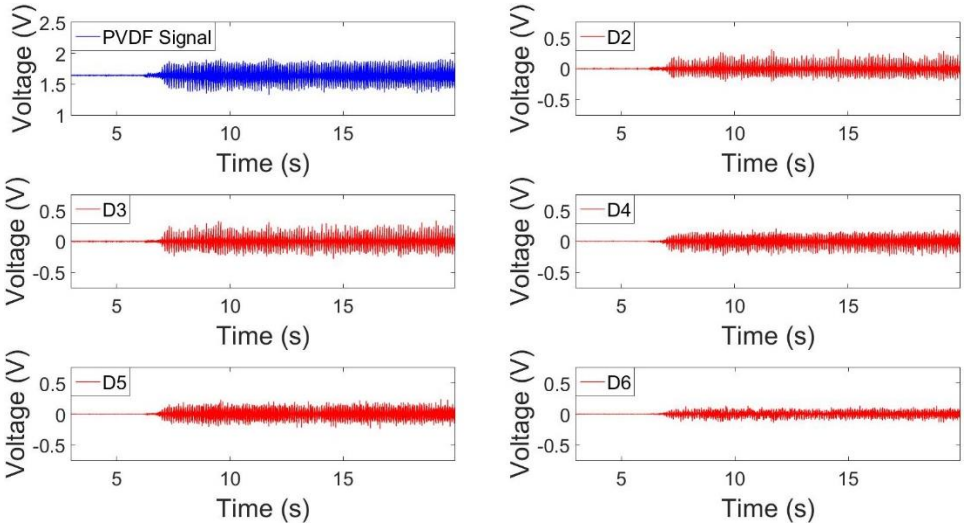


Figure 50. SGWT algorithm results (Test 2).

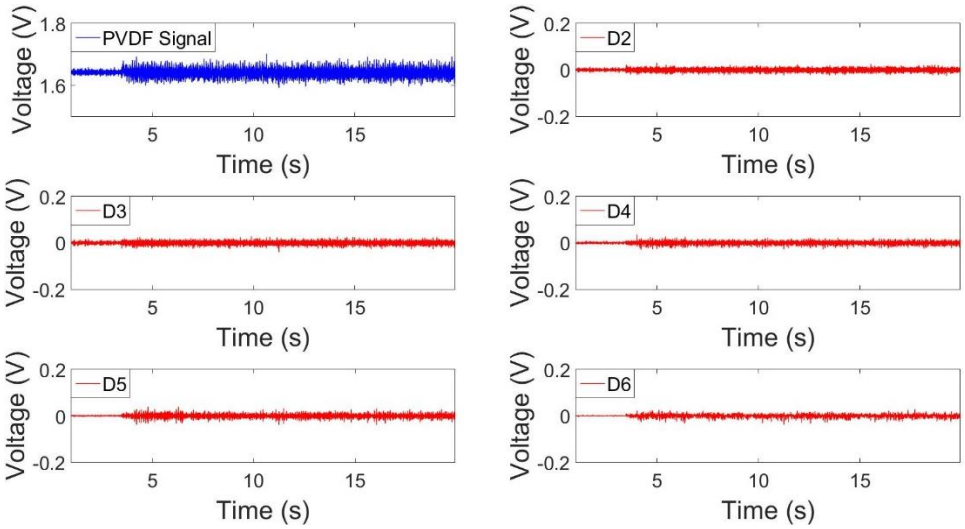


Figure 51. SGWT algorithm results (Test 6).

**Fast Fourier Transform**

In this work, the threshold for the FFT power ratio $P_R$ is taken as 2. As with the autocorrelation algorithm, computer generated normally distributed random numbers were added to the raw force data in order to distinguish between the cutting and non-cutting cases. With the MK20DX256VLH7, a 1024 point FFT appears to be the largest number of possible bins without running into memory constraints. Therefore, a 1024 point FFT was used in the algorithm evaluations. Figure 52 shows the algorithm's application to boring torque data for Test 11, which was an unstable cut. In this case, chatter was detected before the torque signal exploded.

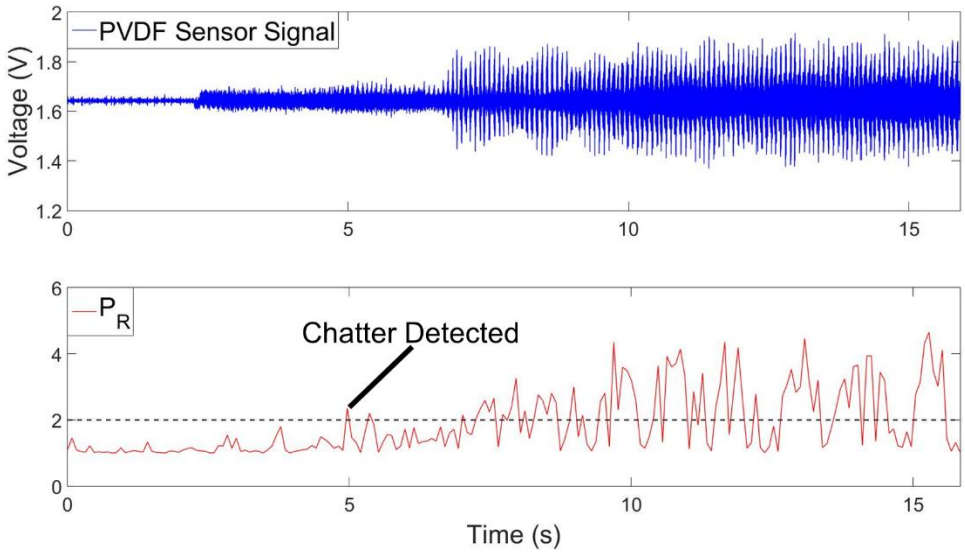


Figure 52. FFT algorithm results (Test 11).

Figure 53 shows the algorithm performance for Test 9. In this test, the algorithm did not trigger a false alarm because even though the total spectrum power increased, no singularly emerging harmonic was produced. However, note that the FFT algorithm's threshold can be tuned for desired levels of sensitivity and robustness.

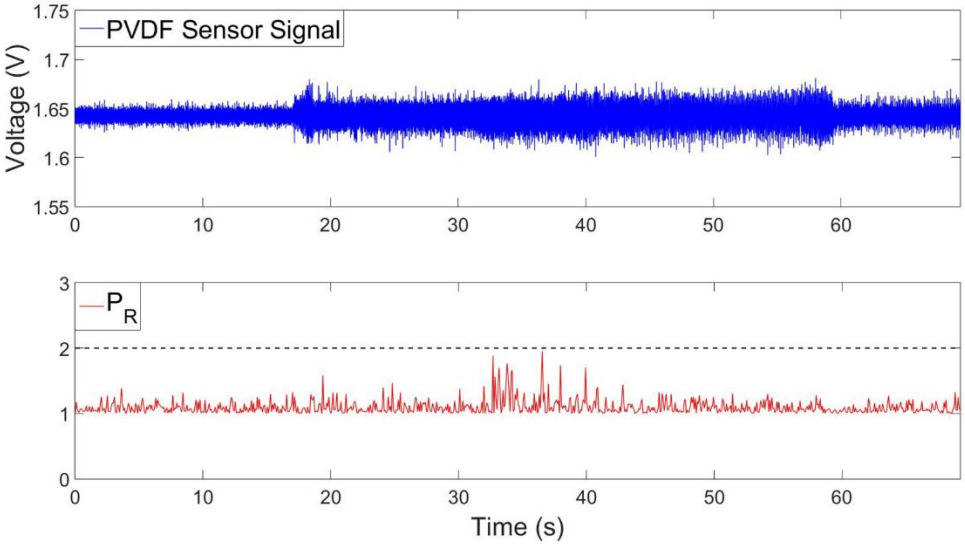


Figure 53. FFT algorithm results (Test 9).

Experimental data show that spectral analysis was found to be the most robust chatter detection method for the three cutting scenarios for turning. Turning generally requires more complicated toolpaths/workpiece geometry, and thus the spectral analysis is recommended for turning processes. However, since boring of holes is a relatively simple and finishing operation, the 1$^{st}$ autocorrelation coefficient method would be recommended for boring processes due to its computational efficiency.

## Summary

Three algorithms were tested for chatter detection in single point cutting operations with a focus on developing low-cost embedded system based real time process monitoring instrumentation. The 1$^{st}$ autocorrelation coefficient was determined to be the most computationally efficient method, but was found to be susceptible to false alarms during stable cutting. Spectral analysis using a ratio of two peaks with the highest power in the FFT was found to be the most robust chatter detection method for the three cutting scenarios analyzed in this study. Spectral analysis is however computationally demanding from a microcontroller (MK20DX256VLH7) performance standpoint. Thus, for boring processes with a single insert where runout is minimal, the 1$^{st}$ autocorrelation function is recommended due to its low computational complexity. Future development of chatter detection algorithms should not only consider variations in the machining parameters, but also variations in the workpiece/tool setup. It is strongly recommended to develop chatter detection methods considering the limits of practical computational hardware for processing sensor-generated data.

# CHAPTER 6

# CONCLUSIONS AND RECOMMENDATIONS

This chapter summarizes the original contributions and main conclusions of this thesis and suggests possible areas for future studies.

## Original Contributions

A set of innovative methods and algorithms for wireless monitoring of single point cutting process has been presented in this thesis, including the PVDF sensor based measurement of turning cutting forces and boring cutting torque. In addition, simplified PVDF rosette configurations consisting of two sensors have been developed for isolation of particular strain components. In addition three computationally efficient algorithms for microcontroller-based on-line chatter recognition were developed and tested in a variety of cutting cases. The originality of this research lies in the modeling of the single-point cutting forces/torque measurement system, the development of various chatter detection algorithms suited for embedded processing, and the proposed cutting condition setups for validating the algorithms. The proposed methods in this thesis represent lower cost but efficient alternatives to the current industry standard for cutting force/torque measurement, and for chatter recognition algorithms that require expensive hardware. Note that the contributions discussed in this thesis can be applied to other applications that require signal recognition of harmonic faults such as bearing fault analysis.

## Main Conclusions

The conclusions for each major section of this thesis are summarized below.

**PVDF Sensor Based Monitoring of Dynamic Cutting Forces in Turning**

- PVDF sensor based dynamic cutting force measurement system was designed, analyzed, prototyped, and experimentally validated for turning processes. The PVDF sensor signal was found to be in reasonable agreement with the standard piezoelectric force dynamometer signal for feed and tangential force components, though not for the radial force component.
- Ideal conditions including facing toolpaths and threading tools were identified for obtaining better agreement with the dynamometer-based reference signal when using a simplified 2 PVDF rosette for measuring radial cutting forces.
- Quantitative, physics based models were established to relate the measured PVDF sensor signals to the dynamic tangential, radial, and feed forces in turning. The model was shown to be independent of the workpiece material and cutting conditions.

**PVDF Sensor Based Monitoring of Cutting Torque in Boring**

- A wireless PVDF sensor based cutting torque measurement system was designed, analyzed, prototyped, and experimentally validated for boring processes.
- When monitoring chatter, better agreement with the dynamometer-based reference signal in both the time and frequency domains was achieved.
- Quantitative, physics based models were established to relate the signal from the simplified 2 sensor PVDF rosette to the dynamic cutting torque in boring. The model was shown to be independent of the workpiece material and cutting conditions.

**Comparison of Chatter Detection Algorithms**

- Three algorithms (1$^{st}$ Autocorrelation, Second Generation Wavelet Transform, Fast Fourier Transform) were tested for chatter detection in single point turning and boring operations with a focus on developing low-cost embedded real time process monitoring instrumentation.

- Spectral analysis using a ratio of two peaks with the highest power in the FFT was found to be the most robust method for chatter detection in turning. The method was able to detect chatter at least 0.5 seconds before chatter occurred on the workpiece and was robust to variations in workpiece geometry and cutting conditions.
- The 1st autocorrelation coefficient was determined to be the most computationally efficient method for chatter detection in boring when effects of runout are minimized.

## Future Work and Recommendations

All the sensing methods and algorithms developed in this thesis can be applied in shop floor applications for a relatively low cost. The PVDF-based sensing technologies are especially useful for high precision applications that require expensive tooling for parts that are too complex for outsourcing or standard tooling. However, a majority of machine tools lack the capability to automatically suppress chatter even after a fault is detected. Chatter is not even on the list of specific machine tool alarms. The primary limitation for integrating the PVDF sensor into an industrial machine tool platform is the lack of open communication protocols for sensor integration. Thus, the modification of machine tool controllers to facilitate integration of chatter detection sensors and embedded tooling would be an interesting topic. This type of development would naturally result in standardized open architecture methodologies for machine tools to override spindle speed and/or feed parameters to suppress chatter.

A particularly interesting subject for future work is further exploration of the nature of chatter in boring bars. As stated in [142, 143], the nature of chatter in boring processes is not entirely due to the regenerative effect, but rather the difference in phase between the two principle axis of stiffness and the cutting force vector. This phenomenon, known as Mode Coupling chatter, occurs in symmetric low stiffness operations including boring bars and robotic milling [144]. However, detailed analysis of the chatter behavior and prevention of this type of chatter is lacking. In particular, there is little work utilizing

analytical models or cutting data to identify/distinguish mode coupling and regenerative effects when chatter occurs. The work reported in [143] identifies the dynamic instability in robotic milling as mode coupling chatter because their data could not be explained by the regenerative chatter stability lobe model. However, the classical stability lobe model is susceptible to various nonlinearities. Thus, a study into the behavior of chatter in boring operations considering both chip regeneration and mode coupling effects is highly recommended to assist in the further development of on-line chatter detection algorithms.

# APPENDIX

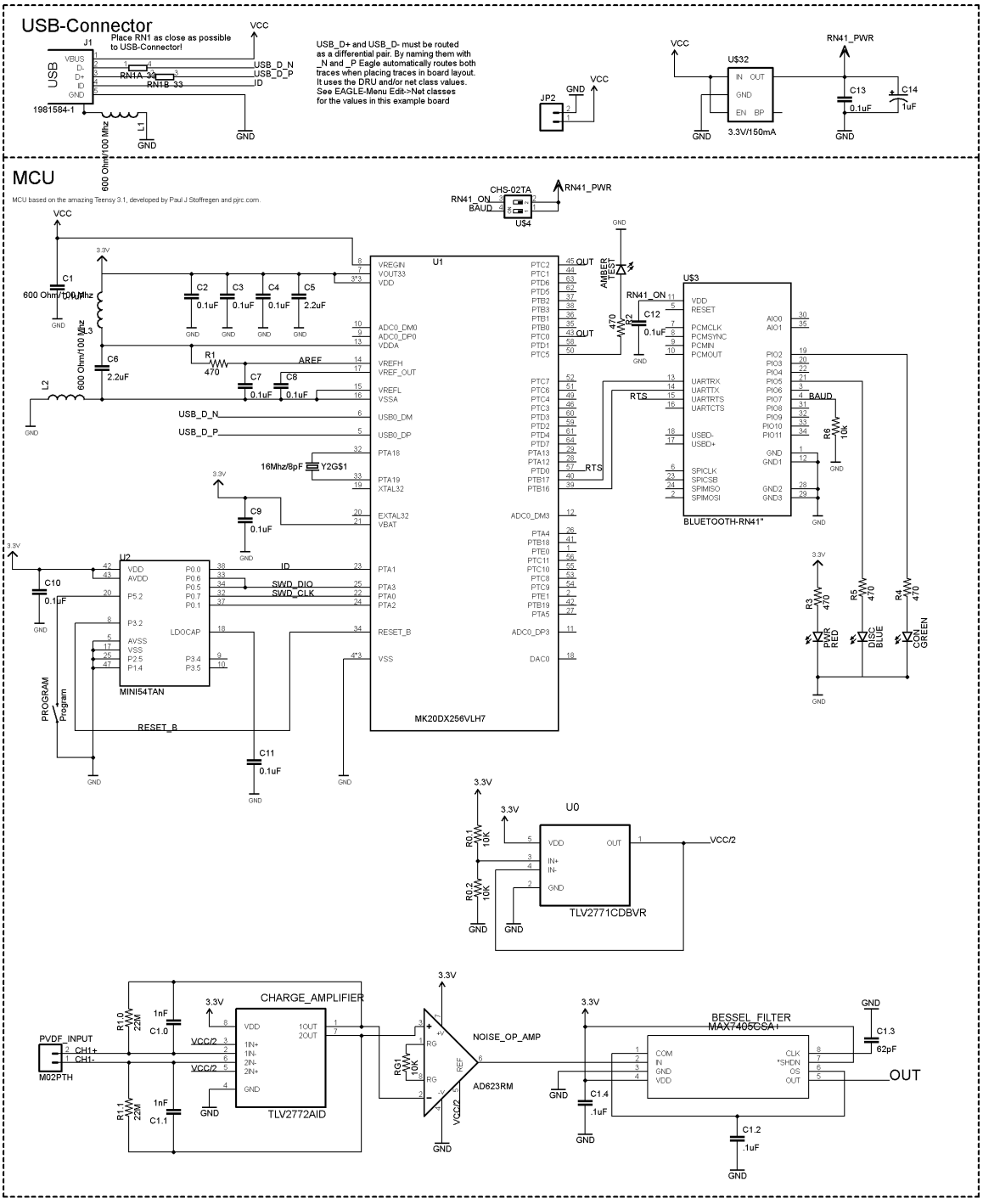


Figure A.1. Wireless PVDF sensor based turning schematic.

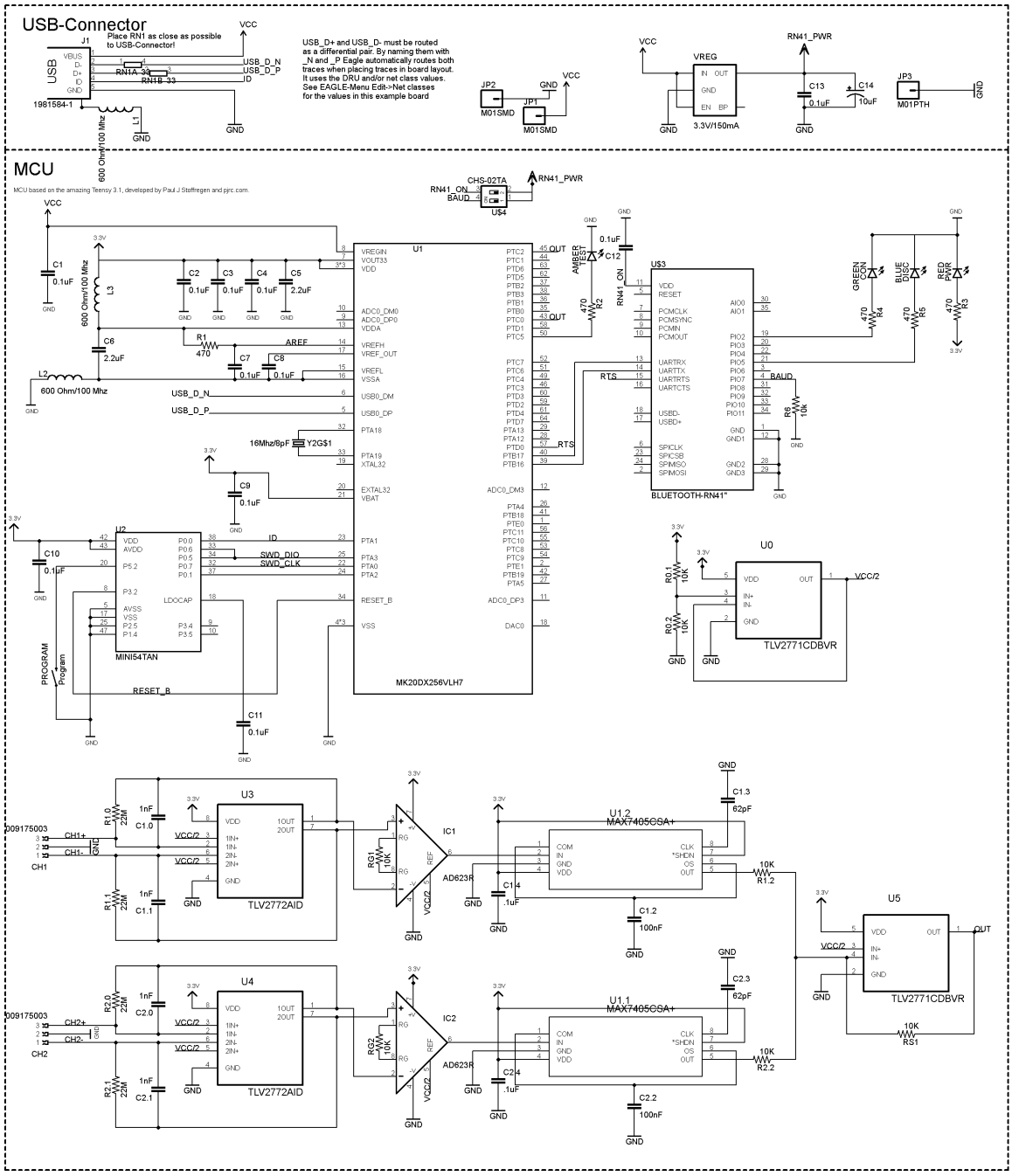


Figure A.2. Wireless PVDF sensor based boring schematic.

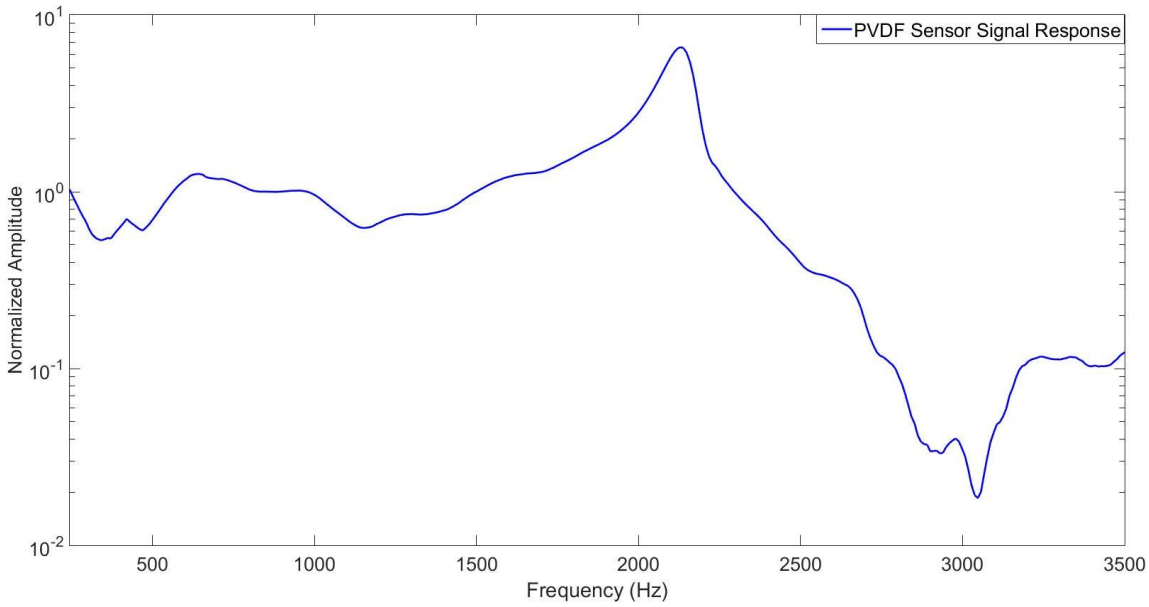


Figure A.3. PVDF sensor response from impulse hammer testing.

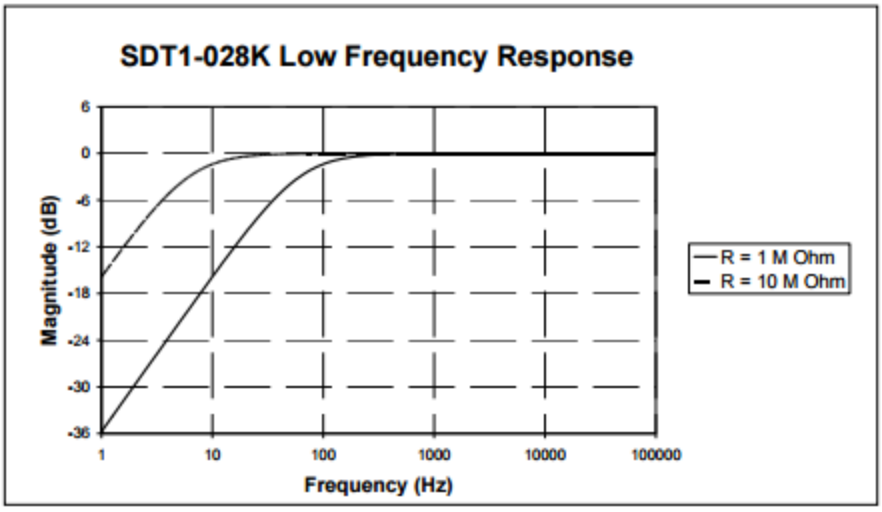


Figure A.4. PVDF sensor response [9].

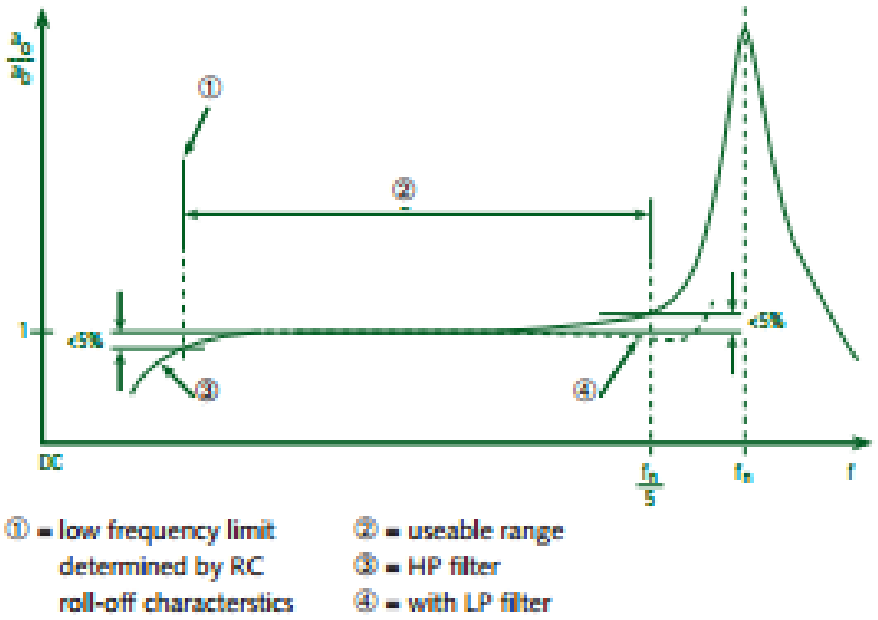


Figure A.5. Typical Kistler quartz-based piezoelectric sensor response [40].

# REFERENCES


[1] Kaymakci, M., Kilic, Z., and Altintas, Y., 2012, "Unified cutting force model for turning, boring, drilling and milling operations," International Journal of Machine Tools and Manufacture, 54, pp. 34-45.

[2] Rao, B. C., and Shin, Y. C., 1999, "A comprehensive dynamic cutting force model for chatter prediction in turning," International Journal of Machine Tools and Manufacture, 39(10), pp. 1631-1654.

[3] Teti, R., Jemielniak, K., O'Donnell, G., and Dornfeld, D., 2010, "Advanced monitoring of machining operations," CIRP Annals-Manufacturing Technology, 59(2), pp. 717-739.

[4] Tlusty, J., and Andrews, G., 1983, "A critical review of sensors for unmanned machining," CIRP Annals-Manufacturing Technology, 32(2), pp. 563-572.

[5] Cardi, A. A., Firpi, H. A., Bement, M. T., and Liang, S. Y., 2008, "Workpiece dynamic analysis and prediction during chatter of turning process," Mechanical Systems and Signal Processing, 22(6), pp. 1481-1494.

[6] Chandiramani, N. K., and Pothala, T., 2006, "Dynamics of 2-dof regenerative chatter during turning," Journal of sound and vibration, 290(1), pp. 448-464.

[7] Deshpande, N., and Fofana, M., 2001, "Nonlinear regenerative chatter in turning," Robotics and Computer-Integrated Manufacturing, 17(1), pp. 107-112.

[8] Ozlu, E., and Budak, E., 2007, "Analytical modeling of chatter stability in turning and boring operations—part I: model development," Journal of Manufacturing Science and Engineering, 129(4), pp. 726-732.

[9] MEAS, 2009, "SDT Shielded Piezo Sensors," http://www.meas-spec.com/downloads/SDT_Series.pdf.

[10] Ma, L., Melkote, S. N., Morehouse, J. B., Castle, J. B., Fonda, J. W., and Johnson, M. A., 2012, "Thin-film PVDF sensor-based monitoring of cutting forces in peripheral end milling," Journal of Dynamic Systems, Measurement, and Control, 134(5), p. 051014.

[11] Galea, S., Chiu, W., and Paul, J., 1993, "Use of piezoelectric films in detecting and monitoring damage in composites," Journal of Intelligent Material Systems and Structures, 4(3), pp. 330-336.

[12] Kim, D., Kim, B., Yun, S., and Kwon, S., "Cellular force measurement for force reflected biomanipulation," Proc. IEEE International Conference on Robotics and Automation, IEEE, pp. 2412-2417.

[13] Li, W. J., and Xi, N., "Novel micro gripping, probing, and sensing devices for single-cell surgery," Proc. 26th Annual International Conference of the IEEE Engineering in Medicine and Biology Society, IEEE, pp. 2591-2594.

[14] Xie, Y., Sun, D., Liu, C., Tse, H. Y., and Cheng, S. H., 2010, "A force control approach to a robot-assisted cell microinjection system," The International Journal of Robotics Research, 29(9), pp. 1222-1232.

[15] Zhang, H., Galea, S., Chiu, W., and Lam, Y., 1993, "An investigation of thin PVDF films as fluctuating-strain-measuring and damage-monitoring devices," Smart Materials and Structures, 2(4), p. 208.

[16] Byrne, G., Dornfeld, D., Inasaki, I., Ketteler, G., König, W., and Teti, R., 1995, "Tool condition monitoring (TCM)—the status of research and industrial application," CIRP Annals-Manufacturing Technology, 44(2), pp. 541-567.

[17] Liang, S. Y., Hecker, R. L., and Landers, R. G., "Machining process monitoring and control: the state–of–the–art," Proc. ASME 2002 International Mechanical Engineering Congress and Exposition, American Society of Mechanical Engineers, pp. 599-610.

[18] Wright, P., Dornfeld, D., and Ota, N., 2008, "Condition monitoring in end-milling using wireless sensor networks (WSNs)," Transactions of NAMRI/SME, 36.

[19] Dornfeld, D., Lee, Y., and Chang, A., 2003, "Monitoring of ultraprecision machining processes," The International Journal of Advanced Manufacturing Technology, 21(8), pp. 571-578.

[20] Jerard, R. B., Fussell, B. K., Suprock, C. A., Cui, Y., Nichols, J., Hassan, R. Z., and Esterling, D., "Integration of wireless sensors and models for a smart machining system," Proc. ASME 2009 International Manufacturing Science and Engineering Conference, American Society of Mechanical Engineers, pp. 119-128.

[21] Yaldız, S., and Ünsaçar, F., 2006, "A dynamometer design for measurement the cutting forces on turning," Measurement, 39(1), pp. 80-89.

[22] Aneiro, F. M., Coelho, R. T., and Brandao, L. C., 2008, "Turning hardened steel using coated carbide at high cutting speeds," Journal of the Brazilian Society of Mechanical Sciences and Engineering, 30(2), pp. 104-109.

[23] O'sullivan, D., and Cotterell, M., 2001, "Temperature measurement in single point turning," Journal of Materials Processing Technology, 118(1), pp. 301-308.

[24] Hou, L., and Bergmann, N. W., "System requirements for industrial wireless sensor networks," Proc. Emerging Technologies and Factory Automation (ETFA), 2010 IEEE Conference on, IEEE, pp. 1-8.

[25] Nethi, S., Nieminen, J., and Jäntti, R., "Exploitation of multi-channel communications in industrial wireless sensor applications: Avoiding interference and enabling coexistence," Proc. Wireless Communications and Networking Conference (WCNC), 2011 IEEE, IEEE, pp. 345-350.

[26] Tang, L., Wang, K.-C., and Huang, Y., 2013, "Study of speed-dependent packet error rate for wireless sensor on rotating mechanical structures," Industrial Informatics, IEEE Transactions on, 9(1), pp. 72-80.

[27] Abrishambaf, R., Bal, M., and Hashemipour, M., 2011, "Distributed control architecture for wireless sensor networks using IEC 61499 function blocks for industrial automation," International Journal of Computer and Electrical Engineering, 3(5), p. 640.

[28] Tan, K. K., Huang, S., Zhang, Y., and Lee, T. H., 2009, "Distributed fault detection in industrial system based on sensor wireless network," Computer Standards and Interfaces, 31(3), pp. 573-578.

[29] Skuta, J., "The control unit with wireless interfaces for CNC model," Proc. Control Conference (ICCC), 2014 15th International Carpathian, IEEE, pp. 570-573.

[30] Moreno-Tapia, S. V., Vera-Salas, L. A., Osornio-Rios, R. A., Dominguez-Gonzalez, A., Stiharu, I., and Romero-Troncoso, R. d. J., 2010, "A field programmable gate array-based reconfigurable smart-sensor network for wireless monitoring of new generation computer numerically controlled machines," Sensors, 10(8), pp. 7263-7286.

[31] Ho, C. Y., Lee, Y. C., and Tzeng, Y. S., "Measurement of cutting temperature using wireless sensing system," Proc. Materials Science Forum, Trans Tech Publications, pp. 949-952.

[32] Guha, A., Werschmoeller, D., and Li, X., "Wireless acquisition of temperature data from PCBN embedded thin film sensors," Proc. ASME 2010 International Manufacturing Science and Engineering Conference, American Society of Mechanical Engineers, pp. 467-471.

[33] Liu, Z., Quan, Y. M., and Liang, L., "A wireless system for cutting temperature measurement," Proc. Advanced Materials Research, Trans Tech Publications, pp. 475-480.

[34] Werschmoeller, D., Ehmann, K., and Li, X., 2011, "Tool embedded thin film microsensors for monitoring thermal phenomena at tool-workpiece interface during machining," Journal of Manufacturing Science and Engineering, 133(2), p. 021007.

[35] Aruväli, T., Serg, R., and Otto, T., "In-process vibration monitoring on CNC lathe," Proc. 10th International Symposium, Topical Problems in the Field of Electrical and Power Engineering, pp. 174-178.

[36] Shiba, K., Yamamoto, D., Chanthapan, S., Hosaka, H., Sasaki, K., and Itao, K., 2003, "Development of a miniature abrasion-detecting device for a small precision lathe," Sensors and Actuators A: Physical, 109(1), pp. 137-142.

[37] Prateepasen, A., Au, Y., and Jones, B., "Acoustic emission and vibration for tool wear monitoring in single-point machining using belief network," Proc. Instrumentation and Measurement Technology Conference, 2001. IMTC 2001. Proceedings of the 18th IEEE, IEEE, pp. 1541-1546.

[38] Zhou, J.-H., Pang, C. K., Zhong, Z.-W., and Lewis, F. L., 2011, "Tool wear monitoring using acoustic emissions by dominant-feature identification," IEEE Transactions on Instrumentation and Measurement, 60(2), pp. 547-559.

[39] Smith, G. C., and Lee, S. S., 2005, "A method for detecting tool wear on a CNC lathe using a doppler radar detector," The International Journal of Advanced Manufacturing Technology, 25(3-4), pp. 270-280.

[40] Kistler, 2009, "Type 9257B Multicomponent Dynamometer," http://www.kistler.com/us/en/products/components/force-sensors/

[41] Liao, L., Minhas, R., Rangarajan, A., Kurtoglu, T., and de Kleer, J., "A self-aware machine platform in manufacturing shop floor utilizing MTConnect data," Proc. Annual Conference of the Prognostics and Health Management Society.

[42] Bengtsson, N., Michaloski, J., Proctor, F., Shao, G., and Venkatesh, S., "Towards data-driven sustainable machining: combining MTconnect production data and discrete event simulation," Proc. ASME 2010 International Manufacturing Science and Engineering Conference, American Society of Mechanical Engineers, pp. 379-387.

[43] Vijayaraghavan, A., Sobel, W., Fox, A., Dornfeld, D., and Warndorf, P., 2008, "Improving machine tool interoperability using standardized interface protocols: MTconnect," 2008 International Symposium on Flexible Automation.

[44] Albrecht, A., Park, S. S., Altintas, Y., and Pritschow, G., 2005, "High frequency bandwidth cutting force measurement in milling using capacitance displacement sensors," International Journal of Machine Tools and Manufacture, 45(9), pp. 993-1008.

[45] Jun, M. B., Ozdoganlar, O. B., DeVor, R. E., Kapoor, S. G., Kirchheim, A., and Schaffner, G., 2002, "Evaluation of a spindle-based force sensor for monitoring and fault diagnosis of machining operations," International Journal of Machine Tools and Manufacture, 42(6), pp. 741-751.

[46] Park, S. S., and Altintas, Y., 2004, "Dynamic compensation of spindle integrated force sensors with kalman filter," Journal of Dynamic Systems, Measurement, and Control, 126(3), pp. 443-452.

[47] Liu, M., Zhou, Z., Tao, X., and Tan, Y., "A dynamometer design and analysis for measurement the cutting forces on turning based on optical fiber Bragg Grating sensor," Proc. Intelligent Control and Automation (WCICA), 2012 10th World Congress on, IEEE, pp. 4287-4290.

[48] Pezzullo, V., 2014, "Design of a custom software application to monitor and communicate CNC machining process information to aid in chatter identification," Master's of Science, Clemson University.

[49] Li, C., and Ulsoy, A. G., 1999, "High-precision measurement of tool-tip displacement using strain gauges in precision flexible line boring," Mechanical Systems and Signal Processing, 13(4), pp. 531-546.

[50] Kim, J., and Kim, D., 1997, "Development of a combined-type tool dynamometer with a piezo-film accelerometer for an ultra-precision lathe," Journal of Materials Processing Technology, 71(3), pp. 360-366.

[51] Totis, G., and Sortino, M., 2011, "Development of a modular dynamometer for triaxial cutting force measurement in turning," International Journal of Machine Tools and Manufacture, 51(1), pp. 34-42.

[52] Connectivity, T., 2016, "Piezo film sensors," http://www.te.com/usa-en/product-CAT-PFS0009.html#mdp-tabs-content.

[53] Mohammadi, B., Yousefi, A. A., and Bellah, S. M., 2007, "Effect of tensile strain rate and elongation on crystalline structure and piezoelectric properties of PVDF thin films," Polymer Testing, 26(1), pp. 42-50.

[54] Fu, Y., Harvey, E. C., Ghantasala, M. K., and Spinks, G. M., 2005, "Design, fabrication and testing of piezoelectric polymer PVDF microactuators," Smart Materials and Structures, 15(1), p. S141.

[55] Fung, C. K., Elhaj, I., Li, W., and Xi, N., "A 2-d pvdf force sensing system for micro-manipulation and micro-assembly," Proc. IEEE International Conference on Robotics and Automation, IEEE, pp. 1489-1494.

[56] Shen, Y., Xi, N., Lai, K. W., and Li, W. J., 2004, "A novel PVDF microforce/force rate sensor for practical applications in micromanipulation," Sensor Review, 24(3), pp. 274-283.

[57] Pinnington, R., and Briscoe, A., 1994, "Externally applied sensor for axisymmetric waves in a fluid filled pipe," Journal of Sound and Vibration, 173(4), pp. 503-516.

[58] Paradiso, J. A., and Hu, E., "Expressive footwear for computer-augmented dance performance," Proc. First International Symposium on Wearable Computers, IEEE, pp. 165-166.

[59] Wang, Y., Zheng, J., Ren, G., Zhang, P., and Xu, C., 2011, "A flexible piezoelectric force sensor based on PVDF fabrics," Smart Materials and Structures, 20(4), p. 045009.

[60] Zhang, Y., 2006, "In situ fatigue crack detection using piezoelectric paint sensor," Journal of Intelligent Material Systems and Structures, 17(10), pp. 843-852.

[61] Ma, L., Melkote, S. N., Morehouse, J. B., Castle, J. B., Fonda, J. W., and Johnson, M. A., 2012, "Design of thin-film polyvinylidene fluoride sensor rosettes for isolation of various strain components," Journal of Intelligent Material Systems and Structures, 23(10), pp. 1119-1130.

[62] Ma, L., Melkote, S. N., and Castle, J. B., 2014, "PVDF sensor-based monitoring of milling torque," The International Journal of Advanced Manufacturing Technology, 70(9-12), pp. 1603-1614.

[63] Li, C. J., and Li, S., 1993, "A new sensor for real-time milling tool condition monitoring," Journal of Dynamic systems, Measurement, and Control, 115(2A), pp. 285-290.

[64] Delio, T., Tlusty, J., and Smith, S., 1992, "Use of audio signals for chatter detection and control," Journal of Engineering for Industry, 114(2), pp. 146-157.

[65] Al-Regib, E., and Ni, J., 2010, "Chatter detection in machining using nonlinear energy operator," Journal of Dynamic Systems, Measurement, and Control, 132(3), p. 034502.

[66] Berger, B., Manzari, J., Anand, D., and Belai, C., 2001, "Auto-regressive SVD algorithms and cutting state identification," Journal of Sound and Vibration, 248(2), pp. 351-370.

[67] Berger, B., Minis, I., Harley, J., Rokni, M., and Papadopoulos, M., 1998, "Wavelet based cutting state identification," Journal of Sound and Vibration, 213(5), pp. 813-827.

[68] Clancy, B. E., Rao, B., and Shin, Y. C., 2002, "Time domain chatter prediction including tool wear effects during face turning of nickel based super alloys," Transactions of North American Manufacturing Research Institution, 30, pp. 377-384.

[69] Elias, J., and Namboothiri, V. N., 2014, "Cross-recurrence plot quantification analysis of input and output signals for the detection of chatter in turning," Nonlinear Dynamics, 76(1), pp. 255-261.

[70] Eynian, M., and Altintas, Y., 2009, "Chatter stability of general turning operations with process damping," Journal of Manufacturing Science and Engineering, 131(4), p. 041005.

[71] Hynynen, K. M., Ratava, J., Lindh, T., Rikkonen, M., Ryynänen, V., Lohtander, M., and Varis, J., 2014, "Chatter detection in turning processes using coherence of acceleration and audio signals," Journal of Manufacturing Science and Engineering, 136(4), p. 044503.

[72] Li, X., Wong, Y., and Nee, A., 1997, "Tool wear and chatter detection using the coherence function of two crossed accelerations," International Journal of Machine Tools and Manufacture, 37(4), pp. 425-435.

[73] Lin, S., and Hu, M., 1992, "Low vibration control system in turning," International Journal of Machine Tools and Manufacture, 32(5), pp. 629-640.

[74] Liu, Y., Li, T.-x., Liu, K., and Zhang, Y.-m., 2016, "Chatter reliability prediction of turning process system with uncertainties," Mechanical Systems and Signal Processing, 66, pp. 232-247.

[75] Perez-Canales, D., Vela-Martínez, L., Jáuregui-Correa, J. C., and Alvarez-Ramirez, J., 2012, "Analysis of the entropy randomness index for machining chatter detection," International Journal of Machine Tools and Manufacture, 62, pp. 39-45.

[76] Siddhpura, M., and Paurobally, R., "Experimental investigation of chatter vibrations in facing and turning processes," Proc. World Academy of Science, Engineering and Technology, World Academy of Science, Engineering and Technology (WASET), pp. 968-973.

[77] Sun, Y., Zhuang, C., and Xiong, Z., "Real-time chatter detection using the weighted wavelet packet entropy," Proc. 2014 IEEE/ASME International Conference on Advanced Intelligent Mechatronics (AIM), IEEE, pp. 1652-1657.

[78] Tansel, I., Wagiman, A., and Tziranis, A., 1991, "Recognition of chatter with neural networks," International Journal of Machine Tools and Manufacture, 31(4), pp. 539-552.

[79] Tansel, I., Wang, X., Chen, P., Yenilmez, A., and Ozcelik, B., 2006, "Transformations in machining. Part 2. Evaluation of machining quality and detection of chatter in turning by using s-transformation," International Journal of Machine Tools and Manufacture, 46(1), pp. 43-50.

[80] Thomas, M., and Beauchamp, Y., 2003, "Statistical investigation of modal parameters of cutting tools in dry turning," International Journal of Machine Tools and Manufacture, 43(11), pp. 1093-1106.

[81] Wang, M., and Fei, R., 2001, "On-line chatter detection and control in boring based on an electrorheological fluid," Mechatronics, 11(7), pp. 779-792.

[82] Wu, Y., and Du, R., 1996, "Feature extraction and assessment using wavelet packets for monitoring of machining processes," Mechanical Systems and Signal Processing, 10(1), pp. 29-53.

[83] Zhang, C. L., Yue, X., Jiang, Y. T., and Zheng, W., "A hybrid approach of ANN and HMM for cutting chatter monitoring," Proc. Advanced Materials Research, Trans Tech Publ, pp. 3225-3232.

[84] Bao, S., Zhang, W., Yu, J., Qiao, S., and Yang, F., 1994, "A new approach to the early prediction of turning chatter," Journal of Vibration and Acoustics, 116(4), pp. 485-488.

[85] Grabec, I., Gradišek, J., and Govekar, E., 1999, "A new method for chatter detection in turning," CIRP Annals-Manufacturing Technology, 48(1), pp. 29-32.

[86] Kayhan, M., and Budak, E., 2009, "An experimental investigation of chatter effects on tool life," Proceedings of the Institution of Mechanical Engineers, Part B: Journal of Engineering Manufacture, 223(11), pp. 1455-1463.

[87] Peng, W., Hu, Z., Yuan, L., and Zhu, P., "Chatter identification using HHT for boring process," Proc. International Conference on Optical Instruments and Technology (OIT2013), International Society for Optics and Photonics, pp. 904316-904311-904316.

[88] Pour, D. S., and Behbahani, S., 2015, "Semi-active fuzzy control of machine tool chatter vibration using smart MR dampers," The International Journal of Advanced Manufacturing Technology, pp. 421-428.

[89] Qian, S., Sun, Y., and Xiong, Z., "Intelligent chatter detection based on wavelet packet node energy and LSSVM-RFE," Proc. IEEE International Conference on Advanced Intelligent Mechatronics (AIM), IEEE, pp. 1514-1519.

[90] Yeh, L., and Lai, G., 1995, "A study of the monitoring and suppression system for turning slender workpieces," Proceedings of the Institution of Mechanical Engineers, Part B: Journal of Engineering Manufacture, 209(3), pp. 227-236.

[91] Matsumoto, Y., Tjiang, N., Foote, B., and Naerheimh, Y., 1990, "Tool wear monitoring using acoustic emission in the existence of chatter," International Journal of Production Research, 28(10), pp. 1861-1869.

[92] Yu, S., and Shah, V., 2008, "Theoretical and experimental studies of chatter in turning for uniform and stepped workpieces," Journal of Vibration and Acoustics, 130(6), p. 061005.

[93] Nair, U., Krishna, B. M., Namboothiri, V., and Nampoori, V., 2010, "Permutation entropy based real-time chatter detection using audio signal in turning process," The International Journal of Advanced Manufacturing Technology, 46(1-4), pp. 61-68.

[94] Zhu, P., Peng, W., Yuan, L., and Hu, Z., "Feasibility study of detection of chatter by using FBG during boring," Proc. Sixth International Symposium on Precision Mechanical Measurements, International Society for Optics and Photonics, p. 891622.

[95] Ramesh, K., Alwarsamy, T., and Jayabal, S., 2013, "Investigation of chatter stability in boring tool and tool wear prediction using neural network," International Journal of Materials and Product Technology, 46(1), pp. 47-70.

[96] Lange, J., and Abu-Zahra, N., 2002, "Tool chatter monitoring in turning operations using wavelet analysis of ultrasound waves," The International Journal of Advanced Manufacturing Technology, 20(4), pp. 248-254.

[97] Chen, H.-M., Fan, K.-C., Kuo, T.-H., and Wang, C.-H., 2012, "Development of a low cost in-process chatter suppression system in milling process," Chinese Journal of Mechanical Engineering, 33(5), pp. 419-426.

[98] Colak, O., Oral, O., Caglayan, N., and Kazanci, H., "Wireless tool vibration monitoring for milling," Proc. 11th International Conference on Management of Innovative Technologies and 2nd International Conference on Sustainable Life in Manufacturing, pp. 178-183.

[99] Siddhpura, M., and Paurobally, R., 2012, "A review of chatter vibration research in turning," International Journal of Machine tools and Manufacture, 61, pp. 27-47.

[100] Soliman, E., and Ismail, F., 1997, "Chatter detection by monitoring spindle drive current," The International Journal of Advanced Manufacturing Technology, 13(1), pp. 27-34.

[101] Kuljanic, E., Sortino, M., and Totis, G., 2008, "Multisensor approaches for chatter detection in milling," Journal of Sound and Vibration, 312(4), pp. 672-693.

[102] Heidenhain, 2013, "Dynamic efficiency: working efficiently and with process reliability," http://heidenhaingb.com/wp-content/uploads/pdf-files/Dynamic_Efficiency_en.pdf.

[103] Lewis, J., and Moss, B., "MEMS microphone: the future for hearing aids," Analog Dialogue, 47(11).

[104] Altintas, Y., 2012, Manufacturing automation: metal cutting mechanics, machine tool vibrations, and CNC design, Cambridge University Press.

[105] Altintas, Y., Eynian, M., and Onozuka, H., 2008, "Identification of dynamic cutting force coefficients and chatter stability with process damping," CIRP Annals-Manufacturing Technology, 57(1), pp. 371-374.

[106] Wang, J., Liang, S. Y., and Book, W. J., 1994, "Convolution analysis of milling force pulsation," Journal of Engineering for Industry, 116(1), pp. 17-25.

[107] Sutherland, J. W., 1988, "A dynamic model of the cutting force system in the end milling process," 49, University of Illinois at Urbana-Champaign.

[108] Wan, M., and Zhang, W., 2009, "Systematic study on cutting force modelling methods for peripheral milling," International Journal of Machine Tools and Manufacture, 49(5), pp. 424-432.

[109] Merdol, S., and Altintas, Y., 2004, "Multi frequency solution of chatter stability for low immersion milling," Journal of Manufacturing Science and Engineering, 126(3), pp. 459-466.

[110] Ma, L., Melkote, S. N., and Castle, J. B., 2013, "A model-based computationally efficient method for on-line detection of chatter in milling," Journal of Manufacturing Science and Engineering, 135(3), p. 031007.

[111] Kakinuma, Y., Sudo, Y., and Aoyama, T., 2011, "Detection of chatter vibration in end milling applying disturbance observer," CIRP Annals-Manufacturing Technology, 60(1), pp. 109-112.

[112] Seguy, S., Insperger, T., Arnaud, L., Dessein, G., and Peigné, G., 2011, "Suppression of period doubling chatter in high-speed milling by spindle speed variation," Machining Science and Technology, 15(2), pp. 153-171.

[113] Lamraoui, M., Barakat, M., Thomas, M., and El Badaoui, M., 2015, "Chatter detection in milling machines by neural network classification and feature selection," Journal of Vibration and Control, 21(7), pp. 1251-1266.

[114] Suprock, C. A., Hassan, R. Z., Jerard, R. B., and Fussell, B. K., "Predicting endmill tool chatter with a wireless tool tip vibration sensor," Proc. 11th CIRP Conference on Modeling of Machining Operations.

[115] Messaoud, A., Weihs, C., and Hering, F., 2008, "Detection of chatter vibration in a drilling process using multivariate control charts," Computational Statistics & Data Analysis, 52(6), pp. 3208-3219.

[116] Choi, T., and Shin, Y. C., 2003, "On-line chatter detection using wavelet-based parameter estimation," Journal of Manufacturing Science and Engineering, 125(1), pp. 21-28.

[117] Tarng, Y., Li, T., and Chen, M., 1994, "On-line drilling chatter recognition and avoidance using an ART2 - a neural network," International Journal of Machine Tools and Manufacture, 34(7), pp. 949-957.

[118] Ghosh-Dastidar, S., Adeli, H., and Dadmehr, N., 2007, "Mixed-band wavelet-chaos-neural network methodology for epilepsy and epileptic seizure detection," IEEE Transactions on Biomedical Engineering, 54(9), pp. 1545-1551.

[119] Übeyli, E. D., 2009, "Combined neural network model employing wavelet coefficients for EEG signals classification," Digital Signal Processing, 19(2), pp. 297-308.

[120] Subasi, A., and Ercelebi, E., 2005, "Classification of EEG signals using neural network and logistic regression," Computer Methods and Programs in Biomedicine, 78(2), pp. 87-99.

[121] Webber, W., Litt, B., Wilson, K., and Lesser, R., 1994, "Practical detection of epileptiform discharges (EDs) in the EEG using an artificial neural network: a comparison of raw and parameterized EEG data," Electroencephalography and Clinical Neurophysiology, 91(3), pp. 194-204.

[122] Li, B., Chow, M.-Y., Tipsuwan, Y., and Hung, J. C., 2000, "Neural-network-based motor rolling bearing fault diagnosis," IEEE Transactions on Industrial Electronics, 47(5), pp. 1060-1069.

[123] Samanta, B., and Al-Balushi, K., 2003, "Artificial neural network based fault diagnostics of rolling element bearings using time-domain features," Mechanical Systems and Signal Processing, 17(2), pp. 317-328.

[124] Paya, B., Esat, I., and Badi, M., 1997, "Artificial neural network based fault diagnostics of rotating machinery using wavelet transforms as a preprocessor," Mechanical Systems and Signal Processing, 11(5), pp. 751-765.

[125] Sirohi, J., and Chopra, I., 2000, "Fundamental understanding of piezoelectric strain sensors," Journal of Intelligent Material Systems and Structures, 11(4), pp. 246-257.

[126] Arduino, 2016, "Arduino," https://www.arduino.cc/.

[127]ARM Limited, 2016, "mbed," https://www.mbed.com/en/.

[128] Beagleboard.org Foundation, 2016, "BeagleBoard," https://beagleboard.org/.

[129] Atmel, 2015, "SAM3X / SAM3A Series," http://www.atmel.com/Images/Atmel-11057-32-bit-Cortex-M3-Microcontroller-SAM3X-SAM3A_Datasheet.pdf.

[130] Freescale Semiconductor Inc., 2012, "K20 Sub-Family Reference Manual," https://www.pjrc.com/teensy/K20P64M72SF1RM.pdf.

[131] National Institute of Science and Technology, 2013, "Autocorrelation Plot," http://www.itl.nist.gov/div898/handbook/eda/section3/autocopl.htm.

[132] Chapeau-Blondeau, F., 2007, "Autocorrelation versus entropy-based autoinformation for measuring dependence in random signal," Physica A: Statistical Mechanics and its Applications, 380, pp. 1-18.

[133] Cohen, L., 1998, "Generalization of the Wiener-Khinchin theorem," IEEE Signal Processing Letters, 5(11), pp. 292-294.

[134] Kondo, E., 2016, "Chatter vibration detection method, chatter vibration avoidance method, and machine tool," U. S. P. Office, ed., Makino Milling Machine Company.

[135] Kwak, J.-S., 2006, "Application of wavelet transform technique to detect tool failure in turning operations," The International Journal of Advanced Manufacturing Technology, 28(11-12), pp. 1078-1083.

[136] Yao, Z., Mei, D., and Chen, Z., 2010, "On-line chatter detection and identification based on wavelet and support vector machine," Journal of Materials Processing Technology, 210(5), pp. 713-719.

[137] Rein, S., and Reisslein, M., 2011, "Low-memory wavelet transforms for wireless sensor networks: a tutorial," IEEE Communications Surveys and Tutorials, 13(2), pp. 291-307.

[138] Polikar, R., 1996, "The wavelet transform second edition part I, fundamental concepts and an overview of the wavelet theory," University of Nevada, Reno.

[139] Sweldens, W., 1998, "The lifting scheme: a construction of second generation wavelets," SIAM Journal on Mathematical Analysis, 29(2), pp. 511-546.

[140] Weisstein, E. W., 2015, "Fast Fourier Transform," http://mathworld.wolfram.com/FastFourierTransform.html.

[141] Ammar, G., Gragg, W., and Reichel, L., "Determination of Pisarenko frequency estimates as eigenvalues of an orthogonal matrix," Proc. 31st Annual Technical Symposium, International Society for Optics and Photonics, pp. 143-145.

[142] Stone, B., 2014, "Extension of Chatter Theory," Chatter and Machine Tools, Springer, pp. 27-55.

[143] Pratt Jr, J. R., 1997, "Vibration control for chatter suppression with application to boring bars," PhD, Virginia Polytechnic Institute and State University, Blacksburg, Virginia.

[144] Pan, Z., Zhang, H., Zhu, Z., and Wang, J., 2006, "Chatter analysis of robotic machining process," Journal of Materials Processing Technology, 173(3), pp. 301-309.